Modelling of Landfill Gas Adsorption with Bottom Ash for Utilization of Renewable Energy

Dissertation submitted to the Department of Civil Engineer,
University of Duisburg-Essen
for the degree of “Doktor-Ingenieur” (Dr.-Ing.)

by Chen Miao
born on January 5, 1979 in Jiangsu, P.R. China

Date of examination: 06 October 2011

Reviewer: Prof. Dr.-Ing. Renatus Widmann
Prof. Dr.-Ing. Tim Ricken

Preface and Acknowledgement

This work is carried out at the ‘Abteilung Siedlungswasser- und Abfallwirtschaft’ of Faculty of Engineering in Duisburg-Essen University in close cooperation with the ‘Lehrstuhl Mechanik-Statik-Dynamick’ of Faculty of Architecture and Civil Engineering in TU Dortmund.

I am heartily grateful to my doctoral supervisor Professor Renatus Widmann for supporting me in terms of development of my scientific and professional skills through my study in University of Duisburg-Essen. I particularly thank the supervisor Professor Tim Ricken of Faculty of Architecture and Civil Engineering in TU Dortmund. He gives me great support in modelling development.

This work could never be realized without the opportunity offered by Professor J.-D. Herbell at Institute of Waste Technology of Duisburg-Essen University, that is my first chance to study abroad in life. I am thankful for the support of the China Scholarship Council. As a beneficiary of ‘State-Sponsored Graduate Scholarship Program for Building High-level Universities’, I am able to give undivided attention to scientific research.

Many thanks belong to my colleagues and every one who gives me advice and help. I particularly thank Mr. Serdar Serdas and Mr. Daniel Werner. Their warm and friendly cooperation touches me deeply.

I wish to extend to my personal thanks:

To my beloved family. Thanks for my parents’ great support, their encouragement gives me intense confidence and passion in study through these years.

I also owe my sincere gratitude to my friends. They give me their time in listening to me and accompanying me patiently during the difficult course of the thesis.

Chen Miao

Duisburg, Germany
August 2011

Summary

Energy crisis, environment pollution and climate change are the serious challenges to people worldwide. In the 21st century, human being is trend to research new technology of renewable energy, so as to slow down global warming and develop society in an environmentally sustainable method.

Landfill gas, produced by biodegradable municipal solid waste in landfill, is a renewable energy source. In this work, landfill gas utilization for energy generation is introduced. Landfill gas is able to produce hydrogen by steam reforming reactions. There is a steam reformer equipment in the fuel cells system. A sewage plant of Cologne in Germany has run the Phosphoric Acid Fuel Cells power station with biogas for more than 50,000 hours successfully. Landfill gas thus may be used as fuel for electricity generation via fuel cells system. For the purpose of explaining the possibility of landfill gas utilization via fuel cells, the thermodynamics of landfill gas steam reforming are discussed by simulations.

In practice, the methane-riched gas can be obtained by landfill gas purification and upgrading. This work investigate a new method for upgrading-landfill gas adsorption with bottom ash experimentally. Bottom ash is a by-product of municipal solid waste incineration, some of its physical and chemical properties are analysed in this work. The landfill gas adsorption experimental data show bottom ash can be used as a potential adsorbent for landfill gas adsorption to remove CO_2. In addition, the alkalinity of bottom ash eluate can be reduced in these adsorption processes. Therefore, the interactions between landfill gas and bottom ash can be explained by series reactions accordingly.

Furthermore, a conceptual model involving landfill gas adsorption with bottom ash is developed. In this thesis, the parameters of landfill gas adsorption equilibrium equations can be obtained by fitting experimental data. On the other hand, these functions can be deduced with theoretical approach. In this thesis, both of them are discussed respectively. Additionally, the diffusion phenomena of landfill gas mixtures can be expressed by Maxwell-Stefan equations and Fick's law. According to the relation between Maxwell-Stefan equations and Fick's law, the diffusion coefficients of landfill gas mixtures can be estimated in theory.

The major part of this model is based on the theory of mass transfer through porous media. In which, mass balance, momentum balance and constitutive relations among multi-phase are employed for modeling. Landfill gas adsorption processes in two-dimension porous media can be thus simulated with application of this model.

Contents

List of Figures

List of Tables

List of Symbols and Abbreviations

Latin letters

a_i	activity
$\mathbf{b}^\alpha$	external body force
$B^{\alpha\alpha}$	inverse of binary diffusion coefficient
$[B]$	square matrix of inverted binary diffusiion coefficients
B_S	deformed control space in actual placement, solid skeleton of investigated porous body
$\partial\mathrm{B}_S$	boundary of control space
C	concentration
C^0	inlet concentration of gas
C_0^α	reference molar concentration of constituent
$\mathrm{C_v}$	heat capacity at constant volume
$\mathrm{C_p}$	heat capacity at constant pressure
$\Delta\mathrm{C_p}$	heat capacity change at constant pressure
$\mathbf{C}_\mathrm{S}$	right CAUCHY-GREEN tensors according to the solid
$\mathrm{d}v^\alpha$	partial volume element
$\mathrm{d}v$	average volume element
D	dissipation
$D^{\alpha\beta}$	Maxwell-Stefan binary diffusion coefficient
$\mathrm{D}_{Fick}^{\alpha\beta}$	Fick diffusion coefficient of substance
$\mathrm{D}_{multi}^{\beta\alpha}$	Fick diffusion coefficient of multicomponent
$[\mathrm{D}]_{Fick}$	Fick diffusion coefficients matrix of multicomponenet
$D^{\alpha\beta}$	diffusion coefficient according to Chapman-Enskog theory
$\mathbf{D}_\alpha$	symmetric part of the special velocity gradient
$\hat{\mathrm{e}}^\alpha$	energy supply
$\mathrm{E}^\ominus$	ideal potential at standard
E^α	internal energy
f_i	fugacity of constituent
$f_i^\ominus$	the fugacity of constituent i in standard state
F	Faraday's constant
F	volumetric flow rate
$\mathbf{F}_\alpha$	deformation gradient tensor of constituent
grad...	gradient operator referring to the spatial point
$\Delta\mathrm{G}$	Gibbs free energy change
$\Delta\mathrm{G}^\ominus$	Gibbs free energy change in standard state
$\Delta_\mathrm{r}\mathrm{G}$	Gibbs energy change of a reaction at constant pressure
$\Delta\mathrm{H}$	enthalpy change
$\Delta_\mathrm{r}\mathrm{H}$	enthalpy change of a reaction
$\Delta_\mathrm{r}\mathrm{H}^\ominus$	standard enthalpy change of a reaction
I	current

$\Delta \mathrm{I}$	current change
J^{α}	diffusion fluxes
$\mathbf{J}_{\mathrm{S}}$	Jacobian
K^{α}	kinetic energy
$(\mathrm{K}_a)_r$	equilibrium constant of the r-th reaction
M^{α}	mass of constituent
$\mathrm{M}^{\alpha}_{\mathrm{ol}}$	molar mass
n_i	molar amount of constituent
$n_i^{\ominus}$	amount of moles of constituent i in the initial mixture
n	amount of electrons transferred, sum of molar amount of n_i
$\mathrm{n}^{0\alpha}$	volumetric composition of input gas
$\mathrm{n}^{\alpha}_{mol}$	mole fraction of constitutent
$\mathrm{n}^{\alpha}(\mathrm{x},t)$	volume fraction of constituent
$\mathbf{n}$	normal to boundary
$\delta \mathrm{n}^{\mathrm{S}}$	weight function
N_{α}	molar flux of constituent
N	breakthrough capacity of the bottom ash
$\hat{\mathbf{p}}^{\alpha}$	interaction force of constituent
p^{GR}	pressure of gas phase
P_i	partial pressure of constituent
P	pressure of gas mixture
q^{α}	equilibrium concentration
$\mathbf{q}^{\alpha}$	heat influx vector
Q	heat flux
Q_f	the input gas flow rate
Q^{α}	molar amount of gas
r^{α}	external heat supply
r_{p}	radius of the pores
R	electric resistance
R	gas constant
$\mathrm{S}_i^{\ominus}$	standard entropy of compound
$\Delta \mathrm{S}$	entropy change
$\Delta_{\mathrm{r}}\mathrm{S}$	entropy change of a reaction
t	time
T	temperature
$\nabla \mathrm{T}$	temperature gradient
$\mathbf{T}^{\alpha}$	partial Cauchy stress tensor of constituent
u_{α}	velocity of constituent
$\Delta \mathrm{U}$	internal energy change
v^{α}	real volume
V_p	the total pore volume of solid
V_a	the apparent volume of solid

V_{cell}	voltage of a fuel cell unit
$\Delta\mathrm{V}$	voltage degradation
w	work
W	work
W^{α}	mechanical work
$\mathbf{w}_{\mathrm{G}\alpha}$	seepage velocity in connection with gas and constituent
$\mathbf{x}_{\alpha}^{''}$	acceleration field of constituent
$\mathrm{x}_{\alpha}^{'}$	velocity
$\mathrm{x}^{'}$	molar average velocity
x	position
$\mathbf{x}_{\mathrm{b}}$	boundary

Greek letters, symbols

α	1, . . ., κ individual constituent(phases)
$\delta\ldots$	weight function
ϵ	porosity of solid
ε^{α}	specific internal energy
$\varepsilon_{\alpha\beta}$	geometric average of contributions from the two constituents
$\mathrm{tr}\varepsilon$	linear strain tensor
φ^{α}	constituent
γ^{α}	activity coefficient of constitute
$\Gamma^{\alpha\beta}$	thermodynamic factor for binary system
η	power efficiency
η^{α}	specific entropy of the constituent
κ	amount of individual constituent
$\kappa_{\mathrm{SG}}^{\alpha\mathrm{S}}$	mass transfer coefficient
λ^{α}	Lagrange multiplier of constituent
$\mu_i^{\ominus}$	standard chemical potential of constituent
μ_0^{α}	reference chemical potential of constituent
ν_i	the stoichiometric coefficient
ν_r	total stoichiometric coefficient change of constituent i in r-th reaction
θ	absolute temperature

ρ^{α}	partial densities of constituent
$\rho^{\alpha\mathrm{R}}$	realistic densities of constituent
$\rho_{0\mathrm{S}}^{\mathrm{SR}}$	reference realistic densities of solid
$\hat{\rho}^{\alpha}$	the local mass supply of constituent
$\bar{\rho}^{\alpha}$	average amount adsorbed of constituent
$\rho^{*\alpha\mathrm{S}}$	adsorbed density of constituent in equilibrium
$\sigma_{\alpha\beta}$	arithmetic average of the two constituents
Ω^{α}	specified distribution of the domain
Ω_{D}	function of temperature and intermolecular potential field
ξ_r	reaction coordinate
ψ^{α}	Helmholtz free energy
Ψ^{α}	reduced chemical potential
k_{T}	thermal conductivity

k_B	Boltzmann constant

Subscripts/Superscripts

$\ldots^{\alpha}$, $\ldots_{\alpha}$	constituent of porous body
$\ldots^{i}$	chemical compound, chemical constituent
$\ldots^{\ominus}$	standard state
$\ldots^{0}$	chemical compound in initial condition
$\ldots_{0}$	value of the quantity to the reference time

1 Introduction

1.1 Overview and Problem Analysis

In recent years, human beings are alarmed in climatic change by consuming fossil fuels overly. Some states are trying to reduce the emission of greenhouse gas and cost in economic activities with utilization of nuclear energy, rather than depending on conventional energy. However, the nuclear disaster of Fukushima in Japan confirmed nuclear energy remains a double-headed creature. As consequence, renewable energy receives even more attention than before.

Germany, keeping the leading edge in the field of renewable energy, have generated power by renewable energy. By the end of 2010, the fraction of power generated by renewable energy has achieved to 17 % [1]. It is remarkable that China has been the largest investor in renewable energy, followed by Germany in 2010 [2].

In China, landfilling is the dominating method in municipal solid waste treatment in urban areas. For this reason, landfill gas is a great source of greenhouse gas in cities. In addition, there are more than 13,077 million cubic meters methane produced from biomass in China's rural areas in 2009 [3]. Such huge amount of methane might be an potential climate warming source if it emits without any monitoring or collection; on the other hand, it might be an gaseous biofuel for energy generation with some methods.

In Germany, municipal solid waste incineration is extensive after landfilling of degradable waste was banned. The bulk of total ash from incinerator is bottom ash. It is a coarse, heterogeneous mixture of slag and other material. In Europe, bottom ash can be recycled and used in the construction industry and road building [4].

Furthermore, after the landfill site is closed, landfill gas will go on emitting throughout the municipals waste degradation process. Consequently, waste landfill is a long-term process, in terms of aftercare monitoring and control of emissions. Recently, the investigation in bottom ash used for biogas and waste water purification begin to receive attention [5].

For these reasons, a new method could be researched on landfill gas utilization, as a source of renewable energy. Taking into account of landfill gas composition, it can be used as fuel for power generation. Meanwhile, bottom ash can be employed as adsorbent for removal of CO_2, in order to obtaining purified CH_4 from landfill gas. The performance of landfill gas upgrading by bottom ash can be estimated with experiment. Actually, gas adsorption with porous medium is a complex process. This process can be described by models, therefore, the adsorption processes in various conditions can be predicted by simulations further.

1.2 Scope of This Thesis

This thesis seeks to present the alternative methods on landfill gas utilization and purification by means of experiments and simulations. Section 2 reviews the municipal waste management across some developed and developing countries.

Among the treatment and disposal routines, waste landfill is more popular with advantage of low cost. However, landfill gas is composed of CO_2 and CH_4, which would contribute to global warming. Landfill gas can be collected and used for heating or power generation. Section 3 represents the utilizations of landfill gas as a fuel for energy generation.

Section 4 is concerned with the performance of fuel cells supplied with gaseous biofuel. The fundamentals of electrochemistry in fuel cells are introduced in theories. Then, the properties and performance of a Phosphoric Acid Fuel Cell (PAFC) system in a sewage plant of Cologne in Germany are analysed. In the fuel cells systems, landfill gas can be used as fuel by means of converting CH_4 into H_2. This view is illustrated by landfill gas reforming simulations.

The next part, consisting of section 5, section 6, and section 7, is concerned with landfill gas adsorption with bottom ash. Bottom ash is a kind of by-product of municipal solid waste incineration. It is a sort of potential adsorbent for landfill gas upgrading. In this thesis, the experiments on landfill gas adsorption with bottom ash are discussed in section 5.

Section 6 discusses the Maxwell-Stefan equations and Fick's law for binary and multicomponent systems. In addition, an usable method of estimation diffusion coefficients in landfill gas mixtures is introduced.

The modelling and simulation involving multiphase flow and transport through porous media are described in section 7. Mass balance and momentum balance equations are developed with constitutive relations among phases. They are most important models with capabilities to predict the performance of adsorption processes. The application of models to landfill gas adsorption are detailed in this section as well.

2 Municipal Waste Management

2.1 Waste Management

The waste is actually the material and energy source been put into an unsuitable place. In order to encourage the development of environmentally friendly economic activity and achieve the higher living standard for society and human, the concept of 'hierarchy of waste management' was promoted in European Union (EU) in 1989 [6]. Waste management, aiming to minimise the amount of waste and to minimise pollution on environment, is one of the main subjects of 'hierarchy of waste management'.

Waste management is usually implemented through some waste management strategies and subsequent directives, regulations and decisions [7] [8] [9]. Through the waste management, waste would be recovered and disposed of with harmless methods to human health and environment; the waste treatment and disposal processes could be applied with improved technologies; waste could be recycled, re-used, and utilized as an energy source.

The waste management involves the following details:

2.1.1 Waste reduction

It is an significant saving on raw material, energy use and waste disposal cost in industries. Waste production can be reduced with the development of new technologies and processes in manufacturing. On the other hand, the less production of waste may be arising from the manufacture of longer lasting products. Meanwhile, the hazard waste should be avoided in manufacture processes.

2.1.2 Recycling

Recycling is a process to recover materials, like glass, paper and so on, from waste and to produce a marketable product with them. The potential for recycling material from waste is high. However, as figure 2-1 showed, the abundance of waste should be collected and sorted in the process of recycling.

2.1.3 Composting

Composting is a method to produce a stable product by decomposing organic waste. Composting of garden and municipal solid waste is a direct way of recycling. Normally, biological would produce biogas in the process of composting. The methane-riched biogas can be used as source of energy. Figure 2-2 showed a bio-compost plant for power generation in western Germany.

2.1.4 Re-use

Rather than producing marketable product with recovered materials in recycling, re-use involves collection, cleaning and re-use the same material directly. On account of environmental and economic cost, re-use may not be the optimum method in waste management.

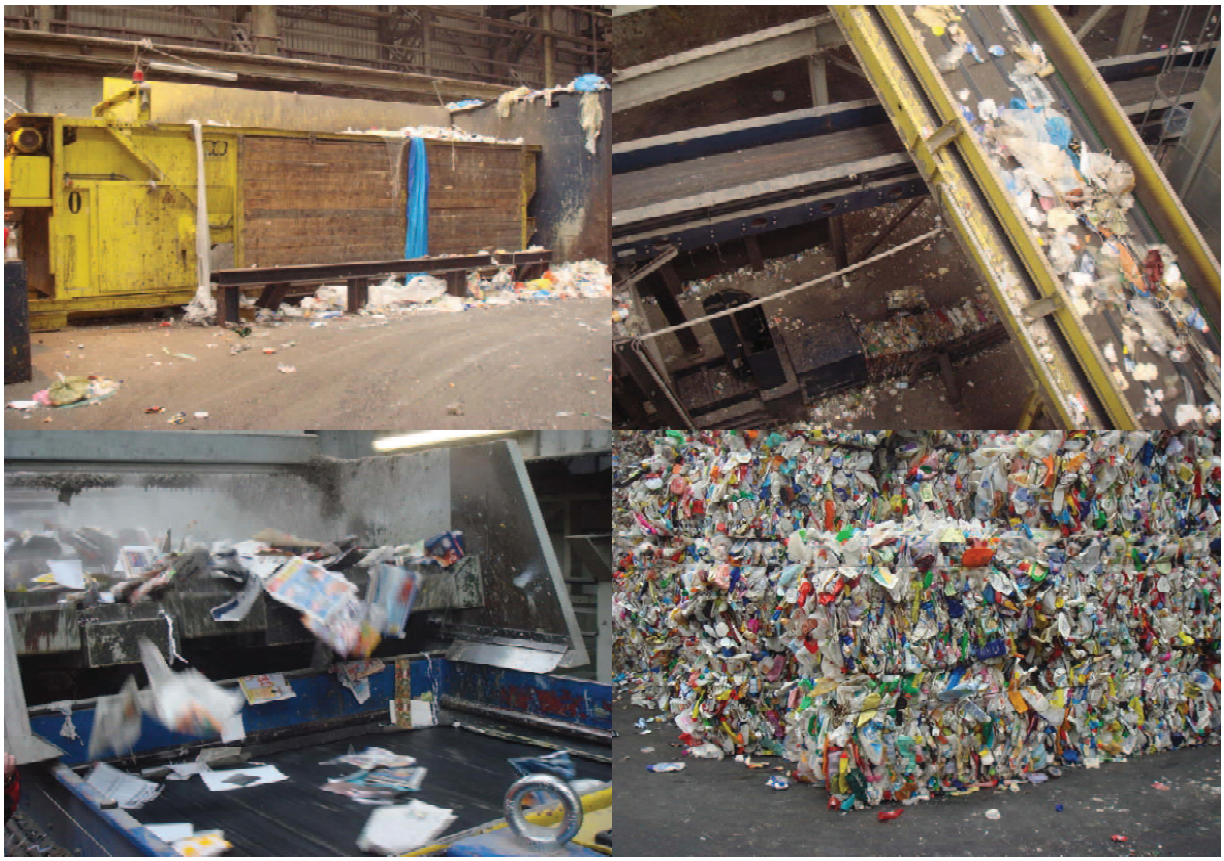

Figure 2-1: Refuse Sorting in Western Germany.

2.1.5 Energy recovery

Energy recovery mainly includes waste incineration and landfill gas utilization. Waste, such as municipal solid waste and sewage sludge, contains organic components which can be incinerated. Energy is able to be recovered by generating steam and electricity via incineration. However, among the outputs of incineration, flue gases are required to be measured and cleaned-up before emission. In addition, the fly ash is potentially hazardous to health, for the sake of containing high concentrations of heavy metals such as lead, cadmium, copper and small amounts of dioxins and furans.

Landfill gas is produced by biodegradation of organic wastes in landfill site. The produced gases, consisting of combustible methane, can be collected and flared off or used to produce heat or electricity. On account of energy costs control and greenhouse gas emissions reduction, landfill gas have caught more attention as a source for energy.

2.1.6 Landfill

In history, landfills have ever been the popular methods of waste disposal and treatment. In a landfill cite, wastes were buried and formed inert materials over a period of time. Consequently, there are many landfill sites around world nowaday. However, the greenhouse gases, CH_4 and CO_2 would be generated throughout the biodegradation period. The European Union member states, as Waste Landfill Directive enforced, begin to reduce the biodegradable waste into landfill

Figure 2-2: Biological Waste Plant for the Methanisation and Composting.

and to focus on greenhouse gas utilization.

2.2 Integrated Waste Management

Integrated waste management is the integration of waste management, centered on wastes collection and sorting. In addition, environmental impact, economic optimisation and societal acceptability would be taken into consideration in any practical system. Integrated waste management implies that for a particular region, the overall waste management system should be friendly to environmental and economical sustainability [10].

On the purpose of sustainable environment, the integrated waste management should be able to reduce the impacts on environment, involving air and water pollution, energy consumption, and so on. Meanwhile, the overall costs level of waste management should be taken into account of the acceptability to society.

In terms of the management of wastes from different sources or from different product areas, integrated waste management may be divided into different categories. On the other hand, according to different functions, the integrated waste management may be categorized into several sections as following:

2.2.1 Waste generation

Waste generation is the method to assess the waste generation and reduction.

2.2.2 Waste pretreatment at source

Before collection and transport to disposal location, waste will be handled, separated and storaged at source. This may include source separation of household waste into recyclable and non-recyclable materials. The pretreatment may involves the processes of compaction or composting of materials at source.

2.2.3 Collection and transport

Collection and transport is an important section in waste management system. In which, waste will be transferred to materials recycling facilities, waste transfer stations or landfill disposal sites via collection vehicles.

2.2.4 Processing of solid waste

Solid wastes are transported to special locations in order to sorting, recycling and processing. The recovery of separated materials, the separation and processing of waste components and transformation of wastes primarily occur in this section. This category includes waste treatment at materials recycling facilities, activities at waste transfer stations, anaerobic digestion, composting and incineration with energy recovery.

2.2.5 Transfer and transport

The transfer usually takes place at a waste transfer station, involving the transfer of wastes from the smaller collection vehicles to the larger transport equipment. The transport usually involves movement to a processing or disposal site over long distances.

It is noteworthy that transboundary movement of waste, especially of the hazardous waste, has been concerned by many countries. In the light of Basel Convention on the Control of Transboundary Movements of Hazardous Wastes, 175 parties are trying to prevent movement of hazardous waste from developed to less developed countries. The provisions of the Basel convention have been integrated into the EU waste shipment regulation [11].

2.2.6 Disposal

Usually, the final disposal is landfill, which involves burying the waste. Among the wastes, they may include the waste directly from source, the residual materials from materials recycling facilities, residue from waste incineration, composting or anaerobic digestion.

A modern landfill site, usually properly designed and well-managed, is a hygienic and relatively inexpensive method for waste disposal. It is able to contain leachate with clay or plastic lining material. The disposed waste is compacted to decrease its volume before landfilling. In addition,

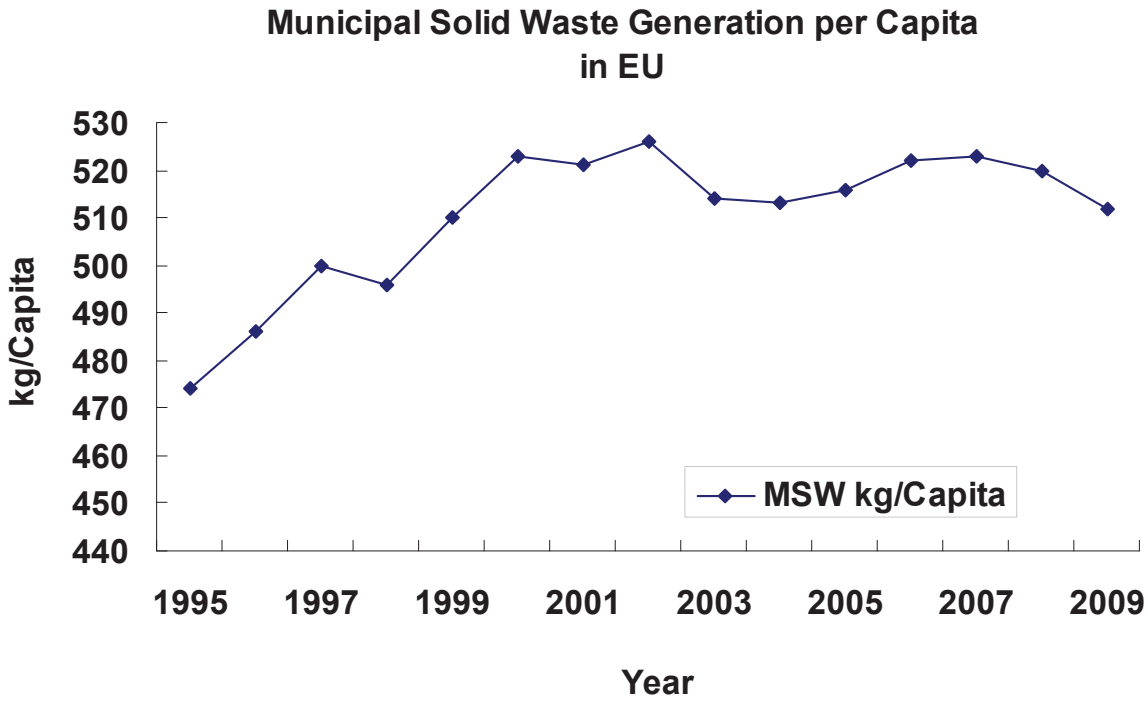

Figure 2-3: Municipal Solid Waste Generation per Capita in EU. Source: European Commission, Eurostat

landfill gas extraction systems are installed to extract the landfill gas. Therefore, landfill gas can be used to generate electricity via flaring off or burning in a gas engine.

2.3 Municipal Solid Waste(MSW)

Municipal waste consists of waste collected by or on behalf of municipal authorities and disposed of through the waste management system. The bulk of this waste stream is from households, though 'similar' wastes from sources such as commerce, offices and public institutions are included [12].

2.3.1 Municipal solid waste generation

Figure 2-3 showed that the quantity of municipal waste generated per inhabitant in the EU (27 countries) grew from 474 Kg in the year 1999 to reach 513 Kg in 2009.

Figure 2-4 showed the total amount of municipal waste of Germany and Chinese urban areas among the year of 2000 and 2009. Seen from figure, the amount of municipal waste was around 50 million tons every year in Germany [13], while China showed a steady increase in waste generation in urban areas [14].

Generally, municipal waste generation is related to a number of factors. It was ever demonstrated a possible linkage between increase in waste generation and economic growth in each countries [15]. It was believed that a rise in income would result in the higher consumption of

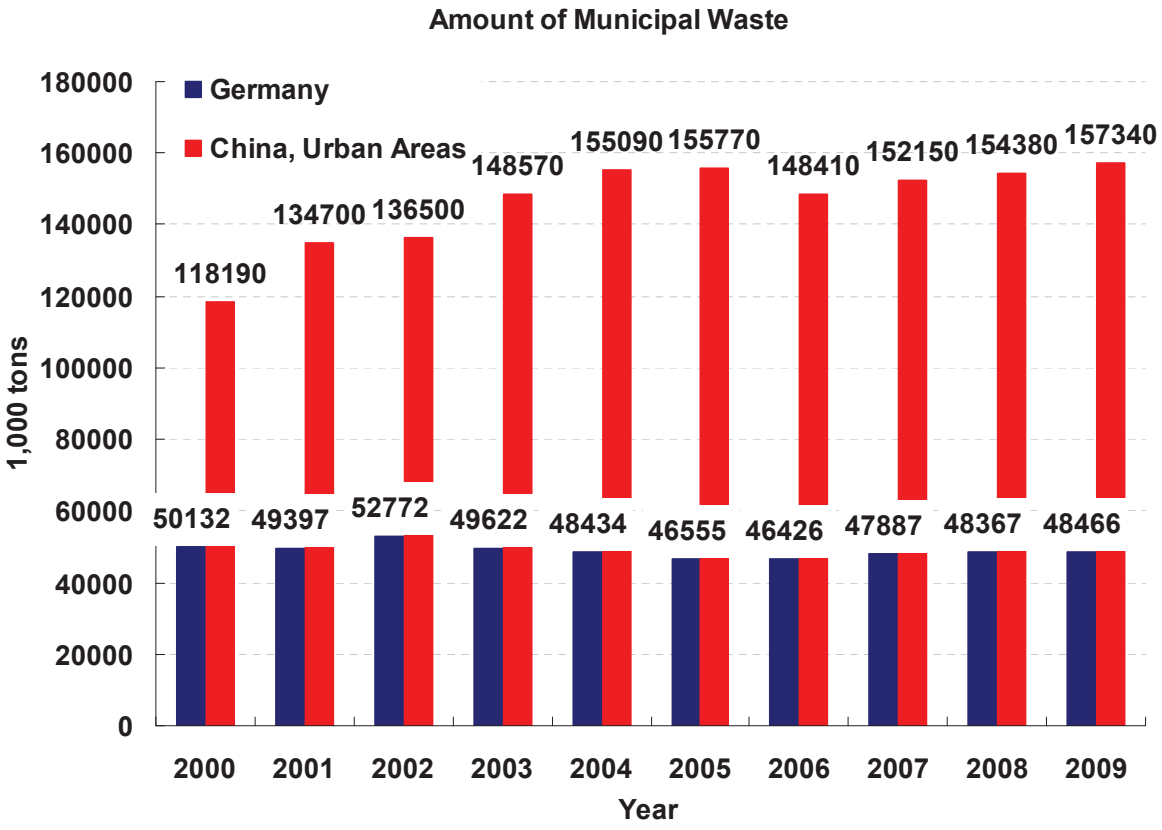

Figure 2-4: Total Amount of Municipal Waste Generation. Source: Federal Statistical Office of Germany,2011; National Bureau Statistics of China,2011.

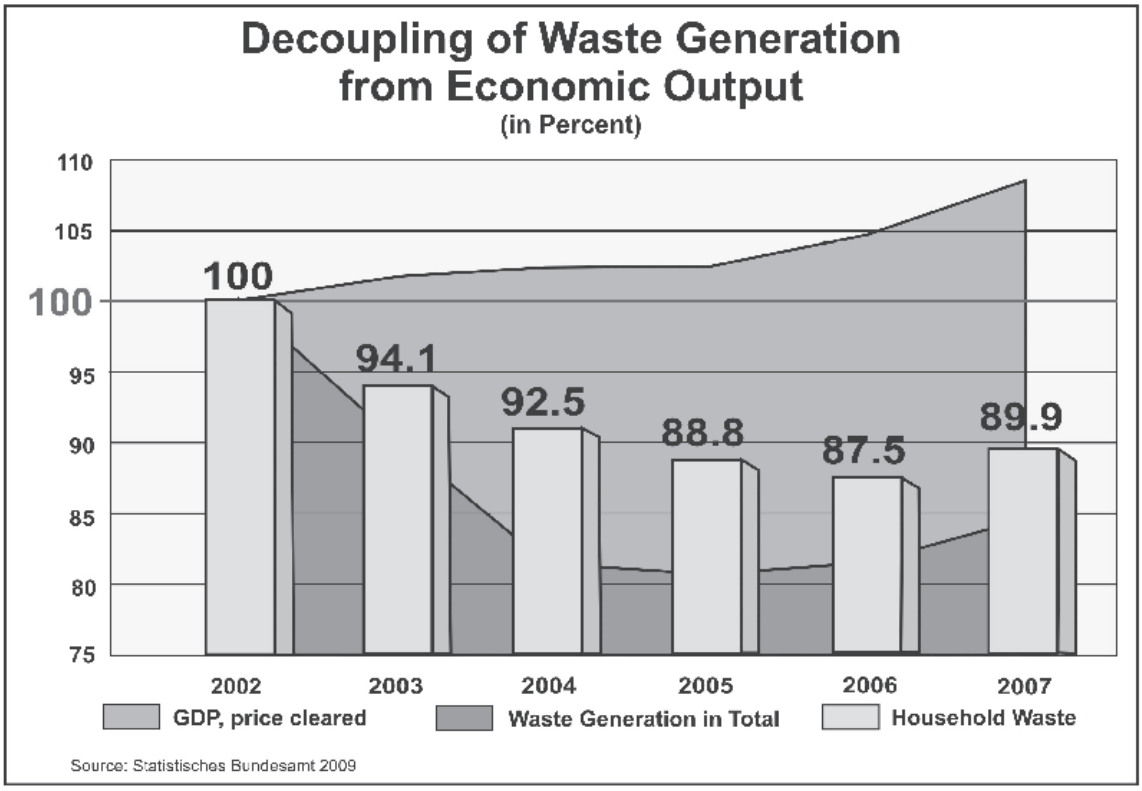

Figure 2-5: Decoupling of Generation from Economic Output.(Cited from Federal Statistical Office of Germany, 2009)

goods and increasing in packaging waste. However, as figure 2-5 [16] shown, overall between 2002 and 2007 in Germany, the waste generation is decoupled from economic output.

In Germany, waste avoidance starts in the shop. Consumers are encouraged to use baskets or shopping bags instead of plastic. Beverages are usually packaged by reusable bottles and cans. It is relatively easy to help avoid waste. In China, for the same purpose, consumers are encouraged to use shopping bags as the 'Restrictions on Manufacture, Sale and Usage of Plastic' enforced in 2008. Accordingly, the plastic bags, of which thickness are less than 0.025 mm, are not allowed to be manufactured, sold and used [17].

The increased generation of municipal waste is reflected in the growth in population. In China, as the rapid development in urbanisation, the fraction of urban population has reached 49.68 % in 2010. It is increased by 13.46 % over the ten-year period [18]. The increased population results in a rise in the amount of municipal waste generation in Chinese urban areas. The amount of municipal waste is increased from 118 million tons in 2000 to 157 million tons in 2009.

2.3.2 Municipal solid waste composition

The municipal solid waste is mainly composed of paper, cardboard, plastic, metals, glass, textiles, food from households, garden waste and other minor fraction of waste. In the aspect of waste incineration, it is an fundamental factor to be considered. Incinerator operators are concerned with calorific value of wastes, the elemental analysis, ash, moisture and combustible

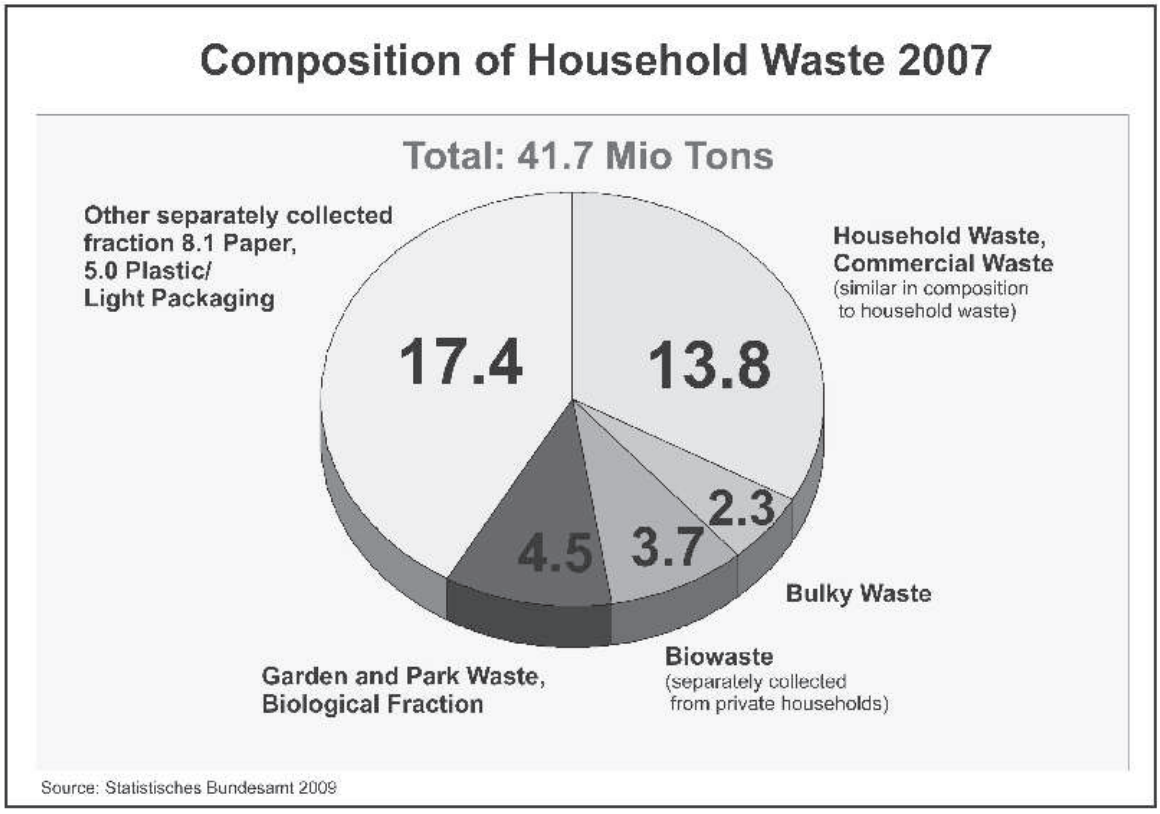

Figure 2-6: Composition of Household Waste of Germany in 2007. Cited from Federal Environment Ministry of Germany.

fraction of wastes. The design, operation and pollutant emissions of the incinerator is determined by all these factors. The composition of municipal solid waste is very dependent on the local conditions. In addition, the methods of sorting, re-use and recycling may inevitably influence the quantities and composition of wastes.

The glass, metals, paper and plastic is the substantial part of the recycling of municipal waste in most countries. As European Topic Centre on Resource and Waste Management (ETC/RWM) reported, in 2005 these fractions accounted for over 35 % among the EU member states excluding France and Spain [19].

Bio waste is also a considerable part of the recycling. It is in the form of green kitchen waste and garden waste among municipal wastes. In most countries bio waste constitutes about 25 %. In Denmark and Luxembourg, the percentage of bio waste recycling is as high as over 40 % of the total recycled municipal waste. But in some countries the recycling of it is only a minor part of the recycling, such as Ireland and Spain.

In some countries of EU, the detailed composition analyses on municipal solid waste are available. For example, the composition of household waste of Germany in 2007 is shown in figure 2-6 [20]. These data are useful for estimate of recycling and re-use strategies, particularly for incineration combustibility.

In China, it is inessential to separate the municipal solid waste at source. Among different areas within China, there are large variations in waste composition. Since the composition of waste is

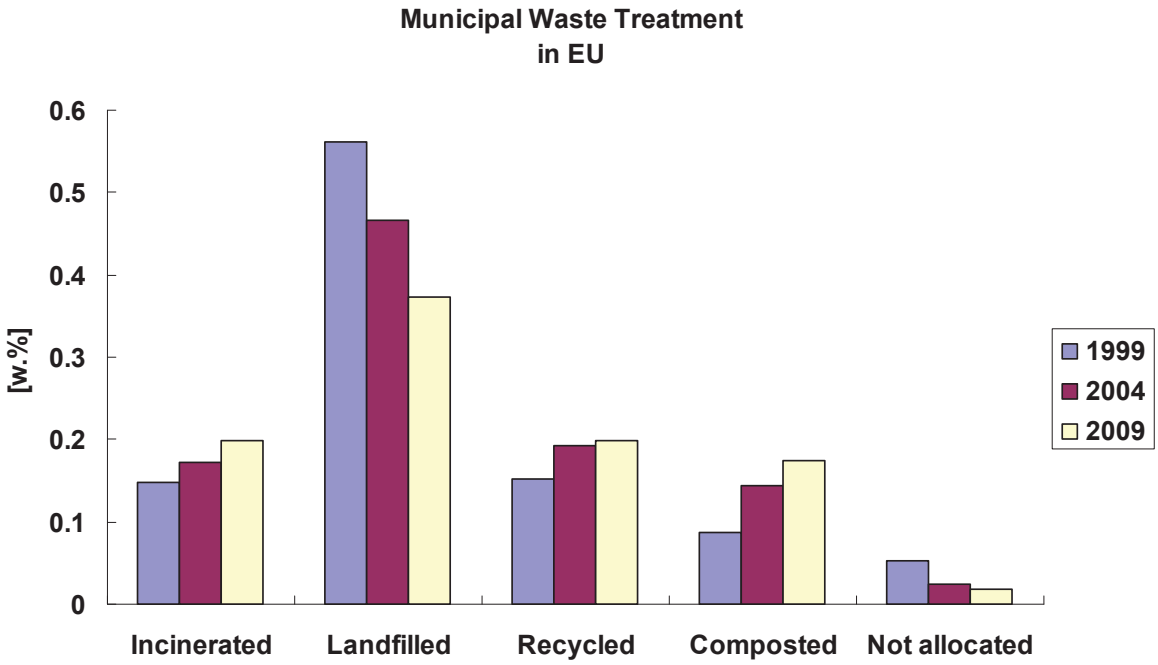

Figure 2-7: Municipal Waste Treatment in EU. Source:Eurostat.

dependent on living habits and consumption patterns heavily, the analyses of waste compositions around China become difficult.

In 2011, 'The Directive on Furthering Treatment of Municipal Solid Waste' is promoted in China [21]. In which, the separation of waste at source will be carried out in some capital cities firstly; the sorting, re-use and recycling will be applied to waste management. In the same period, the management of waste separation, processing at source is activated in 100 residential areas of Shanghai – the largest city of China.

2.4 Municipal Solid Waste Treatment and Disposal

2.4.1 MSW treatment in EU

The political emphasis on municipal waste is very high. The factors of composition, distribution among many waste generators and the links to environment impact and energy recovery, give rise to the complex character of municipal waste. Across the EU member states, the majority treatment of municipal solid waste is waste incineration either with or without energy recovery, landfill, recycling and composting.

As shown in figure 2-7, there was a significant change in the municipal waste treatment during the period of 1999 to 2009. Landfill was the most common option at the start of the period under consideration, with a 56 % share of municipal waste treatment within the EU in 1999; in 2004 the share of landfill fell below 50 %, and by 2009 it had fallen still further to 37 %. Some 15 % of municipal waste was incinerated in 1999 and this share rose to 20 % by 2009, while the share of waste that was recycled or composted rose from 24 % to 37 % at the same time.

During this period, a sustainable waste management strategy was promoted throughout the EU. The member states were encouraged to minimise the production of waste by the use of newer technologies and processes, and to re-use and recycling of waste.

In 1994, a Directive on packaging and packaging waste was promoted in EU [22]. As the results, the member states recovered a minimum of 50 % of all packaging put on the market by the year 2001. At the end of December 2008, the revised recovery target has achieved to 60 %.

In 1999, as the implementation of 'Directive Landfill', the EU member states were required to reduce the amount of biodegradable municipal waste in landfills to 75 % by 16 July 2006, to 50 % by 16 July 2009 and to 35 % by 16 July 2016.

These Directives have led to different strategies preventing the organic fraction of municipal waste from being landfilled, namely composting (including fermentation), incineration and pre-treatment such as mechanical-biological treatment (including physical stabilisation) [23].

Municipal solid waste, mainly consisting of packaging waste, glass and plastics, can be readily segregated in process of recycling. The recyclable materials might be separated at source or at a materials recycling facility. Therefore, the share of municipal solid waste recycled increased from 15 % in 1999 to 20 % in 2009 in EU.

Another increased treatment method for municipal solid waste is composting. Composting is the aerobic biological degradation of biodegradable organic waste such as garden and food waste by micro-organisms. It can be carried out by using organic waste collected from parks, household and garden waste. Composting has accounted for a share of 17-18 % in 2009.

Incineration is looked as one of several Energy-from-Waste (EfW) technologies. The heat produced by an incinerator can be used to generate steam, by which to produce electricity to drive a turbine. Although incineration does not completely replace landfilling, it significantly reduces the necessary volume for disposal. As reported, incineration is able to reduce the solid mass of the original waste by 80-85 % and the volume (already compressed somewhat in garbage trucks) by 95-96 % [24].

As can be seen from figure 2-8, waste incineration has also grown steadily in the reference period. Since 1999, the amounts of municipal waste incinerated in the EU-27 have increased from 76 Kg per capita in 1999 to 89 Kg per capita in 2004, and achieved to 102 Kg per capita in 2009.

It is noteworthy that amount of waste incineration has reached 420 Kg per inhabitant in Denmark in 2009. In the same year, the amount of waste incineration in Sweden was as high as 235 Kg per inhabitant. In Denmark and Sweden, landfilling combustible waste has been banned since 1997 and 2002 respectively. The waste has to be treated by recycling, composting or incineration. This strategy gives these two countries the highest incineration rates for municipal waste among the EU member states.

2.4.2 MSW treatment in Germany

2.4.2.1 Landfill in Germany In Germany, the landfill ban for untreated municipal waste has been entered into force since 1 June 2005. The amount of landfilled waste drops considerably. Over the last decade, the waste treatment methods have mainly replaced by recycling, mechanical-biological treatment and incineration.

Untreated waste contains various types and quantities of both harmful and biologically degrad-

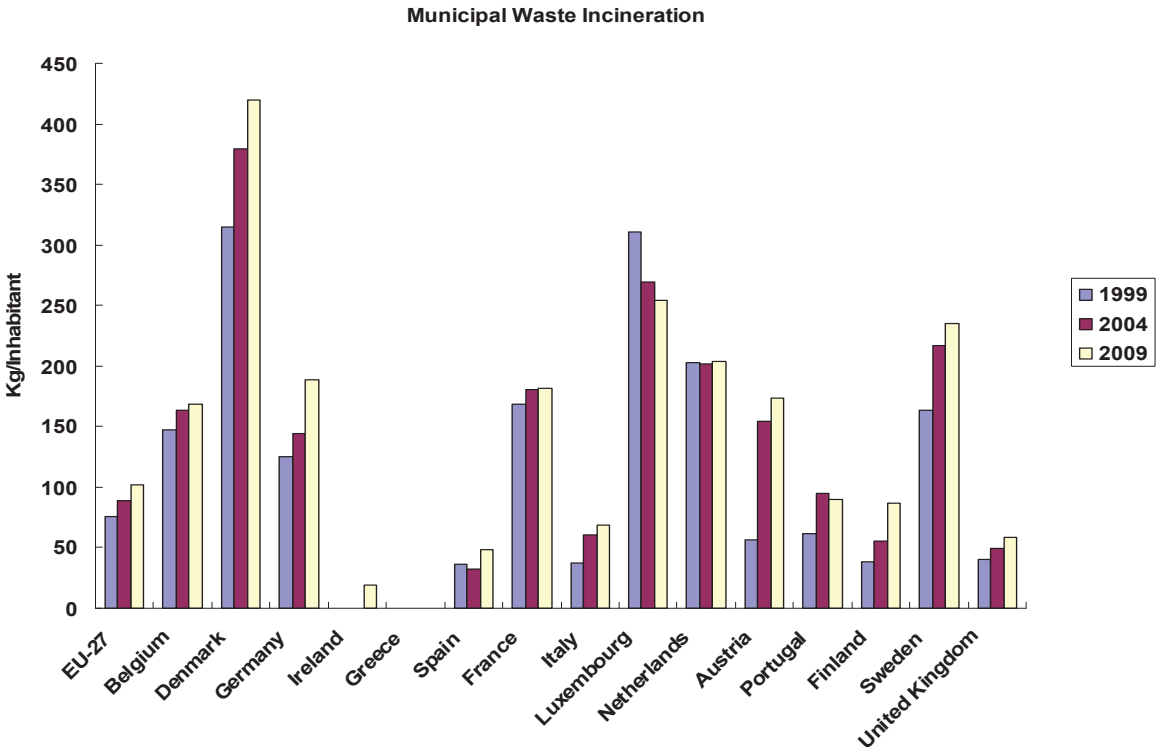

Figure 2-8: Municipal Waste Incinerations in Selected European Countries. Source:Eurostat.

able substances. In a landfill, these wastes would react biologically and chemically. Biological degradation in the landfill body would produce methane-riched landfill gas. This is a significant contributor to global warming, via escaping into the atmosphere. Meanwhile, rainwater can permeate through the landfill body, with which many organic and inorganic substances can be dissolved in landfill site. Consequently, such solution turns into potentially groundwater-polluting leachate.

Thus, conventional landfilling is a major source of the greenhouse gas – methane. To prevent adverse environmental effects, conventional landfilling would therefore require extensive post-closure monitoring and remedial work over many decades, or even centuries, in order to ensure that leachate and landfill gas remain contained. Figure 2-9 shows a post-closed landfill in western Germany.

2.4.2.2 Incineration in Germany Incineration is widespread in Germany. In 2009, the share of waste incineration has achieved to 81 % among the municipal waste disposal operators [25].

Throughout the EU, municipal solid waste incineration is controlled by both the Waste Incineration Directive (WID) and the Large Combustion Plant Directive (LCPD). Thus, the environmental impacts associated with EfW processes should be ensured that certain pollution is kept within recommended limits.

The combustion of waste is a very dusty process. In the processes of combustion, flue gases would load particulate matter. Such particulate is largely composed of ash. In addition, some more toxic pollutants such as heavy metals and dioxins and furans may form into solid particles

Figure 2-9: The Post-Closed Landfill Site in Western Germany.

or adsorbed on the surface of the particles.

The emission of dioxins and furans from waste incineration is highly concerned. In 2005, The Ministry of the Environment of Germany, where there were 66 incinerators at that time, estimated that '...whereas in 1990 one third of all dioxin emissions in Germany came from incineration plants, for the year 2000 the figure was less than 1 %. Chimneys and tiled stoves in private households alone discharge approximately 20 times more dioxin into the environment than incineration plants' [26].

Bottom ash is produced from the furnace grate in a incinerator. It is the bulk of total ash and is a heterogeneous mixture of slag, ferrous and non-ferrous metals, ceramics, glass, other non-combustible material and uncombusted organic material. Bottom ash will be cooled by water and removed from the grate. Bottom ash waste water is alkaline and contains only low levels of dissolved heavy metals, below permitted sewage discharge levels [27].

2.4.2.3 Mechanical-biological treatment in Germany Mechanical-biological treatment as well as sorting of waste are the pre-treatment processes of municipal waste treatment. In the mechanical stages of the processing, high calorific value fractions such as plastics are removed for energy recovery, and metals are separated for materials recycling. The biological treatment stages involves aerobic, anaerobic or combined processes. Anaerobic processes produce biogas which can be used for energy production.

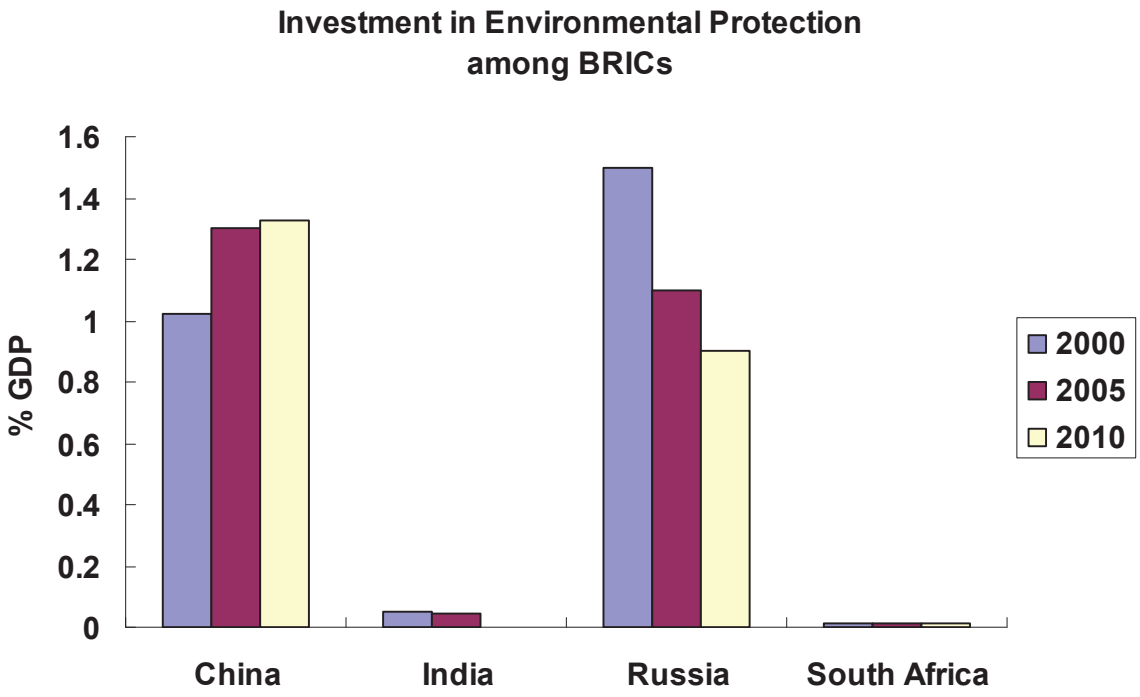

Figure 2-10: Investment in Environment among BRICs. Source:National Bureau of Statistic of China. Note:The data of India is in 2007 and 2008.

2.4.3 MSW treatment in China

2.4.3.1 Overview of MSW Management in China In 1992, China adopted the concept of 'Sustainable Development'. In the later of 1997, this concept was implemented in the 'Long-term Development Plan for Chinese Economics and Society' [28]. It can be seen from figure 2-10, China increased investment in environmental protection from 1.02 % per GDP in 2005 to 1.33 % per GDP in 2010 [29].

The treatment of municipal solid waste is one of the central issues of sustainable development. In 2009, the investment in municipal solid waste treatment throughout Chinese urban areas achieves to 8463 million Yuan (1 Yuan≈0.1 Euro, in 2009), which accounts for 27 % of investment in urban sanitation [30].

By 2009, sanitary landfill is still the major option on municipal solid waste treatment. The fraction of landfill reaches 79 %, followed by incineration at 18 %, whilst waste composting plays a minor role [31].

As figure 2-11 shown, between 2001 and 2009, the fraction of non-hazardous treatment of municipal solid waste increased steadily from 58.2 % in 2001 to 71.4 % in 2009 [32]. However, there was an unusual gap between different regions in China. In 2009, the fraction of non-hazardous treatment is 81.5 % in eastern China, while it is only 42.7 % in northeast region of China.

2.4.3.2 MSW incineration in China There are 19 commercial MSW incinerators operated daily in China. In 2003, a Swiss student of the Hochschule Rapperswil studied the status of

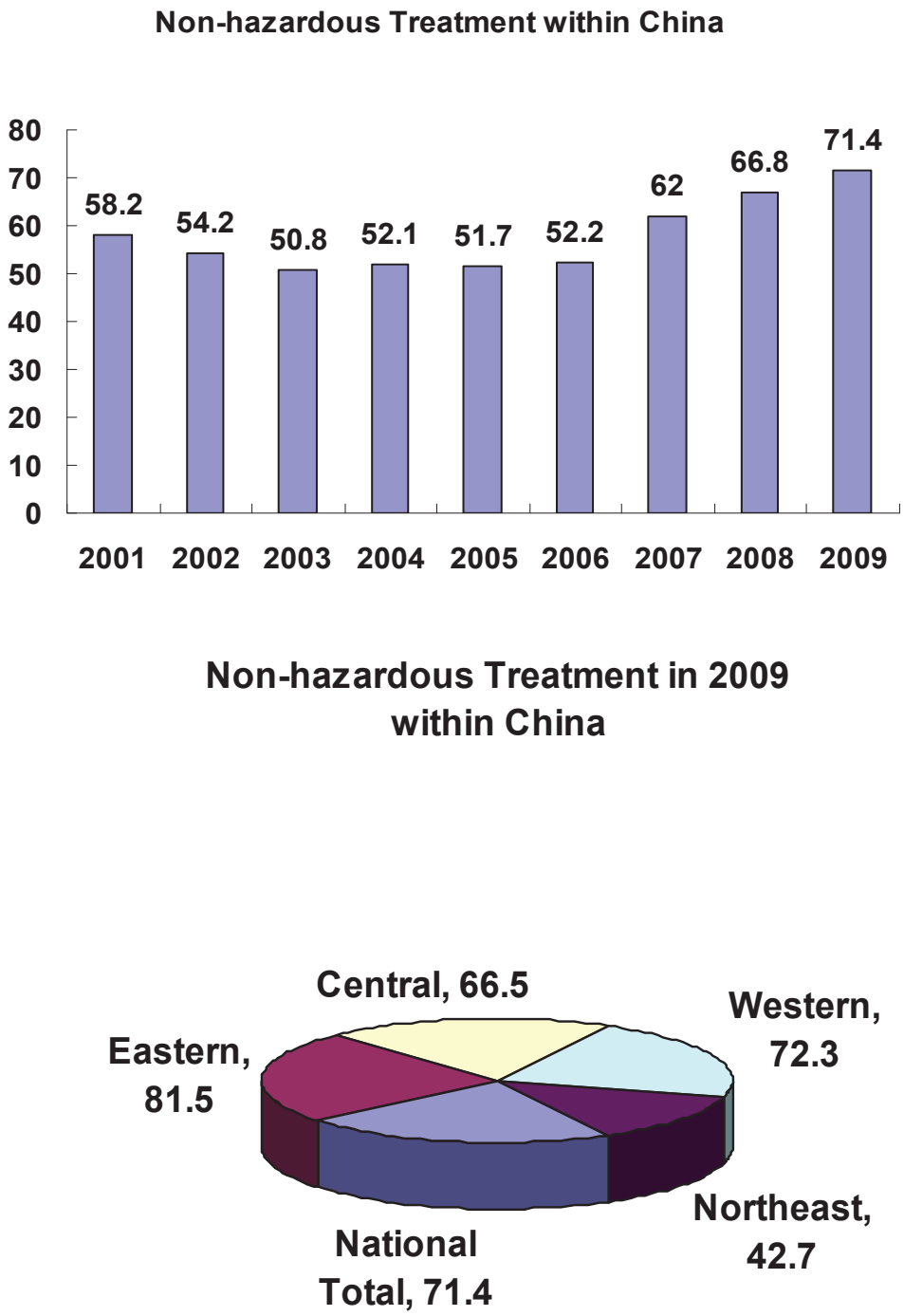

Figure 2-11: Non-hazardour Treatment in China. Source:National Bureau of Statistic of China.

waste incineration in China. According to his findings, Institute for Applied Environmental Technology compared the data of Chinese waste incinerations with those of Switzerland, and made some conclusions: the incineration of municipal waste plays a minor role in China today, as the authorities still focus mainly on incinerating hazardous waste. Because of the lower calorific value of solid waste in China, the fluided bed combustion is more popular, instead of conventional grate firing in Switzerland. In addition, there is no metal recycling from MWS incineration residues. By analyzing residues samples, they found the average metal content of the Chinese slag is lower than that of Swiss slag, 3.3 % over 12.6 % in Switzerland. However, the municipal waste incinerators in China contains higher levels of mercury than the slag from Swiss municipal waste incinerators. They thought it was possibility that not only municipal solid waste is incinerated in Chinese municipal waste incineration, but that some hazardous waste also finds its way there [33].

In 2009, a research team from Dalian of China released their investigation on 19 commercial MSW incinerators in China. The report pointed out that, the emission of PCDD/Fs from 16 MSW incinerators were lower than 1.0 ng I-TEQ Nm^{-3}. While, only 6 of the total incinerators emitted lower level of dioxin than 0.1 ng I-TEQ Nm^{-3}, that is the standard restricted by the European Union Directive [34].

2.4.3.3 Strategies of waste management in China From the later of 1990s, inhabitants were encouraged to separate household wastes at source in some large cities. However, this proposal was performed poorly.

In the early of 21st Century, the advanced managements and technologies on waste treatment were introduced into China. Meanwhile, some Directives on waste management were promoted. According to these Directives, manufacturers were required to produce less waste in industry; inhabitants in urban areas were encouraged to sort household wastes and reduce package wastes [35]; inhabitants in rural areas were encouraged to use renewable methane as energy.

China is actively addressing the problems of environmental pollution, climate change, and energy crisis currently. As the essential aspect of waste to energy, municipal waste management has been the main attraction toward renewable energy in China.

3 Landfill Gas Utilization

3.1 Landfill Gas

Landfill gas is generated through the anaerobic decomposition of organic waste present in municipal solid waste. Generation starts shortly after a landfill begins receiving waste. The average composition of landfill gas is about 50 % CH_4, 45 % CO_2, and 5 % N_2 and other gases. In addition, there are traces amount of nonmethane organic compounds.

The landfill gas production depends on varies of conditions, such as composition of the waste, the moisture of surroundings, the amount of O_2, the temperature, and so on. Among the landfill gases, CH_4 production only occurs when enough O_2 has been absorbed in site. The significate landfill gas production usually occurs about a year after deposit and thereafter gradually declines. Generally, this period will last about 20 years or even more. Landfill design and operation contributes to the decomposition process. The behaviour of landfill gas has already been studied in details [36].

3.2 Landfill Gas Utilization

3.2.1 Overview of landfill gas utilization

In 1994, the US Environmental Protection Agency (EPA) created the Landfill Methane Outreach Program (LMOP) with the goal of reducing landfill greenhouse gas emission by promoting the development of landfill-gas-to-energy projects. In these projects the landfill gas is used as a direct fuel in industrial processes or as the fuel that runs electricity-generating equipment. Since 1996, as enactment of the 'New Source Performance Standard and Emission Guidelines for Municipal Solid Waste Landfills', the LMOP has become a tool to help landfills meet the new regulations. As a result of all these efforts, CH_4 emission from landfill has decreased each passing year in US.

In 2004, The Methane to Markets (M2M) Partnership was launched in Washington, D.C., in US. The M2M program is an international initiative that advances cost-effective, near-term CH_4 recovery and use as a clean energy source. The goal of the Partnership is to reduce global CH_4 emission in order to enhance economic growth, strengthen energy security, improve air quality, improve industrial safety, and reduce emission of greenhouse gases. The Partnership acts as a mechanism to bring together interested parties from governments and the private sector to facilitate CH_4 project development and implementation around the world. The Partnership currently focuses on four sources of CH_4 emission: Agriculture, Coal mines, Landfills, Oil and gas systems.

In 2006, Germany became an official Partner Country to the M2M Partnership. Based on data in EPA's Global Anthropogenic Emission of 'Non-CO_2 Greenhouse Gases' reported, in 2005, Germany's estimated anthropogenic CH_4 emission ranked 20th in the world. Approximately 65 % of its anthropogenic CH_4 emission came from agriculture, coal mines, landfills, and natural gas and oil systems, in which CH_4 emission by landfill source was 13 %.

3.2.2 Utilization of landfill gas

Landfill gas can be captured, converted, and used as an energy source, instead of escaping into the air directly. Gas is collected by a system of wells and pipes installed throughout the landfill. The costs of a collection system depend on some different site factors, as landfill depth, amount of wells required. Utilization of landfill gas helps to prevent CH_4 from migrating into the atmosphere and resulting in local smog and global climate change. There are several practices for using landfill gas:

3.2.2.1 Alternative fuels Landfill gas can be used to offset the using of natural gas, coal, and so on, by producing alternative fuels. It has been successfully delivered to the natural gas pipeline system. CH_4 conversion to methanol CH_3OH has been investigated in US since the early 1980 [37]. As the demand of alternative vehicle fuel and the need to reduce the cost of H_2 from renewable sources [38], the renewable H_2 [39] and CH_3OH [40] production potential from landfill gas was estimated in US recently.

3.2.2.2 Direct use In many cases, landfill gas may be used in a boiler to displace natural gas or other fossil fuel. When an utility power plant or an industrial user is located within several miles of a landfill, it may be feasible to pipe landfill gas to their boilers. Landfill gas also can be used to evaporate leachate [41].

3.2.2.3 Electricity generation Traditionally, landfill gas flaring process is used to reduce odours, safety concerns, and CH_4 emission by burning, in order to comply with the standard. An alternative to flaring is to generate electricity by using landfill gas, instead of just burning. In addition to having the same benefits of flaring, landfill gas to electricity generation could indirectly reduce air pollution from fossil fuel combustion.

Reciprocating Internal Combustion Engine (ICE) The reciprocating internal combustion engine represents the most employed technology for electric energy generation from landfill gas. The reason is mainly due to the compatibility of the power with the economic feasibility of the system. Moreover, ICEs are a consolidated technology, and the related economic risks are very low compared to the other technologies. Another attractive characteristics is that ICEs are compact and easy to transport, and thus, they can be moved from one well to another in case of landfill gas shortage in one well.

But, the main disadvantage is the high air pollution generation. Compared to the other technologies, the amounts of NO_x and CO are very high.

Gas Turbines (GT) Gas turbines represent the second most used technology for landfill gas energy conversion; even though the amount of installations is significantly lower than that of the reciprocating internal combustion engines. GT combusts landfill gas to heat compressed air, making it expand to power a turbine, which in turn drives a generator. The obvious advantage of gas turbines is the dramatically reduced emission respect to ICE.

Gas turbines are not considered as a realistic option for power generation from landfill gas, due to their lower thermal efficiency compared to the ICE [42], the high pressure requirement of

compressing the gas, the damage to turbine blades from siloxanes or corrosion [43].

Steam Turbines (ST) In steam turbines, landfill gas is used to heat up water and produce steam that spins the generator. Unlike ICE and GT, which have lifetimes of over 25 year, ST has a lifetime of up to 50 years [44].

Microturbines Microturbines are new, innovative technologies to generate power [45]. This kind of systems have many advantages over larger-scale, generation facilities, such as shorter lead times from planning to construction, lower air emission. Another advantage is durability and reliability: they perform for about 40,000 hours and require little maintenance. In general, microturbine project costs have been more expensive on a dollar per KW installed capacity basis than internal combustion engine projects [46]. They accept most commercial fuels, such as gasoline, natural gas well as renewable fuels such as biodiesel and biogas. Microturbine systems are recently applied at landfills of US [47].

Stirling-Cycle engines (SCE) In the Stirling engine, gas is contained in a continuous, closed volume that is divided into hot and cold regions. The size of the volume is periodically varied to compress and expand the gas. Heating and cooling are accomplished by periodically transferring working gas between the hot and cold regions. Since the engine derives its heat from an external source, almost any type of fuel (e.g. landfill gas) or combustible material can be used. Up to now, SCE technology is still under development.

Organic Rankine Cycle (ORC) The Organic Rankine Cycle engine is a process that uses an organic fluid in a closed cycle to convert thermal energy into mechanical energy. It may represent a technically feasible alternative for using landfill gas as heat source [47].

Fuel Cells Fuel cells are electrochemical devices that convert chemical energy in fuels into electrical energy directly, promising power generation with high efficiency and low environmental impact. In addition, as combustion is avoided, fuel cells produce power with minor pollutant [48].

There is a fuel processor in fuel cells system, in which CH_4 in the landfill gas stream will be converted into H_2 and CO_2 in an endothermic reaction over a catalyst bed. The specific contaminants in the landfill gas of concern to the fuel cell are sulphur and halides. Both of these ingredients can poison and therefore reduce the life of the fuel cell power plant's fuel processor [49]. Thus, landfill gas pre-treatment is an important issue for fuel cells. There are several types of fuel cells are discussed on landfill gas utilization.

- **Phosphoric Acid Fuel Cell (PAFC)**

  Phosphoric acid is used as the electrolyte in this fuel cell. At lower temperatures, phosphoric acid is a poor ionic conductor, and CO poisoning of the platin electro-catalyst in the anode becomes severe. The relative stability of concentrated phosphoric acid is high compared to other common acids; consequently the PAFC is capable of operating at the high temperature range from 100 to 220 °C.

The demonstration test successfully demonstrated operation of the energy recovery system, including the gas pre-treatment unit and the commercial PAFC modified for operation on landfill gas in US [49].

- **Molten Carbonate Fuel Cell (MCFC)**

  The electrolyte in this fuel cell is usually a combination of alkali carbonates. The MCFC operates at 600 to 700 °C, where the alkali carbonates form a highly conductive molten salt, with carbonate ions providing ionic conduction. In the MCFC, CO is a directly useable fuel. At the high operating temperatures in MCFC, nickel (anode) and nickel oxide (cathode) are adequate to promote reaction. Noble metals are not required for operation, and many common hydrocarbon fuels can be reformed internally.

  A life-cycle-assessment of landfill gas-MCFC system was conducted [50], the results showed that the MCFC-landfill gas system allows to us obtain a relevant reduction in global warming gases and NO_x reduction.

- **Solid Oxide Fuel Cell (SOFC)**

  The electrolyte in this fuel cell is a solid, nonporous metal oxide. The cell operates at 600-1000°C, where oxygen ions conducts ionic. CO is able to be used as fuel in SOFC directly. In the range of operation temperature, natural gas can be reformed in SOFC. There are only a few experiments of SOFC operation on landfill gas reported in the open literature [51].

Environmental impact of electricity generation Landfill gas electricity generators produce nitrogen oxides emission that vary widely from one site to another, depending on the type of generator and the extent to which steps have been taken to minimize emission.

Combustion of landfill gas can also result in the release of organic compounds and trace amounts of toxic materials, including mercury and dioxins, although such releases are at levels lower than if the landfill gas is flared. Fuel cells, on the contrary, are the cleanest energy system among electricity generating technologies.

There is few water impacts associated with landfill gas power plants. Unlike other power plants that rely upon water for cooling, landfill gas power plants are usually very small, and therefore pollution discharges into local lakes or streams are typically quite small.

4 Utilization of Landfill Gas for Fuel Cells

This section provides the fuel cell technologies and biogas/landfill gas utilization for fuel cell. First it discusses the basic fuel cell components. Then, the theory of fuel cell performance, the analyses on Phosphoric Acid Fuel Cells (PAFCs) are introduced. Finally, in order to utilize landfill gas as fuel for fuel cells, the simulation of landfill gas reforming is discussed.

4.1 Fuel Cell Components

As known to all, fuel cells are kinds of devices that are able to convert chemical energy in fuel into electrical energy directly. A wide variety of fuels and oxidants are possible in fuel cells. Of most interest today are those fuel cells that use hydrogen as a reductant, and ambient air as the oxidant. Other fuels include hydrocarbons and alcohols; with chlorine or chlorine dioxide used as oxidants [52].

Fuel cells consist of power system and cooling system usually. In the power system, fuel gases and air are converted into electricity and heat. Meanwhile, cooling system excesses unused heat from the power system to atmosphere. A fuel cell power system comprises a number of components, such as unit cells, cell stack assembly, and some other ancillary subsystems. The details will be discussed as followings:

4.1.1 Unit cells

The core of a fuel cell is unit cells. In which, the chemical energy contained in a fuel is converted into electrical energy by electrochemical reactions. A unit cell is composed of an anode and a cathode, in contact with which is an electrolyte, also named ion conductor [53]. According to the choice of electrolyte and fuel, the type of fuel cells are categorized. This section mainly focuses on the common physical structure and chemical characters of fuel cells.

As shown in figure 4-1, fuel, usually hydrogen, is fed into the anode, at which fuel turns into positive ions and electrons. On the other hand, the oxidant, usually oxygen, is fed into the cathode. The ions are transferred through electrolyte, so that the electrochemical reactions can take place at the electrodes. At the same time, electric currents are drived to perform works on load. In this way, fuel cells produce power as long as fuels are supplied continuously.

4.1.2 Cell stack assembly

Cell stack assembly is the major component in fuel cell power system. It is combined by unit cells in series and parallel circuits to achieve the voltage and power output requirements.

In practice, cell stack assembly cannot work independently. A fuel cell must contain power system and cooling system. The freeze prevention heaters are necessary, for the purpose of preventing the cell stack electrolyte from freezing when the power system is shut down and the thermal management system is disabled. In the case of an electrical short, a ground fault detector is able to provide a safety shutdown function. In order to evaluate the cell stack performance, a voltage monitor is also required [54]. All of these instruments are able to constitute the basic power section.

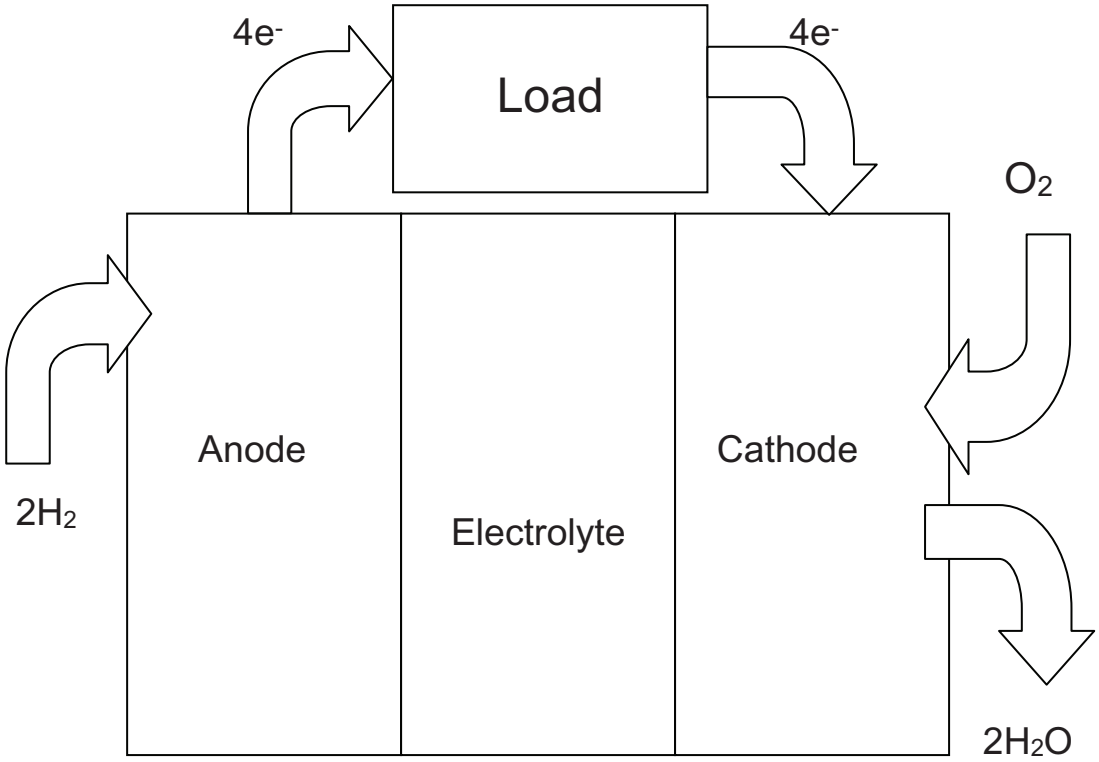

Figure 4-1: A Unit Cell's Working Sketch.

4.1.3 Processing systems

As figure 4-2 shows, a fuel cell is a combination of series of systems. In this section, a UTC fuel cell power plant is taken as an example to illustrate the working processes.

Practically, O_2 is supplied from air for unit cells. Before entering, air is dealt with by an air processing system. Some parts of O_2 are filtered and transferred into cathode, taking part in reactions directly. Some parts are used to ignite reformer burner. At the same time, a part of air is supplied into reformer as the flame sensor cooling air. The air processing system also supplies air to water storage tank, in which CO_2 is removed by dissolving in H_2O properly.

In the fuel processing system, fuel is produced in a steam reformer. In gas reforming processes, not only hydrogen but also natural gas or biogas are able to be used as fuel for fuel cells. A complete fuel process system can recycle remained fuel from cell stack assembly, and flow it to reformer burner to provide thermal energy for reforming process [54].

In a fuel cell, electrochemical reactions would produce water and heat. To keep the proper performance of fuel cells, these by-products must be removed simultaneously. Therefore, water treatment system and thermal management system are necessary in a fuel cell system. A thermal management system takes charge of keeping proper temperature for cell stacks' operation. The heat, produced from reactions, is removed from cell stacks by the cooperation of thermal system and cooling water of water treatment system. When the heat flows through deionized water, the mixture of steam and water is generated. In the thermal loop, the steam is transferred into reformer by a pump. On the other hand, the reformed fuel would exchange heat in the thermal management system before getting into the anode. In a fuel cell, the water treatment loop treats all of water, involving the water in storage tank, the deionized water, and some blowdown water.

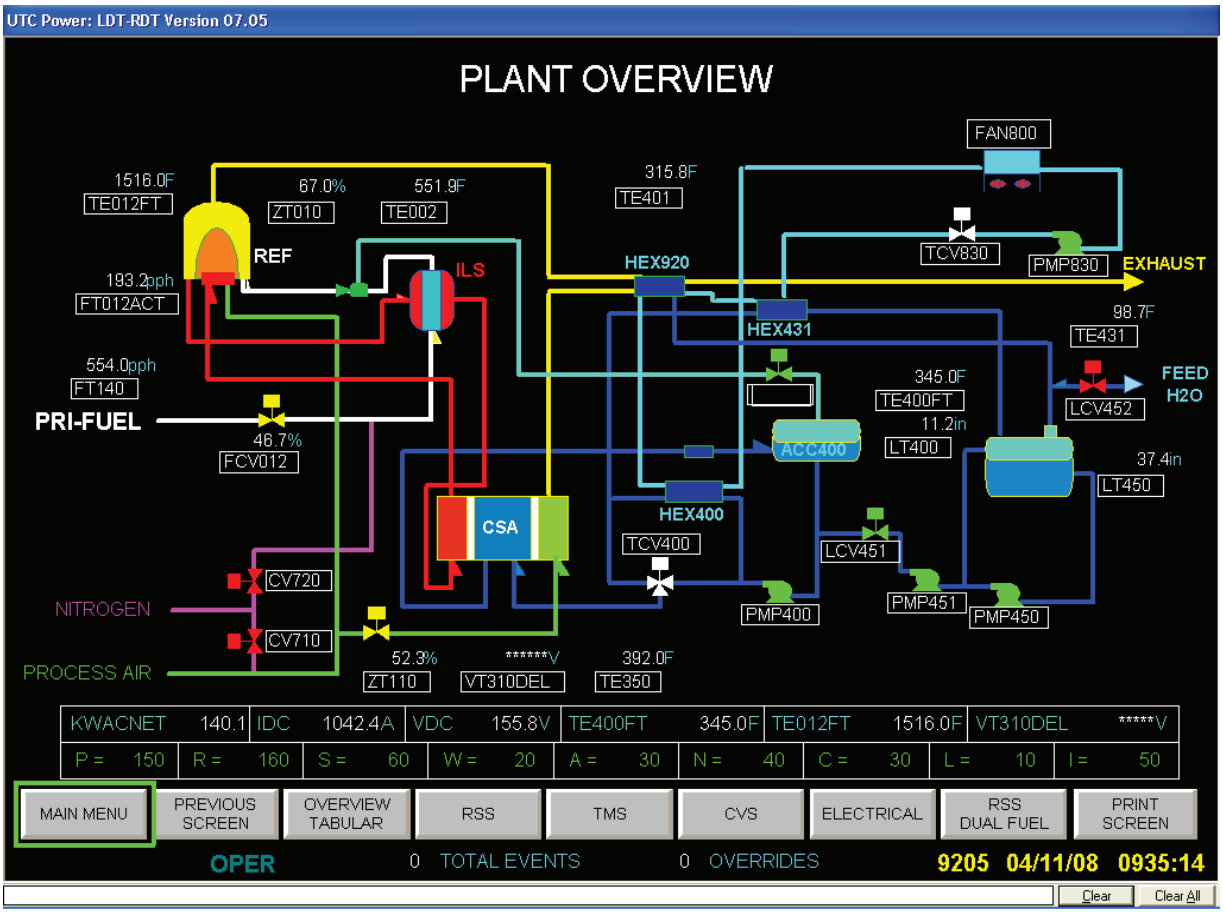

Figure 4-2: Processing of a Fuel Cell.

After closing down or before starting up, fuel cells must be purged with nitrogen, which is supplied by the nitrogen purge system. Generally, in order to prevent the formation of a combustible gas mixture in fuel cells and to exchange heat with atmosphere, a ventilation system must be installed in a fuel cell system as well.

The study on fuel cells is highly attracted nowadays. One of a significant advantage of fuel cells is lower emissions to environment. In addition, fuel cells have possible potential for consuming biogas or landfill gas as fuel. So that, biogas or landfill gas are able to generate renewable energy via fuel cells.

4.2 Fuel Cell Performance

The basic function of fuel cells is to convert chemical energy of fuels into electrical energy and heat. This process is performed via series of electrochemical reactions. Its energy balance is able to be described by thermodynamics. In this section, an ideal performence of a fuel cell will be discussed. As the example, the performance of a PAFCs system is analyzed later.

4.2.1 The Nernst equation

In electrochemistry, an fuel cell's ideal potential equilibrium can be determined by Nernst equation [53]:

$$\mathrm{E} = \mathrm{E}^{\ominus} - \frac{\mathrm{RT}}{nF} \ln \frac{\prod [Product\ fugacity]}{\prod [Reactant\ fugacity]} \tag{4.1}$$

where, n is the amount of electrons transferred, F is Faraday's constant (96.485×10^3 C mol^{-1}), R is the gas constant (8.314 J K^{-1} mol^{-1}), and $\mathrm{E}^{\ominus}$ is the ideal potential of the unit cell at standard pressure and temperature T.

4.2.2 Thermodynamics of a fuel cell

For a fuel cell, the work is obtained from the transport of electrons across a potential difference. Generally, electrical work [53] is described as:

$$\mathrm{W} = -nF\mathrm{E} \tag{4.2}$$

Therefore, in an isobaric process, the total thermal energy attainable from a fuel cell is calculated by:

$$\Delta\mathrm{H} = \mathrm{Q} - nF\mathrm{E} \tag{4.3}$$

in which, ΔH is the enthalpy change.

Assumed the perfect electrochemical reactions take place in a fuel cell, that is the current and all changes following the current are reversible, the amount of heat produced by a fuel cell operation is:

$$\mathrm{Q} = \mathrm{T}\Delta\mathrm{S} \tag{4.4}$$

where, ΔS is the entropy change.

At the constant temperature, the Gibbs free energy change ΔG is given as [53]:

$$\Delta \mathrm{G} = \Delta \mathrm{H} - \mathrm{T}\Delta \mathrm{S} \tag{4.5}$$

As shown above, the total electrical work of a fuel cell is also able to be evaluated by ΔG of electrochemical reactions. So that, at constant pressure and temperature, the relation between chemical energy and electrical energy is expressed as [53]:

$$\Delta \mathrm{G} = -nF\mathrm{E} \tag{4.6}$$

meanwhile,

$$\Delta \mathrm{G} = \Delta \mathrm{G}^{\ominus} - \mathrm{RT} \ln \frac{\prod [Product\ fugacity]}{\prod [Reactant\ fugacity]} \tag{4.7}$$

$\Delta \mathrm{G}^{\ominus}$ is the Gibbs free energy change of reactions on a unit cell at standard state.

4.2.3 PAFC analyses

The PAFCs system is the first commercial fuel cell system in world. In this section, a PAFCs power plant in Cologne of Germany will be studied. As shown in figure 4-3, this PAFCs system had runned more than 50,000 hours by utilizing sewage gas by the end of 2009. From then on, it was shut down completely.

PAFC takes phosphoric acid as an electrolyte. In addition to the fuel cell units, a PAFCs system installs an steam reformer inside. When sewage gas passing through, the hydrogen rich gas is produced. So that, the electrochemical reactions occur in PAFC. At the anode, a reaction is

$$2\mathrm{H}_2 \longrightarrow 4\mathrm{H}^+ + 4\mathrm{e}^-, \tag{4.8}$$

and at the cathode, the reaction is

$$\mathrm{O}_2 + 4\mathrm{H}^+ + 4\mathrm{e}^- \longrightarrow 2\mathrm{H}_2\mathrm{O}. \tag{4.9}$$

According to the total reaction at a fuel cell unit,

$$2\mathrm{H}_2 + \mathrm{O}_2 \longrightarrow 2\mathrm{H}_2\mathrm{O} \tag{4.10}$$

the Nernst equation of a PAFC unit becomes into the form of:

$$\mathrm{E} = \mathrm{E}^{\ominus} - \frac{\mathrm{RT}}{4F} \ln \frac{\mathrm{C}^2_{\mathrm{H_2O}}}{\mathrm{C}^2_{\mathrm{H_2}} \mathrm{C}_{\mathrm{O_2}}} \tag{4.11}$$

where C is the concentration of reactants. PAFC works at 150 °C-220 °C [55], normally. According to the Nernst equation, its ideal voltage would be 1.14V at 205 °C for a unit cell. The performance of PAFC is usually effected by the following factors:

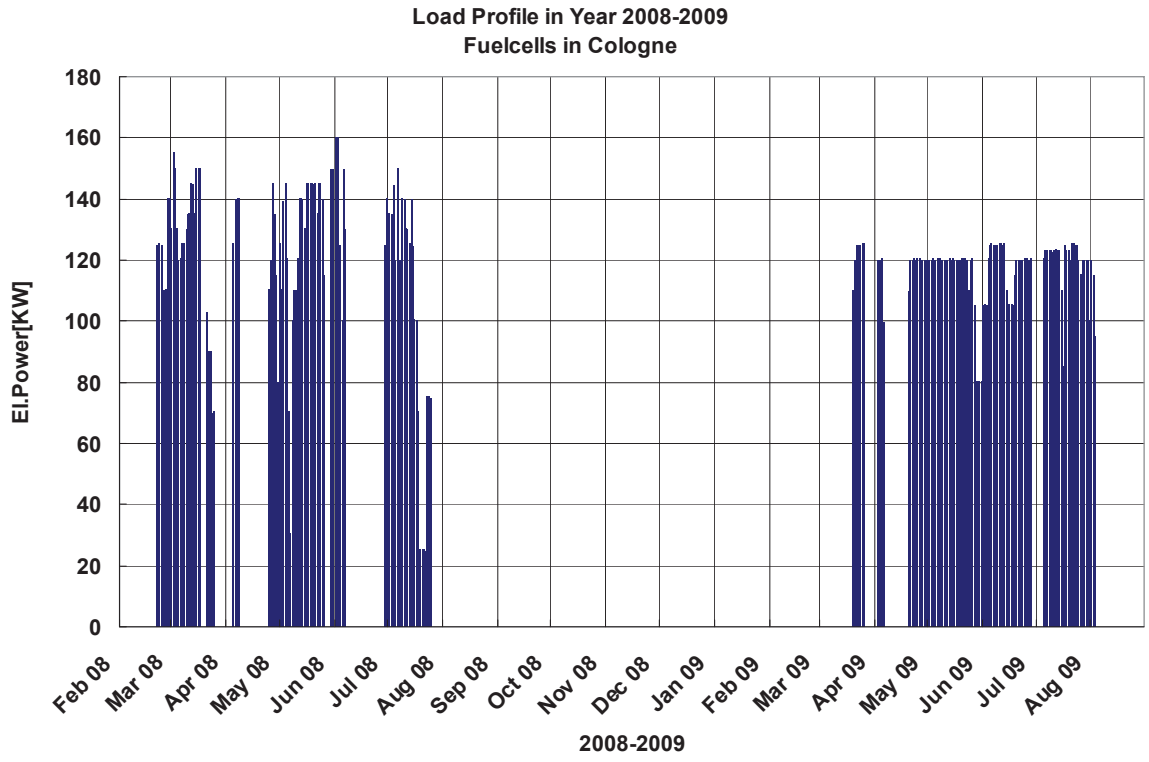

Figure 4-3: Load Profile of PAFCs.(Data source: PAFC power plant in Cologne, offered by TBE.)

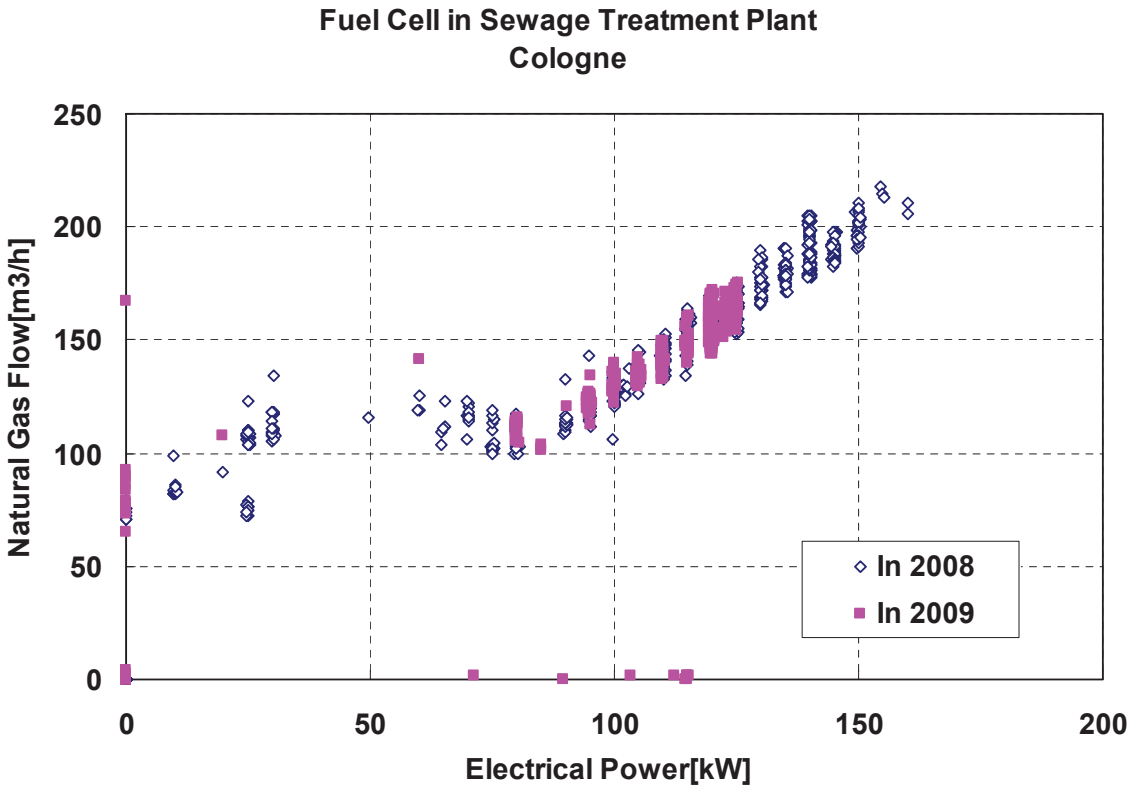

Figure 4-4: Sewage Gas Flow Related to Electrical Power.(Data source: PAFC power plant in Cologne.)

4.2.3.1 Gas flow rate In our case, sewage gas includes 40 % CO_2 and 60 % CH_4 in volume. The composition is similar to those of natural gas. H_2 is produced by biogas-steam reforming in a reformer of PAFC. Assuming the composition of sewage gas is constant, the power of a PAFC would increase as the increasing of sewage gas flow.

The reason is that, keeping the productivity of H_2 as a constance, voltage would increase as increasing fuel gases's concentration. Assumed all the H_2 is consumed in PAFC completely, the power efficiency of a fuel cell unit is related to voltage as following equation

$$\eta = 0.675\mathrm{V}_{cell} \tag{4.12}$$

in theories [53]. As to a PAFC cell unit in practice, it is reported the electrical efficiency is around 37 %-42 % [55]. Therefore, the function of sewage gas flow and electrical power is shown in figure 4-4.

In this figure, the relation of gas flow and power in 2008 is compared with that in 2009. Although the catalyst activity in PAFC, direct current and some operation conditions would impact electrical power, the difference of power beteen year of 2008 and 2009 is too small to be negelected.

4.2.3.2 Gas load time As the load time increasing, the activity of electrolyte and catalyst decreases. So, a fuel cell unit's performance can be estimated by the function of a cell's voltage and gas load time. In the early studies [56] [57] [58], the expected cell life is about 40,000 hours for a PAFCs system. The maximum voltage degradation with time [56] is expressed as

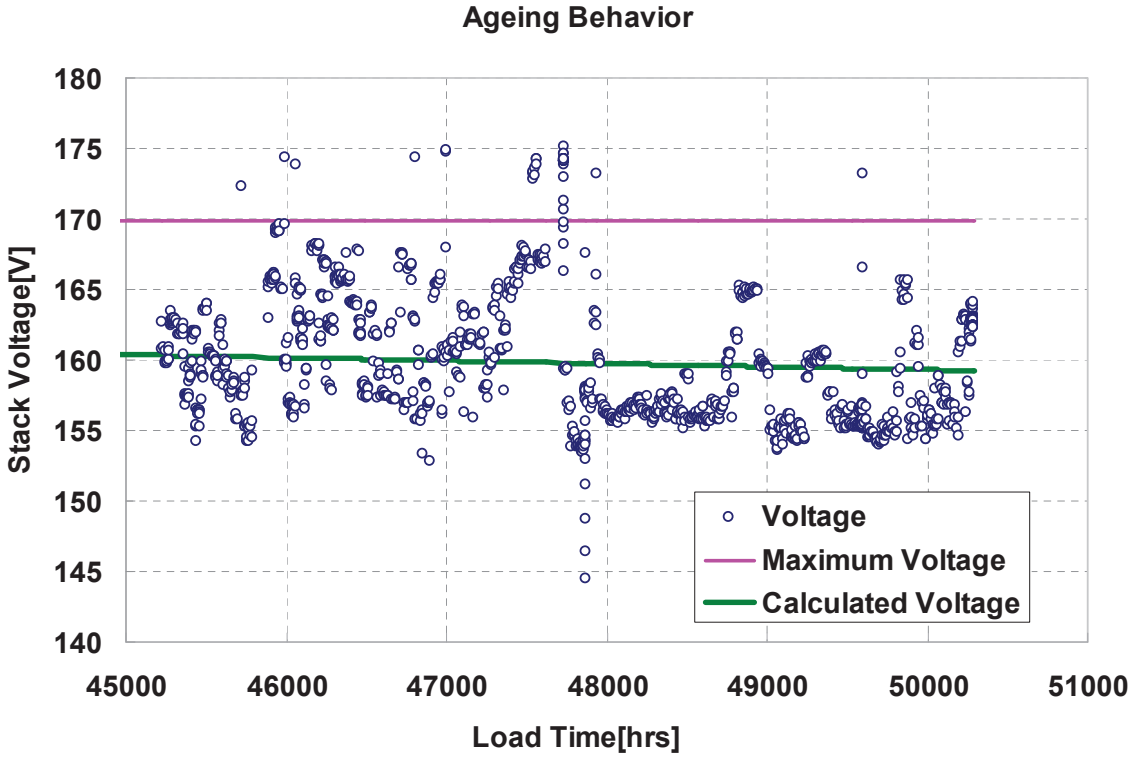

Figure 4-5: Ageing behavior of fuel cell stacks.(Data source: PAFC power plant in Cologne.)

$$\Delta \mathrm{V}(\mathrm{mV}) = -2\mathrm{mV}/1,000\mathrm{hours}. \tag{4.13}$$

As to the PAFCs system in Cologne, it has runned for more than 50,000 hours. Seen from the data of stack voltage after 45,000 hours, the voltage loses significantly. Assuming the voltage can be evaluated with equation 4.13, the value is shown in figure 4-5 as the black line. It is higher than the data of the real situation. In our case, the voltage degradation is expressed by the gray line in figure 4-5. The calculated maximum degradation rate is as high as

$$\Delta \mathrm{V}(\mathrm{mV}) = -213.8\mathrm{mV}/1,000\mathrm{hours}. \tag{4.14}$$

4.2.3.3 Current and voltage Generally speaking, the properties of electric resistance is determined by the materials, cross-section area and length of its own; sometimes the operation temperature is another one factor. As have known, the relation among current I, voltage and electric resistance R is expressed as

$$\mathrm{V} = R\mathrm{I}. \tag{4.15}$$

In this way, the electric resistance is able to be evaluated by voltage and current.

In our case, the function of voltage and current is shown in figure 4-6. The direct current of PAFCs system is linearized to voltage. A function of this relation is derived as

$$\Delta \mathrm{V} = -0.00124\Delta \mathrm{I}. \tag{4.16}$$

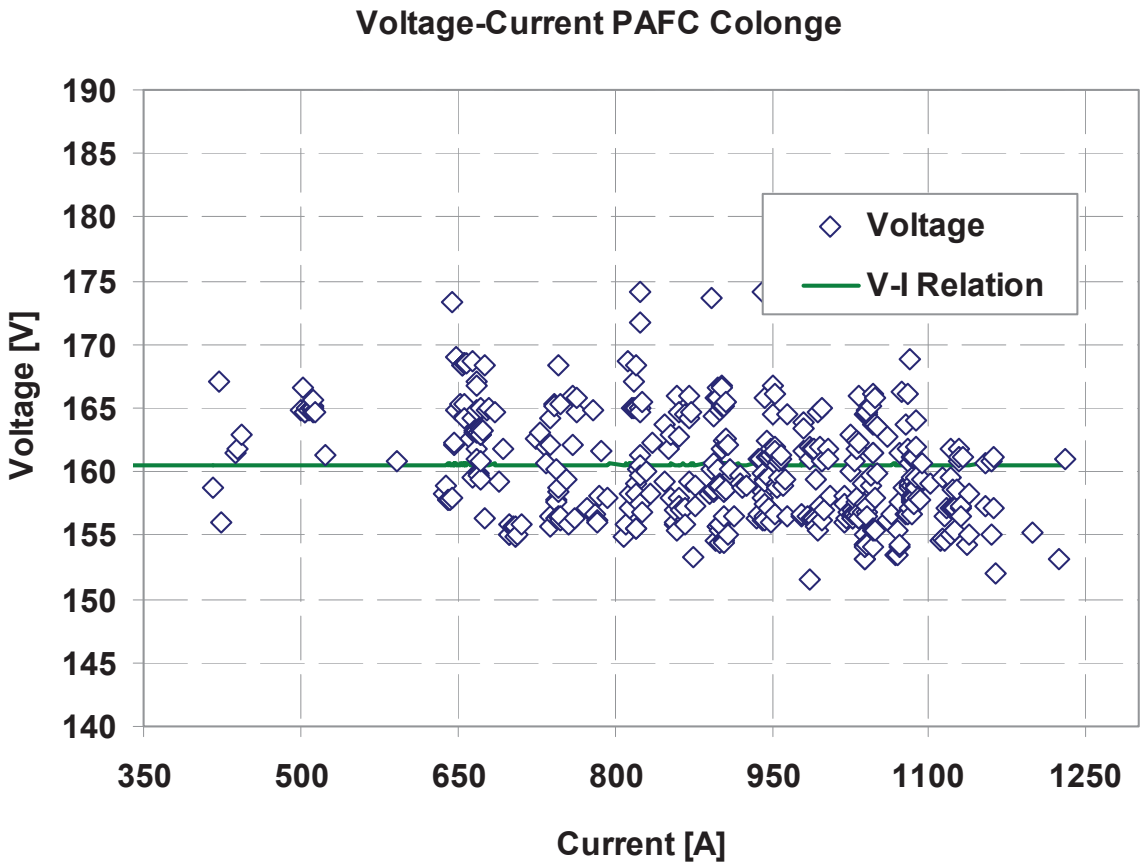

Figure 4-6: Voltage-Current of PAFCs.(Data source: PAFC power plant in Cologne.)

Seen from the data of figure 4-6, in the operation conditions, the resistance of PAFCs system is a constant. That is to say, this PAFCs power plant performs in a stable state.

4.3 Landfill Gas Reforming

Energy from alternative and renewable sources is of vital interest worldwide. H_2 is considered as a most potential energy carrier for the conversion in fuel cells. Besides oil -based liquid fuels, methane -rich gases such as mining gas, digester gas, or landfill gas currently are under research not only for the utilisation in heat engines to produce both mechanical and electrical energy, but for H_2 -production as well. Mining gas actually is a matter of CO_2-trading [59] [60], while anaerobic digestion or fermentation of biodegradable materials such as manure, sewage, or municipal solid waste results primarily in CH_4 and CO_2. This type of biogas mixtures can be converted to H_2.

As mentioned above, the PAFC in Cologne has successfully operated sewage gas since the year of 2000 [61]. Sewage plants are not so numerous in developing countries, while there are lots of and even very big dumping sites for municipal wastes. In those areas and under the regime of CO_2 trading landfill gas comes into the focus again. Actually, such kind of methane-rich biogas is able to be used as fuel gas for fuel cell. After entering the fuel compressor and cleanup device, the cleaned biogas is reformed in the steam reformer in the fule cell system. In order to discuss the thermodynamics of reforming process, the simulation work is studied in this section.

4.3.1 Scope on thermodynamic properties

For a normal reaction

$$\mathrm{aA} + \mathrm{bB} = \mathrm{cC} + \mathrm{dD} \tag{4.17}$$

at 298 **K** and 1 atmosphere, the standard enthalpy change [66] is calculated as

$$\Delta_\mathrm{r}\mathrm{H}^\ominus = \mathrm{c}\Delta\mathrm{H}_\mathrm{C}^\ominus + \mathrm{d}\Delta\mathrm{H}_\mathrm{D}^\ominus - \mathrm{a}\Delta\mathrm{H}_\mathrm{A}^\ominus - \mathrm{b}\Delta\mathrm{H}_\mathrm{B}^\ominus. \tag{4.18}$$

That is, the enthalpy change is related to products and reactants of a reaction. At other temperatures, the enthalpy change is

$$\Delta_\mathrm{r}\mathrm{H} = \Delta_\mathrm{r}\mathrm{H}^\ominus + \int_{298}^{\mathrm{T}} \Delta\mathrm{C}_\mathrm{p}\mathrm{d}\mathrm{T}, \tag{4.19}$$

with

$$\Delta\mathrm{C}_\mathrm{p} = \sum_i \nu_i \mathrm{C}_{\mathrm{p}i}, \tag{4.20}$$

in which, ν_i is the stoichiometric coefficient and $\mathrm{C}_{\mathrm{p}i}$ is the heat capacity of compound i at constant pressure. Additionally, the heat capacity of ideal gas is a function of temperature. With the same method, the entropy change of a normal reaction could be written as

$$\Delta_{\mathrm{r}}\mathrm{S} = \sum_{i} \nu_i \mathrm{S}_i^{\ominus} + \sum_{i} \int_{298}^{\mathrm{T}} \nu_i \mathrm{C}_{\mathrm{p}i} \mathrm{dln T}. \tag{4.21}$$

So that, the Gibbs energy change for a chemical reaction at a constant pressure may be given as

$$\Delta_{\mathrm{r}}\mathrm{G} = \Delta_{\mathrm{r}}\mathrm{H} - \mathrm{T}\Delta_{\mathrm{r}}\mathrm{S}. \tag{4.22}$$

In general, a multi-components system is made up by several elementary reactions. For each kind of constituent in the overall system, the mass balance is able to be expressed by means of stoichiometric coefficients. That is,

$$n_i = n_i^{\ominus} + \sum_{r=1}^{R} \nu_{ri}\xi_r \qquad i = 1, 2, ..., N, \tag{4.23}$$

thus, the derivative is in form of

$$\mathrm{d}n_i = \sum_{r=1}^{R} \nu_{ri}\mathrm{d}\xi_r \qquad i = 1, 2, ..., N. \tag{4.24}$$

Where, $n_i^{\ominus}$ is the amount of moles of constituent i in the initial mixture and ξ_r is so called reaction coordinate.

At a given temperature T and pressure P, the Gibbs function is only the function of ξ_r, which follows

$$\mathrm{dG} = \sum_{r=1}^{R} (\sum_{i=1}^{N} \nu_{ri}\mu_i)\mathrm{d}\xi_r. \tag{4.25}$$

Normally, the relation between the chemical potential and activity is defined as

$$\mu_i = \mu_i^{\ominus} + \mathrm{RTln}a_i, \tag{4.26}$$

where $\mu_i^{\ominus}$ is the chemical potential of constituent i in standard state and a_i is activity [62]. Substituting equation 4.25 into equation 4.26, the differential form of Gibbs function is written as

$$\begin{aligned} \frac{\mathrm{dG}}{\mathrm{d}\xi_r} &= \sum_{i=1}^{N} \nu_{ri}\mu_i \\ &= \sum_{i=1}^{N} \nu_{ri}\mu_i^{\ominus} + \mathrm{RTln}\prod_{i=1}^{N} a_i^{\nu_{ri}} \qquad r = 1, 2, ..., R. \end{aligned} \tag{4.27}$$

With

$$(\Delta\mathrm{G})_r = \frac{\mathrm{dG}}{\mathrm{d}\xi_r} \qquad r = 1, 2, ..., R, \tag{4.28}$$

$$(\Delta \mathrm{G}^{\ominus})_r = \sum_{i=1}^{N} \nu_{ri} \mu_i^{\ominus} \qquad r = 1, 2, ..., R, \tag{4.29}$$

and

$$(\mathrm{K}_a)_r = \prod_{i=1}^{N} a_i^{\nu_{ri}} \qquad r = 1, 2, ..., R. \tag{4.30}$$

The Gibbs energy change of r-th reaction at given temperature T and pressure P may be rewritten as

$$(\Delta \mathrm{G})_r = (\Delta \mathrm{G}^{\ominus})_r + \mathrm{RTln}(\mathrm{K}_a)_r \qquad r = 1, 2, ..., R, \tag{4.31}$$

in which, $(\mathrm{K}_a)_r$ is the equilibrium constant of the r-th reaction in a system.

In general, activity is defined as

$$a_i = \frac{f_i}{f_i^{\ominus}}, \tag{4.32}$$

where f_i is the fugacity of constituent i in the mixture, and $f_i^{\ominus}$ is that of constituent i in standard state. As seen from equation 4.32, the value of activity of each kind of constituent i is related to the fugacity in standard state. Normally, in the ideal gas mixture systems, the standard fugacity is taken at given temperature T and pressure of 1 atm. Considering the value of fugacity coefficient as one in ideal gas systems, so that, the activity of constituent i is

$$a_i = \frac{f_i}{1} = P_i = P\frac{n_i}{n}, \tag{4.33}$$

in which, P_i is the partial pressure of constituent i, P is the pressure of gas mixture, and n is the sum of molar amount of n_i.

Constituting equation 4.33 into equation 4.30, the equilibrium constant of the r-th reaction in a system is expressed as

$$\begin{aligned}(\mathrm{K}_a)_r &= \prod_{i=1}^{N} a_i^{\nu_{ri}} = \prod_{i=1}^{N} f_i^{\nu_{ri}} \\ &= \prod_{i=1}^{N} P_i^{\nu_{ri}} = (\frac{P}{n})^{\nu_r} \prod_{i=1}^{N} n_i^{\nu_{ri}}\end{aligned} \tag{4.34}$$

with $\nu_r = \prod_{i=1}^{N} \nu_{ri}$, which is the total stoichiometric coefficient change of constituent i in r-th reaction.

In a closed system, chemical reactions would arrive at equilibrium at a given temperature T and pressure P. So that, the Gibbs function attains the minimum, thus $\frac{\mathrm{dG}}{\mathrm{d}\xi_r} = 0$, and Gibbs function becomes a function of ξ_r. In this method, the chemical equilibrium can be simulated by calculating a set of reactions in systems.

4.3.2 Steam reforming reactions

According to equation 4.35, the steam methane reforming process is mainly to converts CH_4 into a mixture of H_2 and CO with catalysts. Normally, this reaction is followed by a water gas shift, as shown in equation 4.36, to produce a mixture of H_2 and CO_2. On the other hand, higher fraction of CO_2 in landfill gas or other biogas would result in carbon dioxide reforming at high temperatures.

Steam reforming

$$\mathrm{CH_4(g) + H_2O(g) \rightleftharpoons CO(g) + 3H_2(g)} \qquad \Delta H_{298K} = 206.2 KJ/mol \tag{4.35}$$

Water gas shift

$$\mathrm{CO(g) + H_2O(g) \rightleftharpoons CO_2(g) + H_2(g)} \qquad \Delta H_{298K} = -41.1 KJ/mol \tag{4.36}$$

Carbon dioxide reforming

$$\mathrm{CH_4(g) + CO_2(g) \rightleftharpoons 2CO(g) + 2H_2(g)} \qquad \Delta H_{298K} = 247.0 KJ/mol \tag{4.37}$$

In the gas reforming process, all of the constituents are assumed to be presented in equilibrium according to equation 4.35 to equation 4.37. Furthermore, the reforming systems, with constituents CH_4, CO, CO_2, H_2 and H_2O and elements C, H, O, are simulated by a non commercial program [63] [64] [65]. The numerical method is described in *Thermodynamik der Elektrolytlösungen* [66].

4.3.3 Simulation results and discussion

In this work, the initial composition of gases mixture is made up of 60 % CH_4 and CO_2 40 % in mole, which is similar to those of upgraded landfill gases. The impacts of pressure and temperature on reforming processes will be simulated. Finally, the impact of steam and some hydrocarbons, such as alkenes, alkynes and so on, are taken into account for simulation. In addition, a part of trace gases are to be studied as well.

4.3.3.1 Effect of pressure and temperature As shown in figure 4-7, the reforming was calculated at 1.013bar and various temperature. At the lower temperatures, the exothermic reaction plays a key role in system. Since the water gas shift reaction had a part in process, the product of CO_2 increases rapidly before at 773.15 K. On the contrary, at the higher temperatures, the endothermic reactions, such as equation 4.35 and equation 4.37, became dominant in the methane reforming system. Therefore, H_2 would increase as temperatures increasing. As results, the product of H_2 begin to increase significantly from 873.15 K.

On the other hand, the amount of moles increases in products at equilibrium, as shown in equation 4.35and equation 4.37. This process is associated with an increase in Gibbs change. Therefore, the reactions would take place in reverse at high pressure. So that, the production of H_2 and CO decreases as pressure increasing. Seen from figure 4-8, with the variation of pressure from 1.013 bar to 40.013 bar, the H_2 production decreased from 58.28 % to 42.32 % at 1273.15 K.

In practice, the higher temperature might lead to methane cracking, which is shown in eqaution 4.38.

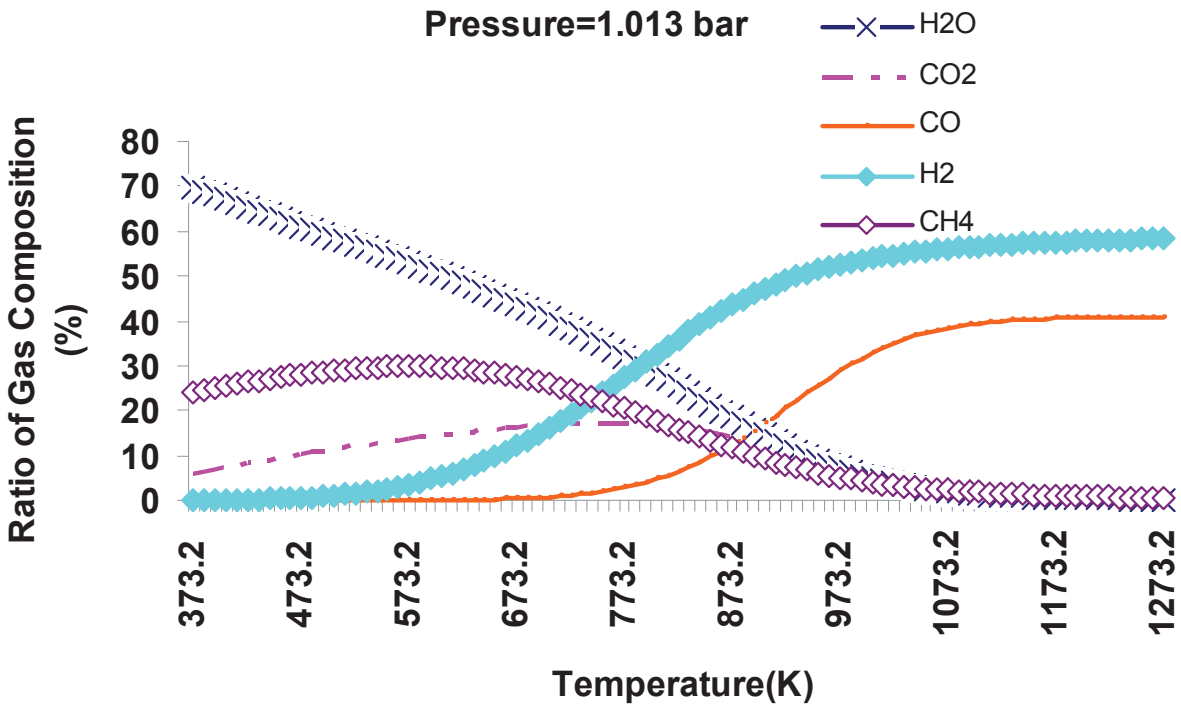

Figure 4-7: Effect of Temperature on Reforming.

Methane decomposition

$$\mathrm{CH_4(g) \rightleftharpoons C + 2H_2(g)} \qquad \Delta H_{298K} = 76.0 KJ/mol. \tag{4.38}$$

Thus, the catalyst of reformer could be polluted by carbon. Normally, a fuel cell system should be maintained in a range of operating temperature. Heat therefore must be removed from equipment. As to the steam reformer in a fuel cell system, a part of heat can be removed directly by the flow of reactants and products. In such a method, the flow rate must be adjusted to make sure the inlet and outlet temperatures of the fuel streams are in a suitable range. The gas flow rate has been discussed in section 4.2.3.

4.3.3.2 Effect of steam concentration on gas production As to these simulation works, the ratio of steam concentration to that of landfill gas varied from 20 % to 100 %. Figure 4-9 showed the gas compositions at 1 bar and 1073.15 K. When the steam was given as 4.0 mol in initial condition, that the steam-gas ratio was 40 %, the composition of H_2 concentrations arrive at maximum.

In the reforming processes, both reforming reactions would be taken into account in systems. When the steam-gas ratio is lower, H_2 production is depended by the concentration of CO_2 more, which is carbon dioxidere forming. As higher steam-gas ratio is considered in simulation, the steam reforming and water gas shift reactions contribute element H much more. Thus, H_2 production increases gradually to maximum with steam concentration increasing.

As shown in equation 4.35 to equation 4.38, the amount of mole of products would increase. Therefore, the reforming processes may result in the higher pressure. In simulations, as more steam was taken into account, H_2 and steam can achieve to maximum under the high pressure.

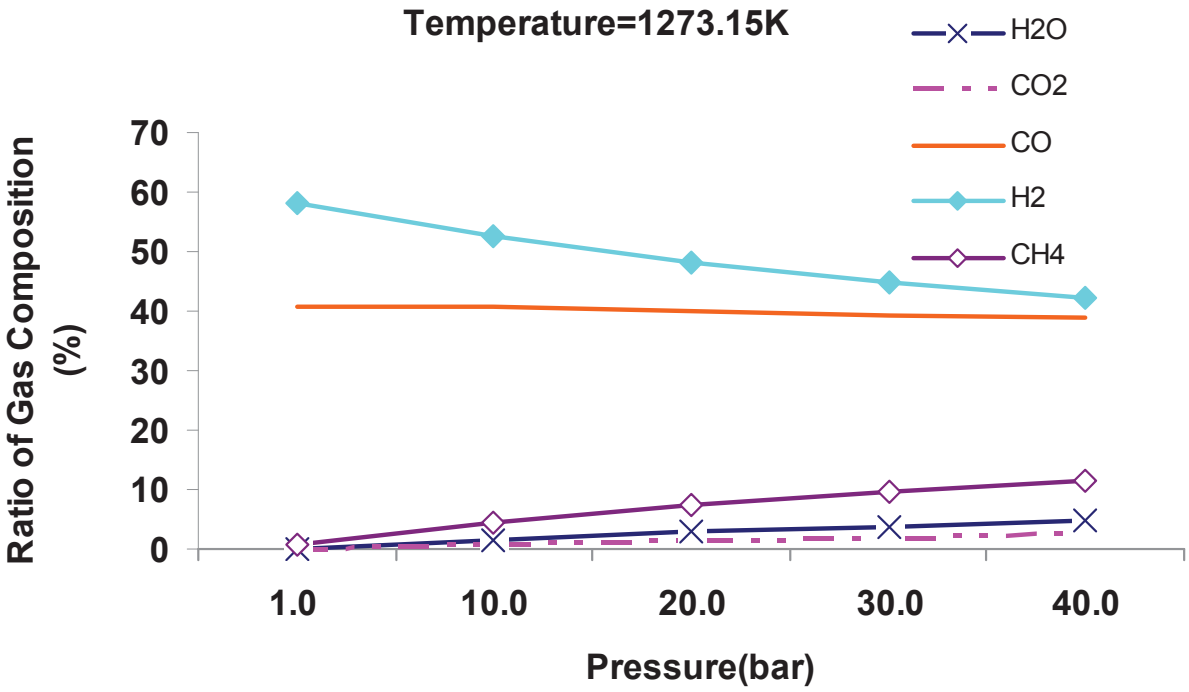

Figure 4-8: Effect of Pressure on Reforming.

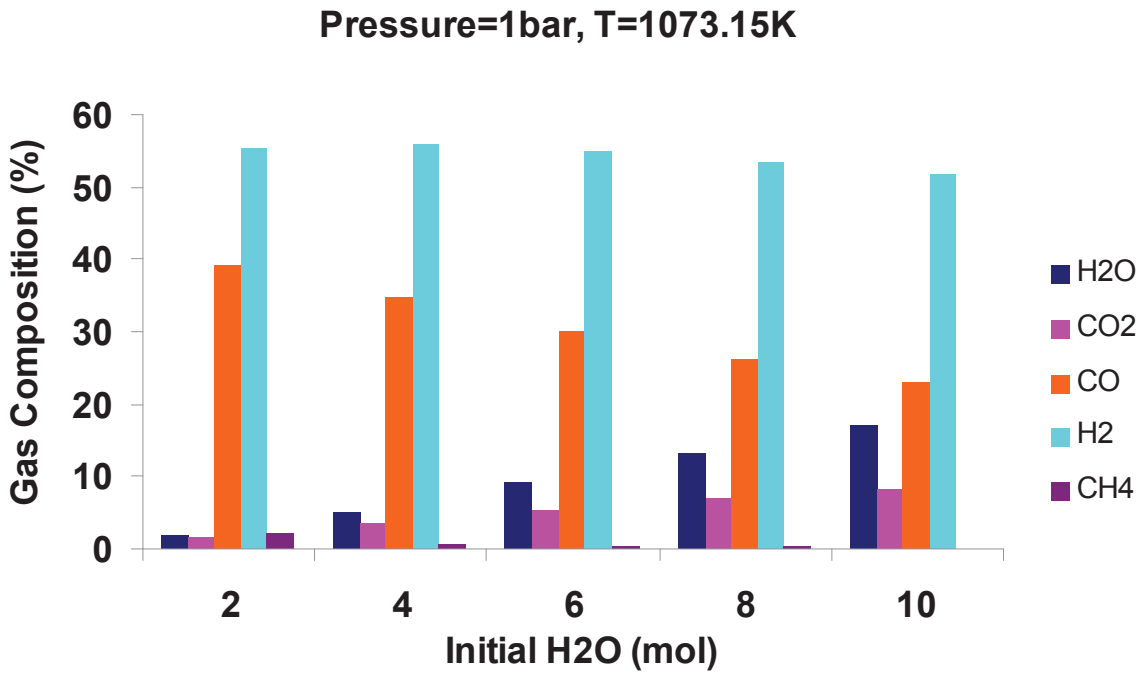

Figure 4-9: Effect of Steam on Reforming.

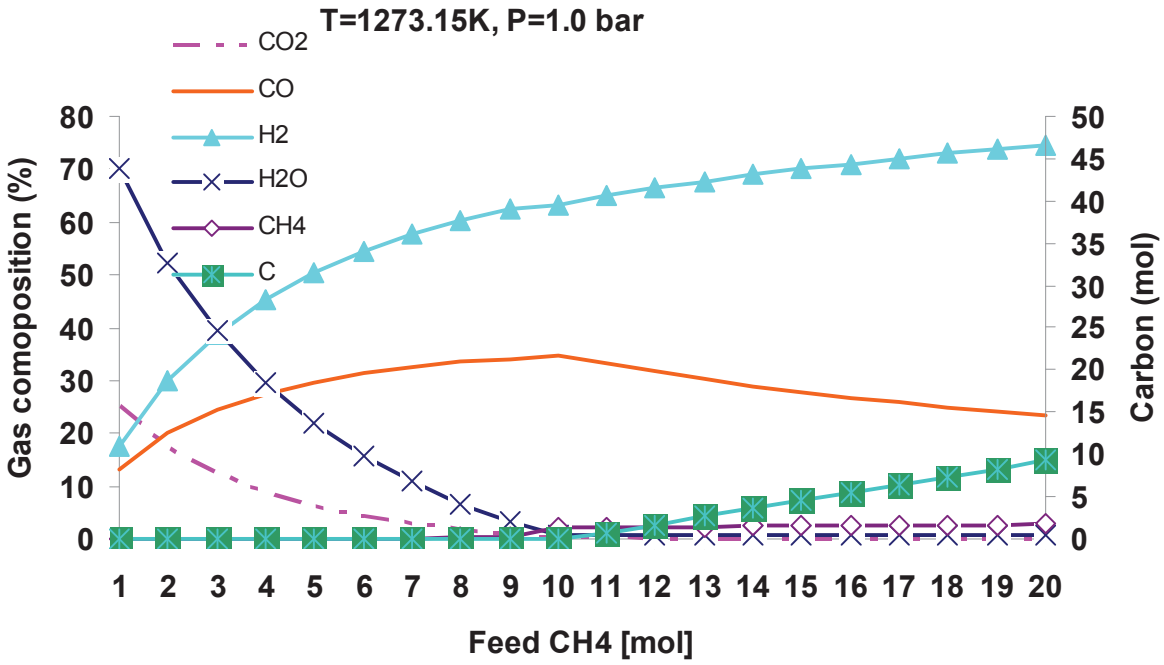

Figure 4-10: Methane Cracking in Reforming.

To keep equilibrium state, the steam reforming and carbon dioxide reforming will take place in reverse direction. So that, the composition of H_2 begin to decrease.

As mentioned above, the deposited carbon must be avoided in reforming process. In general, reforming of CH_4 and steam would produce H_2. The excess CH_4 would be involved in reaction of methane cracking. To describe the damage of lack of steam in reforming, an extreme simulation was performed. At 1 bar and 1273.15 K, 6.0 mol steam and 4.0 mol CO_2 were set in initial conditions; CH_4 was set to vary from 1.0 mol to 20.0 mol in simulation. Seen from figure 4-10, as steam arrived at minimum, the composition of carbon increased rapidly. Meanwhile, the composition of H_2 kept increasing.

By varying the pressure and temperature, the calculation results shows that the maximum of H_2 is various, which depended on steam-gas ratio at different reforming conditions. In practice, the steam-gas ratio is around 66 % at 1033 K-1144 K in the reformer of a PAFCs system. The lower concentration of steam may diminish H_2 production and lead to methane cracking. Thus, stack voltage would drop because of lack of fuel. On the other hand, the higher concentration of steam may contain so much heat, thus resulting in temperature skip of fuel cells system.

4.3.3.3 Effect of trace gases Traces of hydrocarbons, such as alkyls, alkenes, alkynes and benzene, can be found in landfill gas. In this simulation, the effect of ethane (C_2H_6) on reforming system was studied at 1 bar. There were two series of simulations to be calculated. In one series, the purified landfill gas reforming was simulated. In which, the initial conditions were set as 60% CH_4 and 40% CO_2 for gas mixture, and steam-gas fraction was 60 %. In another series, with the same steam-gas ratio, 6 % C_2H_6 was taken into account in initial conditions.The simulation was performed from 973.15 K to 1273.15 K

The results were shown in figure 4-11. As to the series with C_2H_6, from 973.15 K, the com-

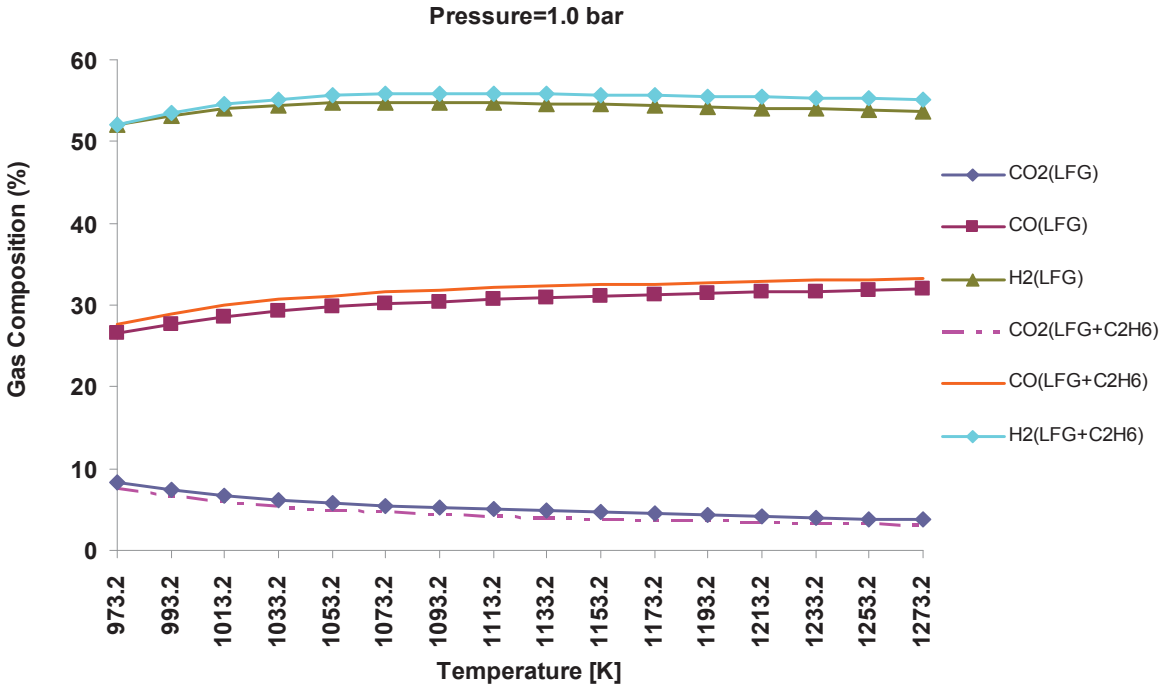

Figure 4-11: Ethane in gas reforming.

position of H_2 and CO were slightly higher (about 1 %) than those of purified landfill gas. In contrast to the production of H_2, the composition of CO_2 decreased around 0.8 % in the series with C_2H_6. This meant that the traces of C_2H_6 could take part in steam reforming, giving rise to the slight increase of H_2.

The further effect of hydrocarbons on methane reforming was studied at 25.013 bar and 40.013 bar respectively. Where, traces of alkenes, alkynes, alkyls and benzene were calculated in program. The results confirmed that hydrocarbons lead to the increment of H_2 and CO in steam reforming. Comparing the results at 25.013 bar and 40.013 bar, the effect of hydrocarbons is insignificant in this work. Just like the purified landfill gas in reforming processes, the higher temperature and lower pressure are the important factors to landfill gas mixed with trace of hydrocarbons.

4.4 Conclusion and Discussion

The purified landfill gas mainly contains 60 % CH_4 and 40 % CO_2. The landfill gas has the same qualities as natural gas, which can be utilized as the fuel for electricity generation. Since the year of 2000, a PAFCs system has operated in the sewage plant of Cologne in Germany. As the case of success in power generation with biogas, it has proved that landfill is possible be used as a kind of biofuel to fuel cell systems.

Fuel cells are designed as devices to convert chemical energy into electrical energy directly. In theory, the performance of fuel cells is related to change of Gibbs energy and Nernst equation. Therefore, the ideal performance of a fuel cell is strongly depending on standard cell potential, reactant concentrations and cell temperature.

In practice, the types of fuel cell systems are categorized by types of electrolyte in a fuel cell.

Generally, the common types include Polymer Electrolyte Fuel Cell(PEFC), Phosphoric Acid Fuel Cell(PAFC), Solid Oxide Fuel Cell(SOFC) and so on. Among them, PAFC is the first fuel cell technology that to be commercialized. The PAFCs system can be equipped with a device to shift CO to H_2 and a reformer to produce H_2. Thus, the biogas may be fuelled by PAFCs system.

The performance of PAFC system in Cologne is analyzed by gas flow rate, gas load time, and the function between current and voltage in fuel cells. Biogas can be supplied into PAFCs system as fuel to produce H_2. Before entering into the reformer, fuel streams must be heated; meanwhile, the effluent fuel streams should be cooled in heat exchanger. To some extent, biogas flow rate plays an important role in heat exchange, which effects the performance of a fuel cell system in power generation indirectly. In our case, the gas flow rate is related to electrical power linearly. Seen from the data of gas load time, the fuel cell systems has operated longer time than expected. Thus, the maximum voltage degradation of PAFCs system is higher than that in theory. Normally, the current-voltage relation is a function to evaluate the electric resistance in systems. As to PAFCs system in Cologne, this value is a constant. So that, it means the performance of fuel cell systems is stable.

As the potential fuel used by fuel cell systems, the landfill gas reforming simulation is discussed in this chapter. As the results showed, pressure and temperature are the key factors in reforming processes. That is, the production of H_2 would decrease as pressure increasing, and increase as temperature increasing. The higher temperature and lower ratio of steam might result in methane decomposing, which should be avoided in real reforming processes. The effected of traces of hydrocarbons and oxygen were discussed as well. As consequence, hydrocarbons and oxygen may take part in reactions, but their effects on reformed gas production can be neglected.

Nowadays, the viability of utilization of landfill gas has been discussed a lot [67] [68] [69]. Recently, landfill gas upgrading and purification have received more and more attention. How to develop an effective and economical method on purification has become an attractive issue.

5 Landfill Gas Adsorption with Bottom Ash

Landfill gas, due to high heating value, can be widely utilized for energy production [70]. But, its quality is depending on the CH_4 content and purity to some extent. Sometimes, for the purpose of improving the energetic content of landfill gas, CO_2 is separated from CH_4. Especially in the terms of combustion, CO_2 is considered as a inert gas.

Pressure swing adsorption has been used for landfill gas purification widely. It involves the physicochemical phenomena to adsorb a species at high pressure. Since different gas possesses different adsorptivity, CO_2 can be separated from CH_4 in landfill gas feed. To improve the behaviour of adsorption bed, the study on various adsorbent has become a field of intense activity. The use of activated carbon [71], impregnated activated carbon [72], molecular sieves [73], and sludge [74] has been researched in adsorption processes. The equilibrium theory of single bed [75] and layered beds [76] in pressure swing adsorption have been discussed as well.

However, in order to remove H_2S and water, pre-treating of gas is necessary for pressure swing adsorption. The energy demand for purification processes, high investment and maintenance costs have displayed the disadvantages of pressure swing adsorption technique.

Recently, a new method of landfill gas purification attracts a lot interest in the field of energy and environment. The experimental results showed that municipal solid waste incineration (MSWI) bottom ash may be served as a adsorbent for landfill gas purification [77]. Furthermore, the removal mechanisms of H_2S with bottom ash are under investigate [78].

In this section, the properties of MSWI bottom ash will be introduced. By analyzing the properties of bottom ash, the potential reactions of adsorption will be explained. The performance of landfill gas adsorption with bottom ash will be introduced by experimental methods.

5.1 Municipal Solid Waste Incineration Bottom Ash

Bottom ash is the primary by-product of municipal solid waste incineration. Generally, the product of MSWI bottom ash is as high as 20 %-30 % from municipal solid waste. Bottom ash is treated for disposal or subsequent utilization, usually. It can be used as the substitute for road construction materials, on account of the geotechnical properties.

MSWI bottom ash may be a potential hazard due to the enrichment of organic compounds and toxic elements in waste. Because of the particularity in the local waste conditions and the techniques in incineration, the properties of bottom ash are various. Thus the study on properties of bottom ash has become one of attractive topics around world for long periods.

5.1.1 Bulk composition of bottom ash

There are three pieces of publications on properties of MSWI bottom ash. Both of them mentioned the bulk composition of bottom ash. The ash samples are taken from USA, Germany, and China respectively.

In 1993, C.S. Kirby collected MSWI ash for study purposes. It was the mixture of bottom and fly ash from the University City Resource Recovery Facility in Charlotte, NC. There were 18 % minerals, 9 % structural and adsorbed water, and 72 % glass in the ash [79]. As the new incineration technologies were developed, and the refuse sorting was promoted in European

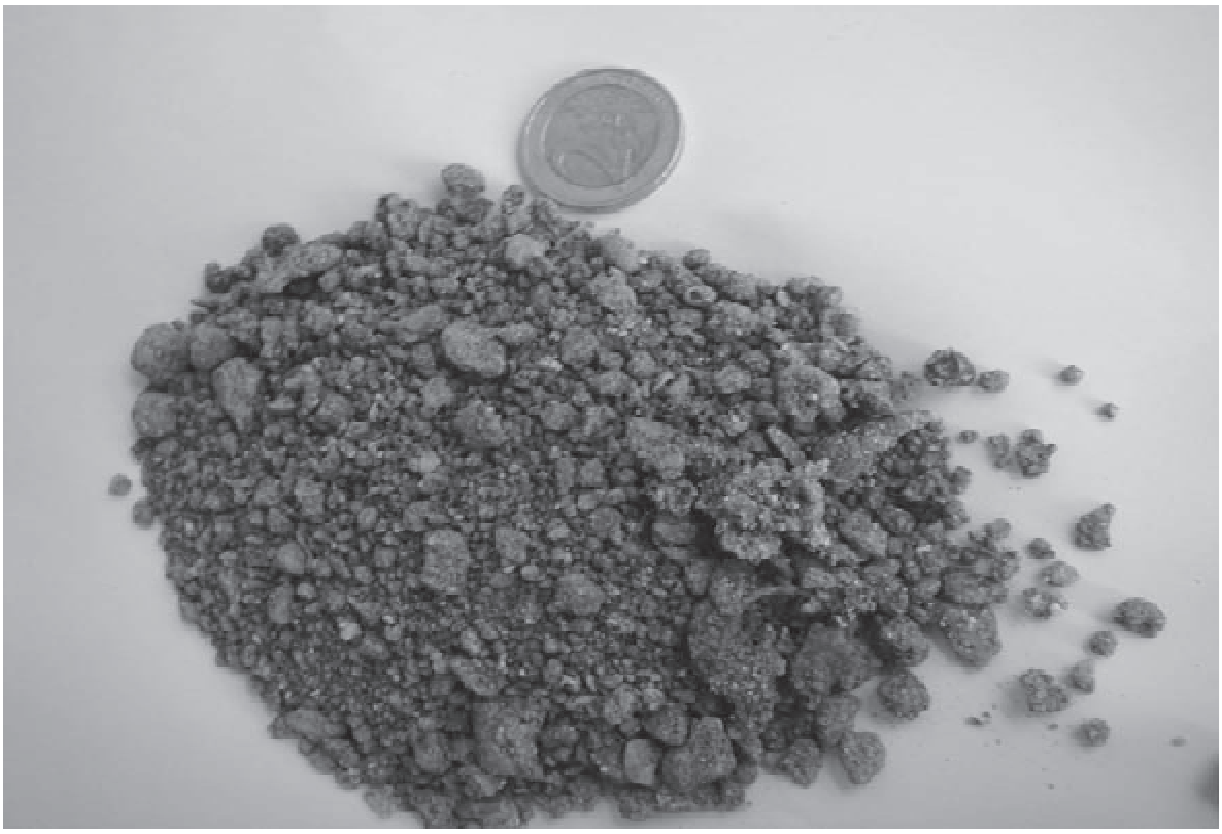

Figure 5-1: Bottom ash from Western Germany.

countries, the bulk composition was different from that of USA. For instance, a publication reported in the year 2000, the bottom ash sample from southern Germany contained 42 % ash, 40 % melting products, 8 % metallic components, and 10 % residual parts [80].

In China, the municipal solid waste incineration management started from the later of 1990s. However, the calorific value of waste was lower through lack of sorting and recycling. The bulk composition of bottom ash was more complicated than that of Germany. Taking an incineration plant of southeastern China as example, the solid waste incinerator operated at 1123.15 K-1473.15 K. The bottom ash mainly consisted of 50.52 % melting products, 17.45 % ash, 2.05 % metallic components, and 28.61 % residual parts, usually stone, glass, and ceramics. In addition to these, there were 1.37% plastic, wood, and cloth in ash, which should have not been found as residue of incineration [81].

In this work, the MSWI bottom ashes were collected from a solid waste incineration plant in western Germany. As figure 5-1 showed, they are coarse granules with various size. However, the bulk composition was not be analyzed in this experiment. To prevent moisture exchange with surroundings, the ashes were stored in a sealed plastic barrel in laboratory.

5.1.2 Chemical properties of bottom ash

The bulk chemistry analyses of bottom ash have been noted by several works [82] [83]. C. S. Kirby has analyzed all major elements and many minor elements in a publication. The results were compared with those from another literatures as well.

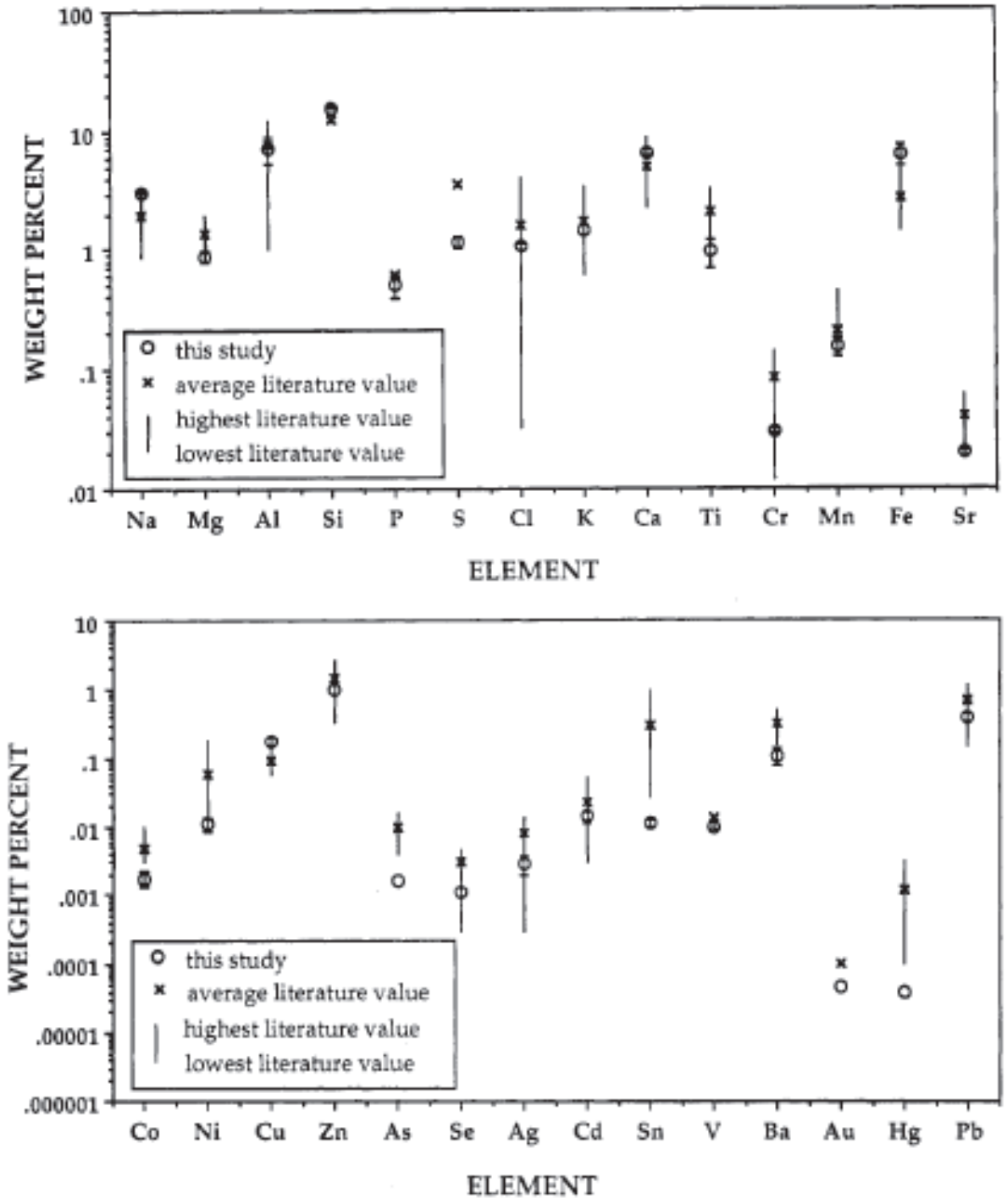

Figure 5-2: Bulk Chemistry of Bottom Ash (Cited from works of C.S. Kirby [79]).

As illustrated in figure 5-2, bottom ash is a very heterogeneous material. But, data presented in the literatures confirms the processes of bottom ash weathering are related to Ca-hydration and carbonation. In the incinerator, $CaCO_3$ would decompose into CaO, and cavities were formed on the surface of bottom ash. In the quenching process, the parts of CaO outside cavities would be hydrated with water. This process can be described by a reaction

$$\textbf{Hydration reaction} \\ \mathrm{CaO} + \mathrm{H_2O} \rightleftharpoons \mathrm{Ca(OH)_2}. \tag{5.1}$$

Furthermore, the hydrate phases would take part in an exothermic reaction on the crystal phases of bottom ash. This process can be written as

$$\mathrm{Ca(OH)_2} + \mathrm{SiO_2} \rightleftharpoons \mathrm{CaH_2SiO_4}. \tag{5.2}$$

Hydrate phases may react with CO_2 as time goes by. This is known as carbonation reaction, and the process can last years, decades or even longer.

$$\textbf{Carbonation reaction} \\ \mathrm{Ca(OH)_2} + \mathrm{CO_2} \rightleftharpoons \mathrm{CaCO_3} + \mathrm{H_2O}. \tag{5.3}$$

Bottom ash would be treated with landfill as the final way, the leachability of bottom ash therefore should be analyzed. The leachate pollution in landfill cites can be categorized as 1) organic solutes; 2) inorganic components; 3) heavy metals including chromium, nickel, and cadmium. The composition of leachate depends on the heterogeneity and solubility of bottom ash. As results, the bottom ash leachability mainly characterized as pH value, hydronium capacity, and electrical conductivity.

In this work, bottom ash is studied as a adsorbent for landfill gas purification. In order to compare the effect of CO_2 on bottom ash leachability, the analyses results of fresh and used bottom ash will be introduced in the later sections.

5.1.3 Water content and ignition loss

The moisture of fresh bottom ash was determined before the processes of landfill gas adsorption. Five samples were taken from bottom ash. Five crucibles with covers were dried in a drying oven (at temperature of 374.15 K) for 10 hours. Then, they were cooled in a desiccator and weighed at ambient temperature.

Five 6 g representative bottom ash samples were weighed to the nearest 1 mg. The samples just covered the bottom of crucibles so as to can be dried to constant weights. Samples were dried, cooled, and weighed as the same processes as those of crucibles. At last, the dried samples were put into muffle furnace, in which the ignition time and temperature have been programmed.

The water content is calculated as

$$\mathrm{Water\ Content, wt\%} = \frac{\mathrm{C} + \mathrm{A} - \mathrm{D}}{\mathrm{A}}, \tag{5.4}$$

and the loss on ignition could be written as

$$\text{Ignition Loss, wt}\% = \frac{\mathrm{D-I}}{\mathrm{D-C}}, \tag{5.5}$$

where:
A— weight of fresh bottom ash, [g];
C— weight of crucible with cover, [g];
D— weight of dried sample, [g];
I— weight of ignited sample, [g].

During the processes of landfill gas adsorption, small quantities of water evaporated and condensed on the cover of reactor. Compared the results of CO_2, the change of water content of used bottom ash could be neglected. As the bottom ash is not heat-sensitive material, the ignition loss would be neglected in adsorption as well. The average data on water content and ignition loss are shown in table 5-1.

5.1.4 Porosity and pore size distribution

Any solid, within which hold cavities, channels or interstices, can be regarded as porous material. Porous materials can be formed in several ways. The porous structure of bottom ash may be by quenching in the processes of incineration. Porosity and pore size distribution are the two of necessary quantitative description of porous structures.

As a good adsorbent, the porous solid must possess good adsorptive capacity as well as good kinetics. That is, the solid must have small pore size and a reasonably high surface area or pore volume, which is related to porosity [84].

Porosity can be defined as the fraction of the total pore volume V_p to the apparent volume V_a of the solid. It is written as:

$$\epsilon = \frac{\mathrm{V_p}}{\mathrm{V_a}}. \tag{5.6}$$

The pore size is an important property of porous materials, but it is impossible to be defined precisely. Usually, the pore shape is irregular and variable, so that makes the specific surface area complicated. The pore size distribution thus is one of best means of characterizing the pore structure. It can provide valuable information on how the pore volume is distributed as a function of pore size for porous solids. Normally, the pore size distribution is represented by the derivatives of $\frac{\mathrm{dV_p}}{\mathrm{dr_p}}$ as a function of $\mathrm{r_p}$, where $\mathrm{r_p}$ is the radius of the pores [85].

In this work, the porosity and pore size distribution of bottom ash are analyzed in the Baustoff Labor, University of Duisburg-Essen. The samples were tested and determined from mercury adsorption and desorption isotherms with Porosimeter (Porosimeter 2000WS). Pore size distributions are shown in figure 5-3. The results confirm that the bottom ash is a highly heterogeneous material, so that the analyses data are different for the same batch of ashes. The average value of porosity is to be listed in table 5-1. In addition, the bulk density of bottom ash is listed as well.

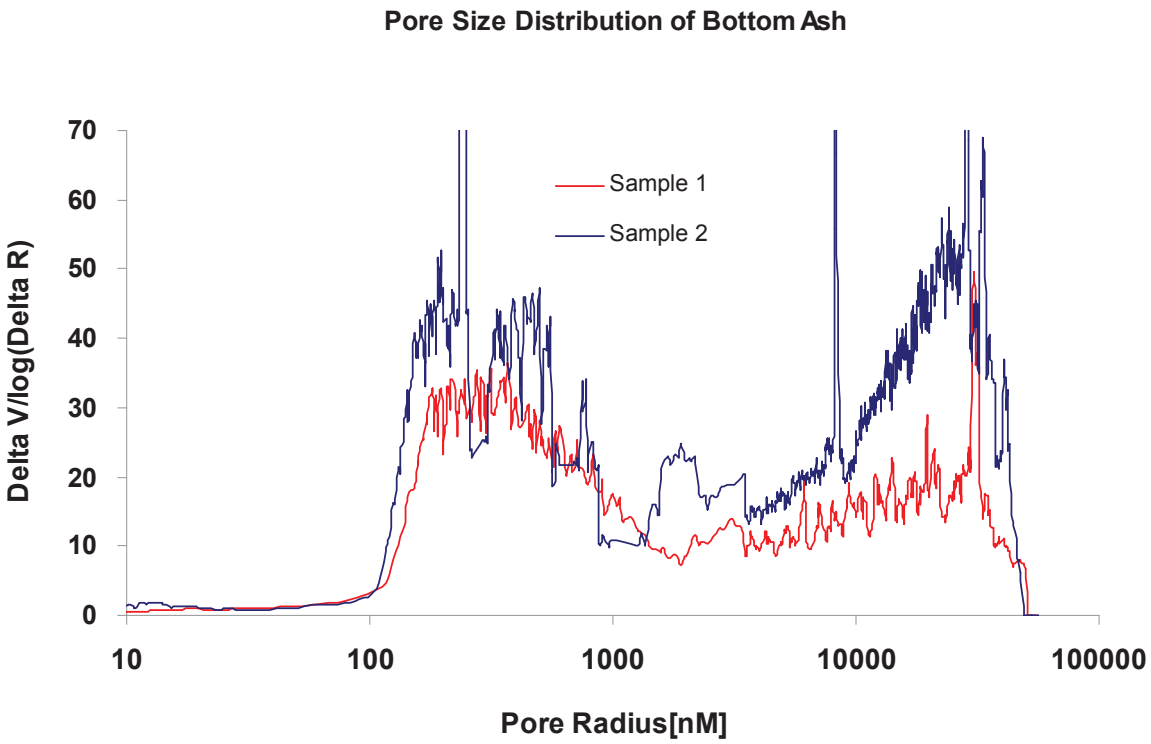

Figure 5-3: The Pore Size Distribution of Bottom Ash.

5.1.5 Heat capacity

In practice, the adsorption in porous solids involves not only mass transfer but also heat transfer. The heat transfer coefficients and thermal conductivities are able to contribute a lot to energy balance.

As Fourier's law expresses, the heat flux Q is proportional to the temperature gradient ∇T:

$$\mathrm{Q} = -k_{\mathrm{T}} \nabla \mathrm{T}. \tag{5.7}$$

In which, k_{T} is the thermal conductivity.

Taking the first law of thermodynamics into consideration, the change in the internal energy is actually a combination of heat added to the system and work done by the system. That is

$$\Delta \mathrm{U} = \mathrm{Q} + \mathrm{W}. \tag{5.8}$$

where, ΔU is the internal energy change in a system, and W is the work preformed on the system by its surroundings. If the process is performed at constant volume, the heat capacity at constant volume $\mathrm{C_v}$ can be defined as

$$\mathrm{C_v} = (\frac{\partial \mathrm{U}}{\partial \mathrm{T}})_{\mathrm{v}}. \tag{5.9}$$

For solids, the value of $\mathrm{C_v}$ is equal to $\mathrm{C_p}$, and almost is a constant.

In this work, heat capacity of bottom ash sample was analyzed in the laboratory of Thermodynamik, IVG, Maschinenbau, University of Duisburg-Essen. The thermal conductivity k_{T} was determined by measuring the temperature drop over a definite length as compared to that found for a substance (stainless steel) in a self made apparatus. The heat capacity C_p was determined from the DTA (commercial DTA/TG apparatus) by comparing the signals with other substances of known heat capacity. The data are listed in table 5-1 respectively.

Table 5-1: **Properties of Bottom Ash**

parameter	**value**	**unit**
water content	14.09	wt.%
ignition loss	3.03	wt.%
porosity	32.80	%
bulk density	1.66	$g{\cdot}cm^{-3}$
thermal conductivity	$0.6{\pm}0.2$	$W{\cdot}(m{\cdot}K)^{-1}$
heat capacity	$1.2{\pm}0.1$	$J{\cdot}(g{\cdot}K)^{-1}$

5.2 Landfill Gas Adsorption with Bottom Ash

From the data reported previously and the analyses in this work, the MSWI bottom ash might be used as a potential adsorbent in landfill gas purification. For the purpose of determining CO_2 breakthrough capacity of the bottom ash, the adsorption experiments are performed in our case. In addition, the physical and chemical properties are analyzed on used ashes.

5.2.1 Fixed bed adsorption processes

The fixed bed adsorption processes were designed and installed at laboratory of Siedlungswasser- und Abfallwirtschaft, University Duisburg-Essen. As figure 5-4 shown, the landfill gas was mixed by pure CH_4 and CO_2 in experiments. N_2 was used as purge and carrier gas during processes. The gas flow rate was adjusted by mass flow controller. Before the experiments, such mass flow controllers have been calibrated.

Temperature would effect on adsorption isotherm and gas diffusion rate, so as to influence on the capacity of adsorbent. In this work, the combined landfill gas was kept at 290.15 K–292.15 K in thermostatic bath before flowing into the adsorbent, and the ambient temperature was kept around 292.15 K. So that, the effect of temperature on adsorption processes could be ignored.

The composition of effluent gas was tested every 5-10 minutes. In order to prevent dusts being blown into gas detector, a filter was installed behind the outlet of fixed bed reactor.

5.2.1.1 Input landfill gas For the laboratory experiments, landfill gas was composed of 70 % CO_2 and 30 % CH_4 in volume. In most of experiments, N_2 was used as carrier gas, so that the composition of input CH_4 was diluted. On the other hand, the gas flow rate was adjusted by changing content of N_2. In this way, the initial volumetric ratio of CH_4 would be varied accordingly. The input gas composition and flow rate would be given in table 5-2.

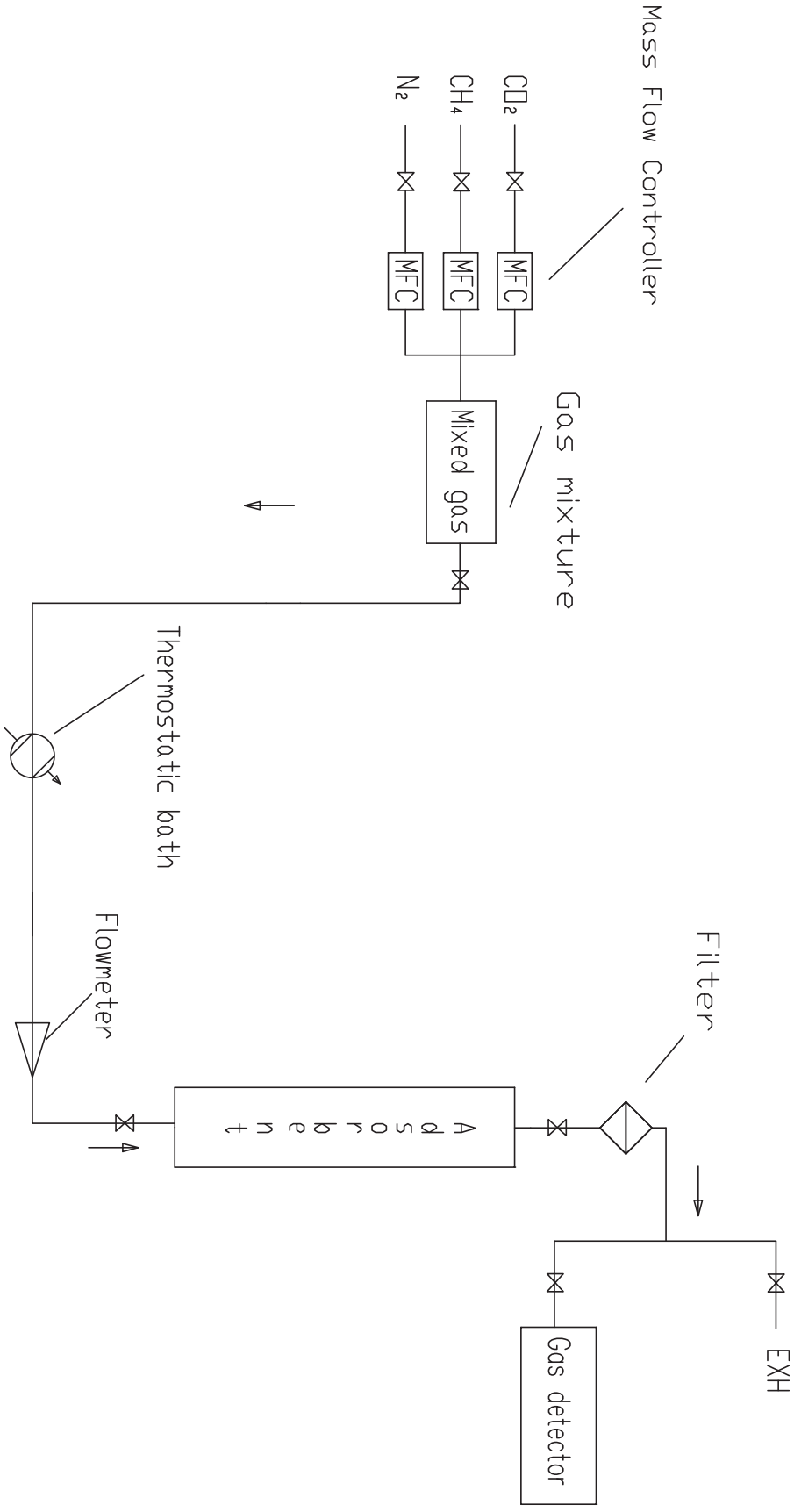

Figure 5-4: The Adsorption Processes.

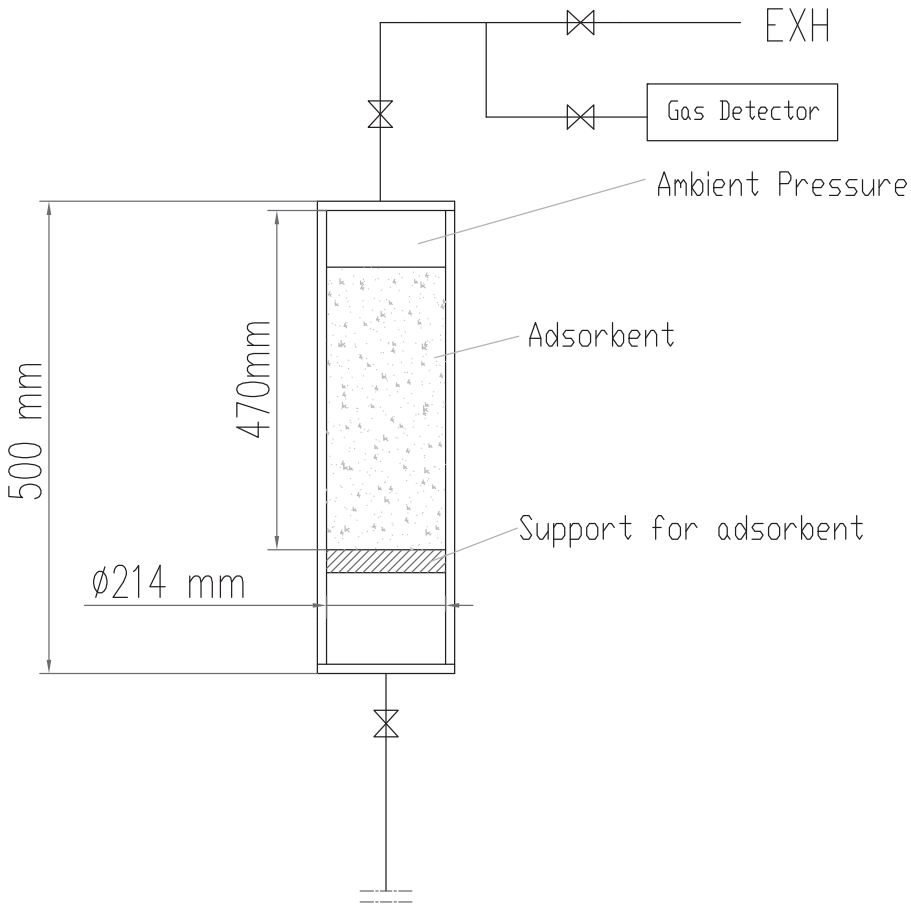

Figure 5-5: Reactor for Fixed Bed Adsorption.

5.2.1.2 Reactor and adsorbent The reactor was utilized as an adsorbent bed. In order to lower the pressure drop and avoid wall effects, the bed diameter must be as large as possible. For the adsorbent with mean particle diameters greater than 2.5 mm, it was required that the ratio of adsorption column inside diameter to mean particle diameters should be greater than 10 [86]. The sketch for reactor was drawn in figure 5-5. Seen from the measurements, the pressure drop was insignificant.

In the experiments of landfill gas purification, one of the important aspects was to evaluate the dynamic capacity of bottom ash for CO_2 in adsorption processes. That was, under the given conditions of gas flow rate, landfill gas composition, temperature, and pressure, a known amount of bottom ash was used as adsorbent, and the time of CO_2 breakthrough was measured. By varying the amount of bottom ash in fixed bed reactor, such measurement was repeated in the same conditions. The dynamic adsorption characteristics could be calculated by the function of breakthrough time and amount of bottom ash.

The amount of bottom ash was varied from 3.6 Kg to 14.4 Kg. In each experiment, the reactor was filled up with fresh bottom ash, tamped in bed, and flushed by N_2. The same procedures were repeated with a series of amount bottom ashes and input gas flow rates. The details were shown in table 5-2.

Table 5-2: **Experimental Conditions**

Series No.	**Bottom Ash [Kg]**	**Flow Rate [L·min^{-1}]**	**Landfill Gas [v.%]**	**Input Gas [v.%]**
1	3.6	0.975	CH_4: 28.9 CO_2: 70.1 O_2: 0.6 BAL.: 0.4	N/A
2	7.2	0.975	CH_4: 28.9 CO_2: 70.1 O_2: 0.6 BAL.: 0.4	N/A
3	10.8	0.975	CH_4: 28.9 CO_2: 70.1 O_2: 0.6 BAL.: 0.4	N/A
4	14.4	0.975	CH_4: 28.9 CO_2: 70.1 O_2: 0.6 BAL.: 0.4	N/A
5	3.6	2.273	CH_4: 30.4 CO_2: 69.6	CH_4: 11.4 CO_2: 18.1 N_2: 70.5
6	7.2	2.273	CH_4: 30.4 CO_2: 69.6	CH_4: 11.4 CO_2: 18.1 N_2: 70.5
7	10.8	2.273	CH_4: 30.4 CO_2: 69.6	CH_4: 11.4 CO_2: 18.1 N_2: 70.5
8	14.4	2.273	CH_4: 30.4 CO_2: 69.6	CH_4: 11.4 CO_2: 18.1 N_2: 70.5
9	3.6	2.143	CH_4: 29.6 CO_2: 70.4	CH_4: 8.9 CO_2: 13.7 N_2: 77.4
10	7.2	2.143	CH_4: 29.6 CO_2: 70.4	CH_4: 8.9 CO_2: 13.7 N_2: 77.4
11	10.8	2.143	CH_4: 29.6 CO_2: 70.4	CH_4: 8.9 CO_2: 13.7 N_2: 77.4
12	14.4	2.143	CH_4: 29.6 CO_2: 70.4	CH_4: 8.9 CO_2: 13.7 N_2: 77.4

Remark: In series of No. 1-No. 4, O_2 and other gas were introduced by gas in the exhaust pipe.

5.2.2 Adsorption results

As the subject for landfill gas purification, the content of CH_4 in effluent gas is one of interest. Before the experiments, fixed bed adsorbent and pipelines should be flushed by N_2, so as to keep CH_4 from gas in the processes. The input gas could be divided into two main categories: without carrier gas and with carrier gas N_2. The results of experiments would be discussed respectively.

5.2.2.1 Adsorption without carrier gas The experiments No. 1-No. 4 were performed without carrier gas. Results of No. 1 are shown in figure 5-6. As a matter of fact, the weight of bottom ash was 3.6 Kg, which occupied only about 20 % of adsorption bed in volume. The lower flow rate ensured the enough contact time between landfill gas and bottom ash.

On the other hand, the purge gas N_2 was not able to be driven out of reactor thoroughly. The volume of residual N_2 would vary as the amount of bottom ash varied in experiments. Although N_2 was just an inert gas in processes, the variable volume fraction might impact on the determination of CO_2 breakthrough time.

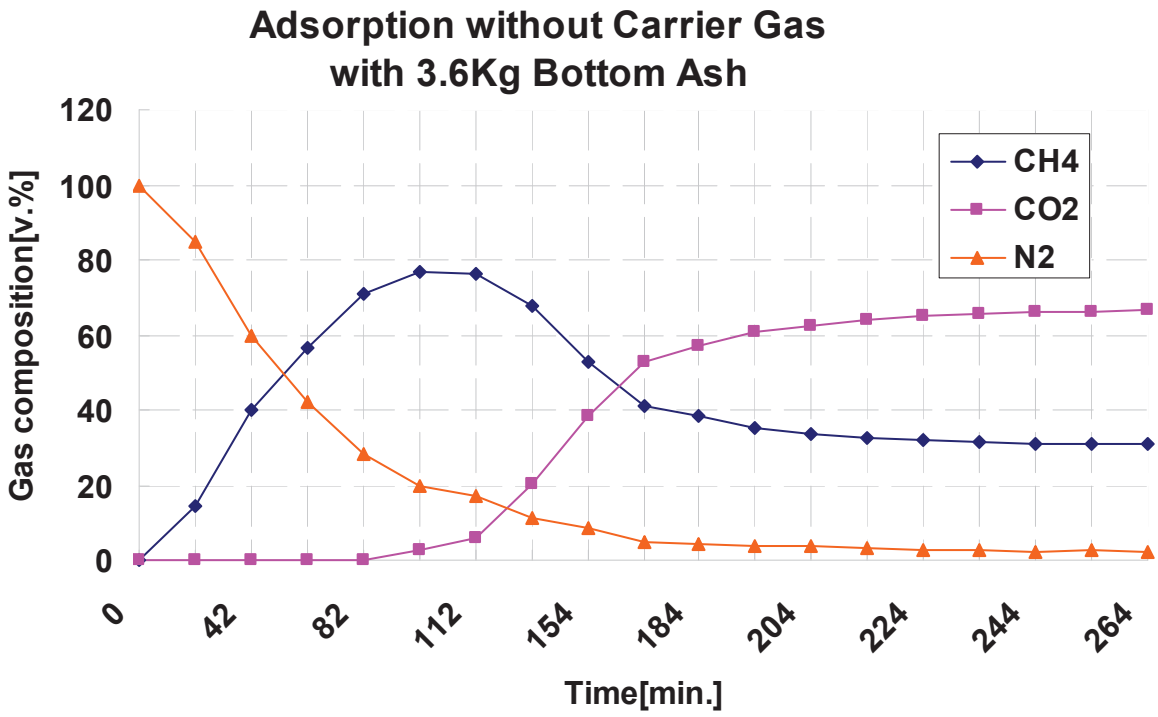

Figure 5-6: Adsorption Without Carrier Gas.

5.2.2.2 Adsorption with carrier gas In experiment No. 5-No. 12, N_2 was used as carrier gas in processes. As consequences, N_2 could keep the constant flow rate among the input gas phase, but the composition of CH_4 would be decreased and flow rate of input gas would be increased in the initial conditions. Figure 5-7 described the process of landfill gas adsorption with 3.6 Kg bottom ash, in which the input gas flow rate was 2.273 $L \cdot min^{-1}$.

On the purpose to record CO_2 breakthrough, a timer was started simultaneously when input gas started flowing into purification systems. The experiments would be ceased as the gas compo-

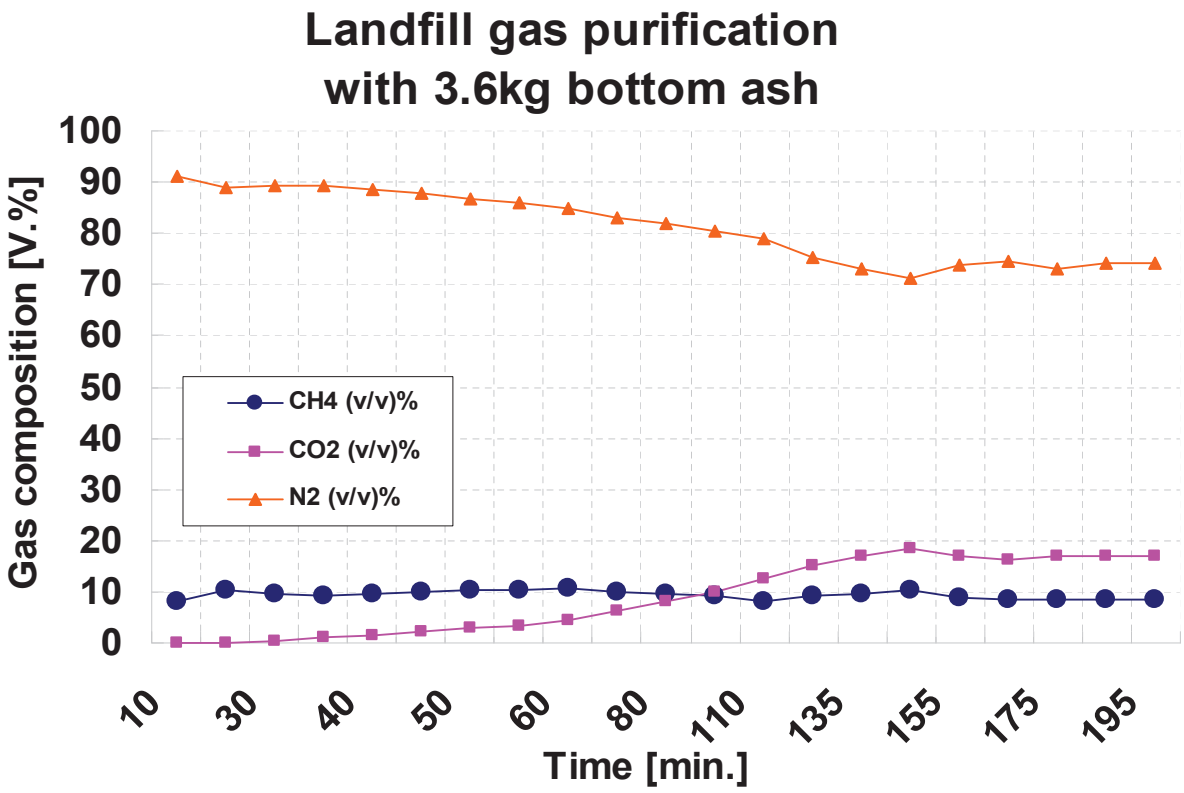

Figure 5-7: Adsorption with Carrier Gas.

sition achieved to constant. The bottom ash dynamic capacity would be calculated on 5 % CO_2 breakthrough. Such breakthrough times increased as amount of bottom ash increasing. Figure 5-8 showed the CO_2 uptake curve at influent rate of 2.273 L$\cdot$ min^{-1}, which corresponding to experiment No. 5-No. 8.

Compared data of figure 5-6 and figure 5-7, the flow rate impact CO_2 breakthrough time significantly. In experiment No. 1, 5 % CO_2 breakthrough time was oberserved after 100 minutes with input gas flow rate of 0.975 L$\cdot$ min^{-1}. By contrast, with the same amount of bottom ash, 5 % CO_2 breakthrough time occurred only 30 minutes later as gas with inflow rate of 2.273 L$\cdot$min^{-1}. Rather than time to breakthrough, breakthrough capacity of bottom ash seemed an necessary parameter to determine adsorption performance.

5.2.2.3 Breakthrough capacity of bottom ash In applications, the best adsorbent should have a high breakthrough capacity for adsorbate under operating conditions [87]. In order to determine the breakthrough capacity of bottom ash for removing CO_2 from landfill gas, the time to breakthrough point was recorded in every experiment. In this work, the breakthrough point was taken when the composition of CO_2 in the effluent gas reached 5 %.

The function of breakthrough time and bottom ash mass was linear, and the slope would equal to the following:

$$A = \frac{N}{C^0 Q_f}. \tag{5.10}$$

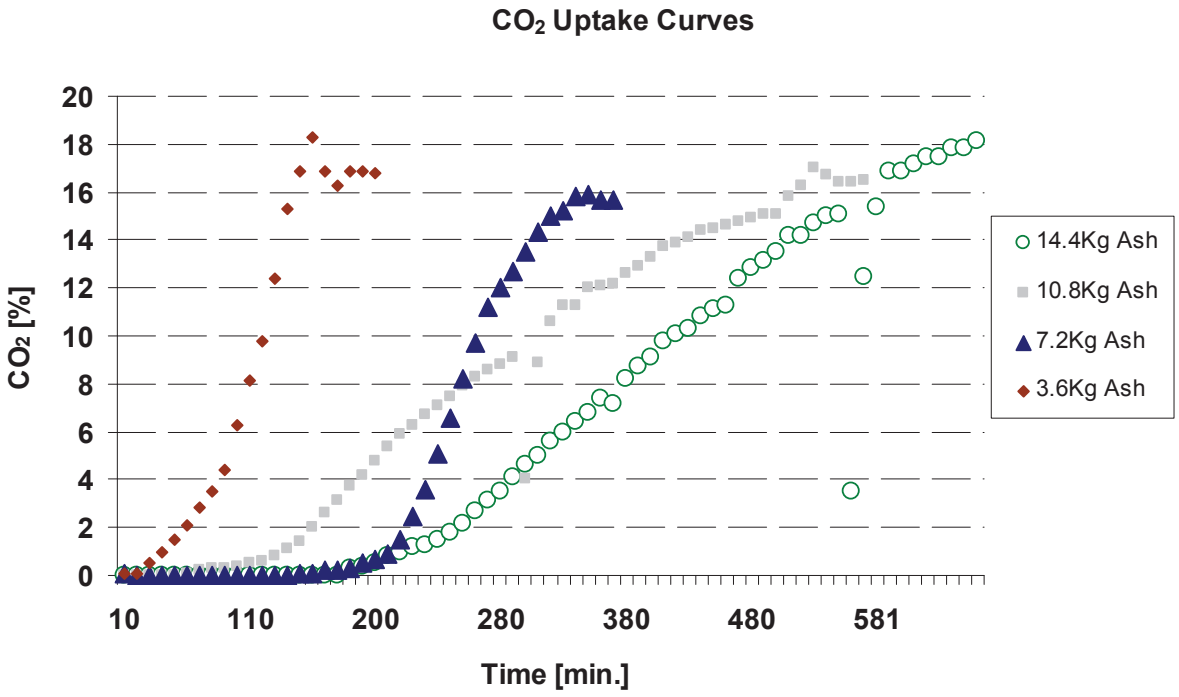

Figure 5-8: CO_2 Uptake Curves.

In which, N was the breakthrough capacity of the bottom ash; C^0 was the inlet concentration of CO_2, which could be calculated by the ratio of CO_2 mass flow rate to the input gas flow rate Q_f. Meanwhile, the interception of this function represented the critical mass for bottom ash.

The tests were taken at flow rate of 2.273 L$\cdot$ min^{-1} and 2.143 L$\cdot$ min^{-1} respectively. The dynamic capacities were listed in table 5-3. It could be observed from data, the breakthrough capacity of bottom ash was not only impacted by influent flow rate, and the inlet concentration of CO_2 should be taken into account. It was widely known that the lower input flow rate could increase contact time between gas and bottom ash. While, it is noteworthy that bottom ash adsorption capacity at high concentration of CO_2 was not necessarily the same as that at low concentration.

5.2.2.4 Bottom ash leachability In addition to landfill gas adsorption capacities, fresh and used bottom ash were analyzed in leachability. That is, around 100 g of each sample was dissolved in 1 L deionized water and shook for 24 hours. Then, bottom ash eluates were filtered and tested.

As table 5-4 shown, an significant reduction of chromium content was obtained with CO_2 adsorption. The chromium maximum average concentration was 0.03 mg/L in fresh sample. Whilst in used bottom ash, it was as low as 0.006 mg/L when 14.4 g bottom ash was used as adsorbent. Meanwhile, the concentration of cadmium in eluates remained very low.

It was noteworthy that, the phosphate content eluated from adsorption with carrier gas was considerably different from those without carrier gas. As the data shown in figure 5-9, taken 7.2 g adsorbent as example, phosphate from adsorption with carrier gas was only 0.024 mg/L, but it was as high as 0.332 mg/L for adsorption without carrier gas. In the adsorptions with carrier gas, both carbonation and hydration reactions could take place in processes. In which,

Table 5-3: **Bottom Ash Breakthrough Capacity**

Flow Rate [L·min^{-1}]	**Inlet CO_2** [g·L^{-1}]	**Ash Mass** [Kg]	**Time*** [min.]	**Breakthrough Capacity** [g CO_2·(Kg Ash)$^{-1}$]	**Critical Mass** [Kg]
2.143	0.2537	3.6	65	8.9858	1.3613
		7.2	100		
		10.8	65		
		14.4	275		
2.273	0.3479	3.6	30	11.0926	1.2475
		7.2	110		
		10.8	90		
		14.4	205		

*__Time__=16.5278·__Mass__$_{Ash}$-22.5000 at 2.143[L·min^{-1}]
*__Time__=14.0275·__Mass__$_{Ash}$-17.5000 at 2.273[L·min^{-1}]

Table 5-4: **Bottom Ash Leachability**

Samples	**Phosphate** [mg·L^{-1}]	**COD** [mg·L^{-1}]	**Chromium** [mg·L^{-1}]	**Cadmium** [mg·L^{-1}]	**Iron** [mg·L^{-1}]	**Nickel** [mg·L^{-1}]
Fresh Ash	0.684	19.4	0.03	<0.02	3.55	0.276
3.6 Kg Ash	0.154	21.7	0.016	<0.02	N/A	N/A
7.2 Kg Ash	0.178	25.1	0.012	<0.02	N/A	N/A
10.8 Kg Ash	0.361	22.2	0.005	<0.02	N/A	N/A
14.4 Kg Ash	0.175	21.3	0.006	<0.02	N/A	N/A

the excess $Ca(OH)_2$ produced by hydration would go on to react with phosphate in the surface of bottom ash. On the contrary, during the processes without carrier gas, both carbonation and hydration reactions were restrained by residual N_2. So that, phosphate was not able to take part in the further reactions completely.

5.2.2.5 Ks, pH value of bottom ash eluate Alkalinity determines the ability of a solution to react with protons to the equivalence point. The alkalinity is equal to the stoichiometric sum of the bases in solution. In the bottom ash eluate, carbonate and hydrogen carbonate tends to compose a majority of the total alkalinity.

Acid-base titration could be used to measure alkalinity. In this work, this method was performed according to standard DIN 38409. In the process of titration with 0.1 mol·L^{-1} hydrochloric acid, there were two turning points at curve. At pH value of 8.2, carbonic acid and its ions in solution would change into hydrogen carbonate ions mostly. In which point, the alkalinity could be calculated and denoted as $Ks_{8.2}$. At pH value of 4.3, both carbonic and hydrogen carbonate ions would change into dissolved carbon dioxide in eluate. So that, the total amount of alkalinity could be calculated with $Ks_{4.3}$, and the methods were given below:

$$\begin{aligned} \mathrm{Ks}_{8.2} &= \frac{\mathrm{C}_{\mathrm{HCl}} * V1 * 1000}{V3}, \\ \mathrm{Ks}_{4.3} &= \frac{\mathrm{C}_{\mathrm{HCl}} * V2 * 1000}{V3}. \end{aligned} \tag{5.11}$$

Where concentration of hydrochloric acid $\mathrm{C}_{\mathrm{HCl}}$ was given as 0.1 mol·L^{-1}, $V1$ was the volume

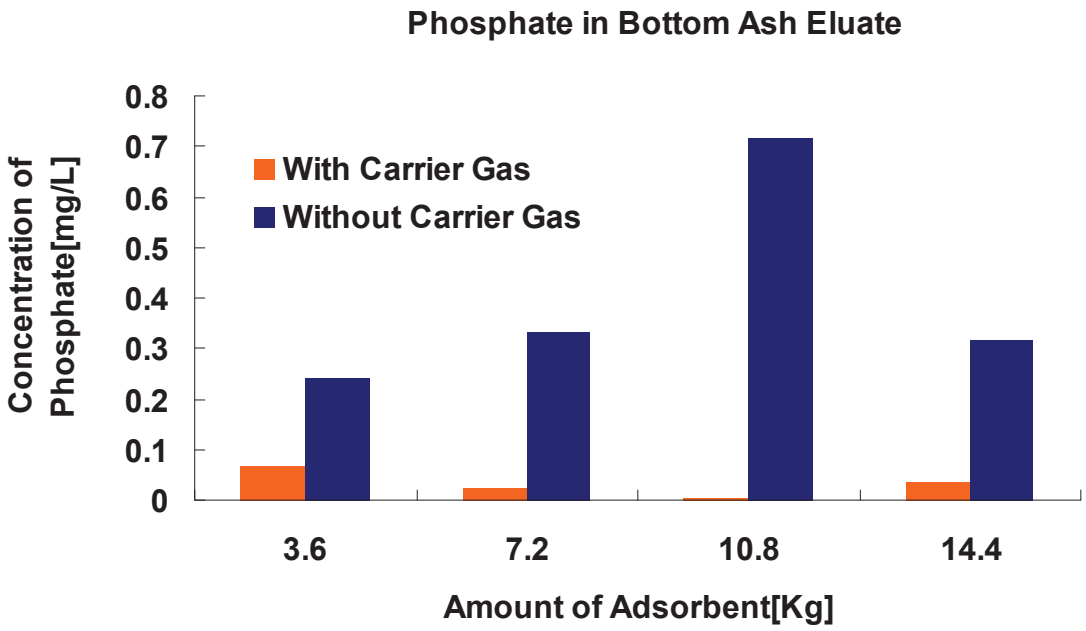

Figure 5-9: Phosphate in Bottom Ash Eluate.

Table 5-5: **Physical Parameters of Eluate**

Samples	**Ks$_{8.2}$** **[mol·L^{-1}]**	**Ks$_{4.3}$** **[mol·L^{-1}]**	**pH value**	**Electrical Conductivity [mS·cm^{-1}]**
Fresh Ash	36.06	38.13	12.83	7.92
3.6 Kg Ash	2.18	2.67	11.41	2.23
7.2 Kg Ash	1.78	2.46	11.77	2.10
10.8 Kg Ash	1.75	2.34	11.42	2.19
14.4 Kg Ash	1.70	2.12	11.26	2.30

of consumed hydrochloric acid at pH 8.2 in ml, $V2$ was the volume of consumed hydrochloric acid at pH 4.3 in ml, and $V3$ was the volume of bottom ash eluate, which was taken around 48 ml in test. The unit of alkalinity was described as mol·L^{-1}.

Besides, the pH was tested in every sample. Seen from the data in table 5-5, adsorption of CO_2 could effect alkalinity of bottom ash significantly. At the same time, although the pH value of eluate could be decreased in processes, it remained in alkaline conditions.

5.2.2.6 Electrical conductivity of bottom ash eluate Normally, the electrical conduction is contributed by ions in solution. The conductivity is not only related to the types of electrolyte, but to the concentration of them.

The electrical conductivities of bottom ash eluates were tested based on standard CEN 27888(C8). The data were listed in table 5-5. In the eluate of fresh bottom ash, the average electrical conductivity was as high as 7.92 mS·cm^{-1}. With application of adsorption, the value of conductivities could fall into range of 2.1 mS·cm^{-1}-2.3 mS·cm^{-1}.

Table 5-6: **Fitting Parameters**

Gas	**a**	**b**	**c**
CO_2	0.0329	1.5299	600.0035
CH_4	200.9744	-46.8905	N/A
N_2	29.0620	-57.5666	N/A

5.3 Landfill Gas Adsorption Equilibrium

In practice, the experiment on adsorption breakthrough was essential. The results of breakthrough curve at small scale could be used to design the adsorption column at a large scale.

As to this landfill gas adsorption experiment, input gas flow rate was low, and the adsorption pressure drop was ignorable. The adsorbed CO_2 could be assumed to be in the equilibrium state. The equilibrium was related to input gas flow rate, and the parameters could be obtained from the plot of concentration vs. time.

It was obvious that the total amount fed of gas φ^{α} to the fixed bed was:

$$\mathrm{Q}^{\alpha} = \int_{0}^{\mathrm{t}} \mathrm{F}\mathrm{c}^{0\alpha}\mathrm{d}\mathrm{t} = \mathrm{F}\mathrm{c}^{0\alpha}\mathrm{t} \tag{5.12}$$

in which, Q^{α} was molar amount of gas φ^{α}; F was the volumetric flow rate. And, $\mathrm{c}^{0\alpha}$ was the initial concentration of φ^{α}, which was related to volumetric composition of input gas φ^{α}:

$$\mathrm{c}^{0\alpha} = \frac{\mathrm{n}^{0\alpha}\rho^{\alpha\mathrm{R}}}{\mathrm{M}^{\alpha}_{\mathrm{ol}}} \tag{5.13}$$

where $\mathrm{n}^{0\alpha}$ was volumetric composition of input gas φ^{α}; $\rho^{\alpha\mathrm{R}}$ was the real density; and $\mathrm{M}^{\alpha}_{\mathrm{ol}}$ was the molar mass of gas φ^{α}.

For gas CH_4 and N_2 in mixture, the fraction of $\frac{\mathrm{Q}^{\alpha}}{\mathrm{q}^{\alpha}}$ was related to input molar amount Q^{α} linearly. Thus, the equilibrium concentration of gas φ^{α}, q^{α}, were written as:

$$\mathrm{q}^{\alpha} = \frac{\mathrm{Q}^{\alpha}}{\mathrm{a}\mathrm{Q}^{\alpha} + \mathrm{b}}. \tag{5.14}$$

Where, a and b are fitting parameters. On the other hand, CO_2 breakthrough curve was an ideal S-shaped. Therefore, its equilibrium function was given in form of:

$$\mathrm{q}_{\mathrm{CO_2}} = \frac{\mathrm{a}(\mathrm{Q}^{\mathrm{CO_2}})^2}{\mathrm{b}(\mathrm{Q}^{\mathrm{CO_2}})^2 + \mathrm{c}}. \tag{5.15}$$

Equation 5.14and 5.15are written in the similar form to that of the multisite Langmuir model [71], where a, b and c are fitting parameters respectively. Both the equations were fitted to the experimental data by numerical methods. The parameters are listed in table 5-6. And the plots of fitting results were shown in figures 5-10 - 5-12.

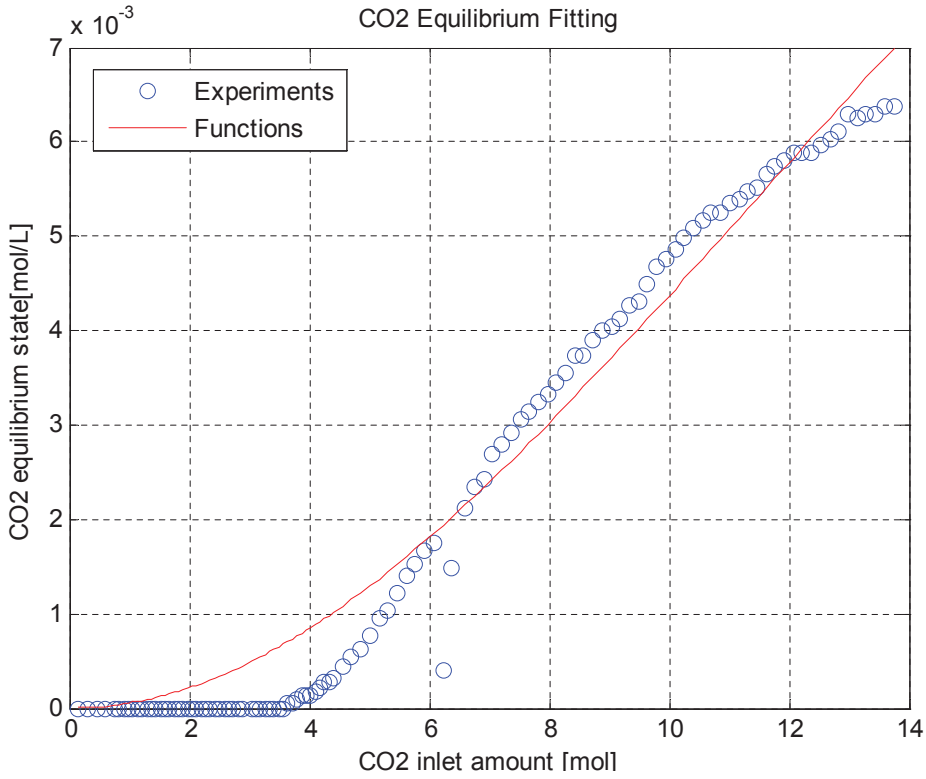

Figure 5-10: CO_2 Adsorption Equilibrium (Functions are described in form of equation 5.15).

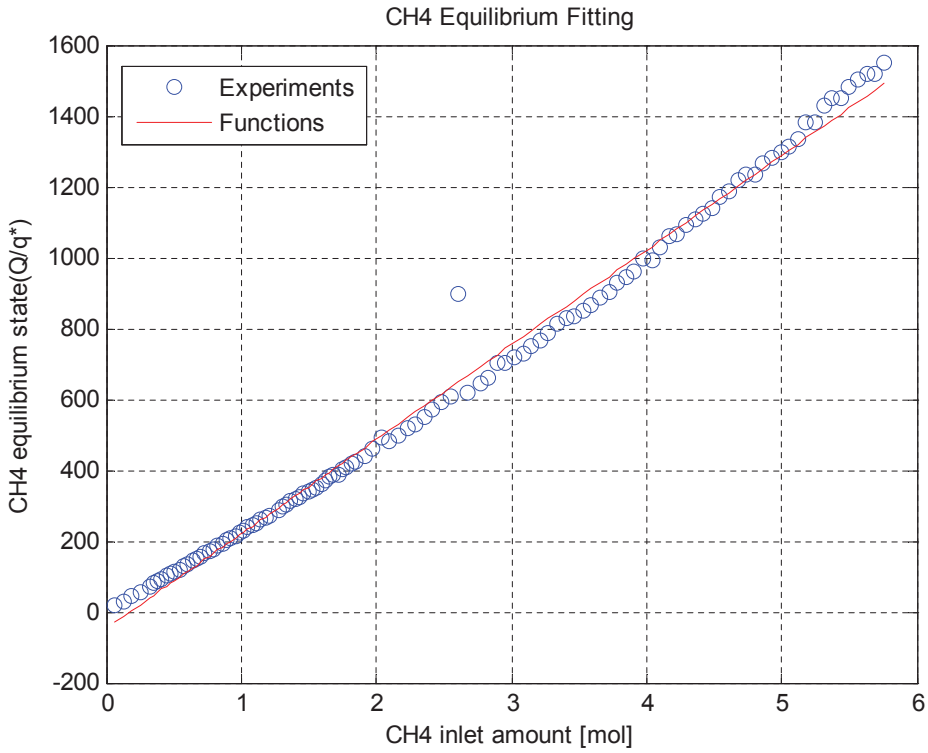

Figure 5-11: CH_4 Adsorption Equilibrium (Functions are described in form of equation 5.14).

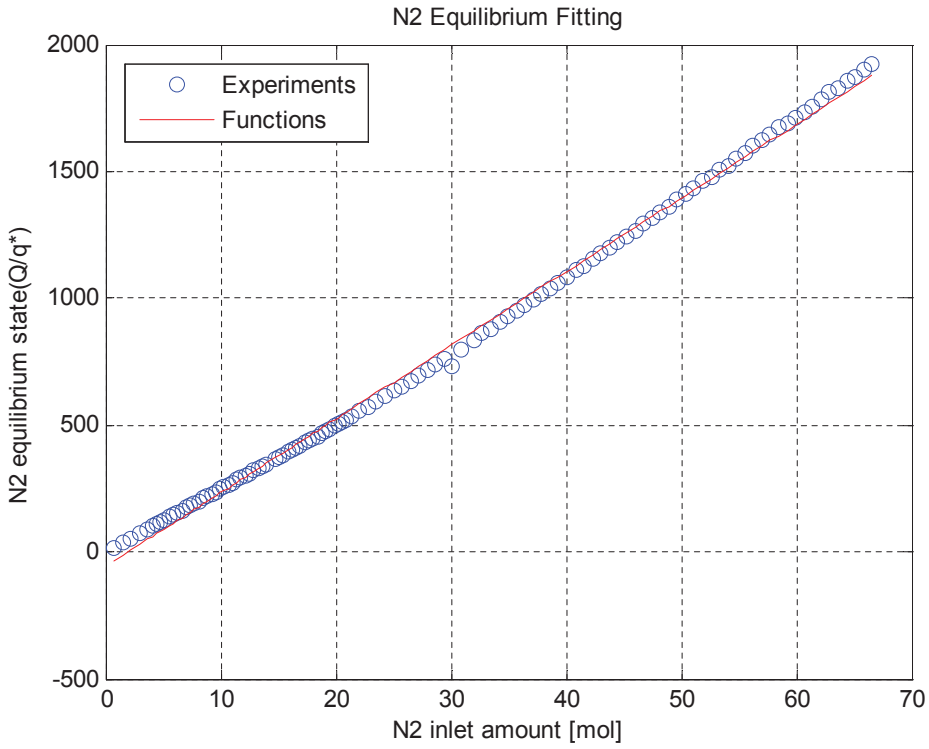

Figure 5-12: N_2 Adsorption Equilibrium (Functions are described in form of equation 5.14).

5.4 Interactions Between Landfill Gas and Bottom Ash

As the main constituents of landfill gas are CH_4 and CO_2, the purification of landfill gas with bottom ash have been caught more attention. Especially for the purpose of removing CO_2 for renewable energy utilization, the interact of CH_4 with bottom ash becomes essential. The solubility of CH_4 in water is low, and it is inert to mineral components of bottom ash. Thus, it is sensible to assume that CH_4 is not retained by bottom ash.

With respect to CO_2, it is well known for the carbonation reaction with bottom ash. The mechanisms are normally described as following: in the prior process, CO_2 is adsorbed on the bottom ash surface by pore water. In the aqueous medium, CO_2 reacts with calcium or other cations of bottom ash. As consequence, CO_2 is seized in the form of carbonate. The main irreversible reaction is the same as shown in equation 5.3.

In our laboratory, bottom ash samples were analyzed in elements (Elementar Analysensyteme GmbH). The data showed that bottom ash was a very heterogeneous material, but the difference between fresh and used bottom ash could be observed clearly. For the fresh bottom ash, C/N average value was 52.065, but the average value of used bottom ash has reached 78.819. As figure 5-13 showed, sample series 1 was taken from fresh bottom ash, the others were the representative samples of used bottom ashes. The analysis data confirmed that CO_2 could be connected by chemical bonds with bottom ash further.

Recently, the removal of H_2S in real landfill gas is studied as well [78]. In the aqueous phase of bottom ash, H_2S would dissociate in the following ways:

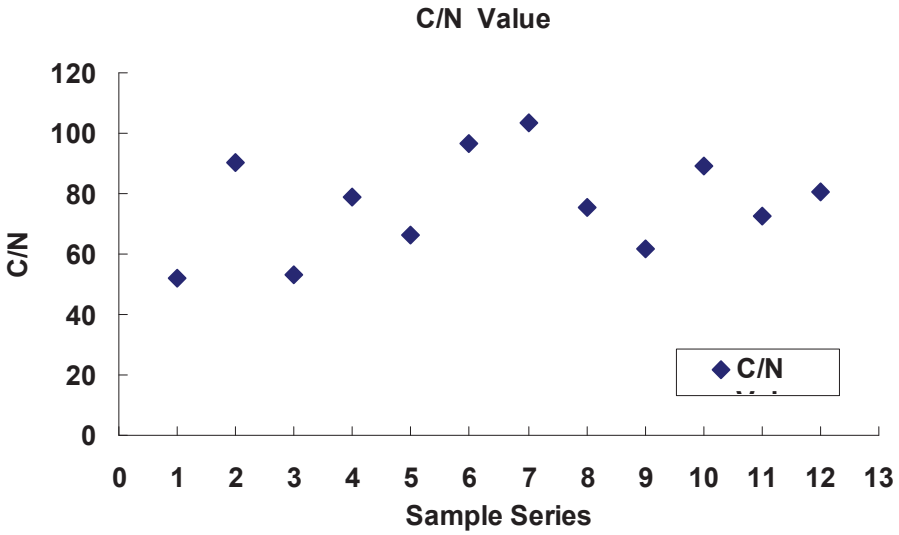

Figure 5-13: Element Analyses of Bottom Ash.

$$\begin{aligned} H_2S + H_2O &\rightleftharpoons HS^- + H_3O^+, \\ HS^- + H_2O &\rightleftharpoons S^{2-} + H_3O^+. \end{aligned} \tag{5.16}$$

It was obvious seen from the reactions of equation 5.16, the water content of bottom ash would effect the removal of H_2S. Furthermore, both of the fresh and carbonated bottom ash could be useful in the purification towards H_2S.

5.5 Conclusions

Landfills and incineration are the two main municipal solid waste management methods. As a by-product of landfills, landfill gas can be used as renewable energy source-CH_4 could be obtained by landfill gas purification.

With respect to municipal solid waste incineration, bottom ash is the most significant by-product. Nowadays, the utilization of bottom ash has received a lot of interest. The analyses of bottom ash physicochemical properties indicate that it is potentially be used for CO_2 removal.

Therefore, landfill gas adsorption with bottom ash was investigated in this work. The tests of bottom ash eluate showed alkalinity, phosphate and chromium contents reduced as CO_2 was adsorbed. The experiments of CO_2 breakthrough capacity with bottom ash were performed. The experimental and calculated data showed CO_2 capacity was related to input gas flow rate and composition.

According to the plot of breakthrough curves, landfill gas equilibrium equations were fitted as well. The data would offer some details in simulations. At last, landfill gas interaction with bottom ash was discussed. Owing to the carbonation reaction on bottom ash, CO_2 could be removed in the adsorption processes.

6 Diffusion Coefficients of Landfill Gas

Diffusion normally occurs in gases systems. Maxwell-Stefan diffusion equation and Fick's law can be used to describe diffusions. In this section, both of them will be discussed and compared. In order to meet particlar applications in engineering, diffusion coefficients can be estimated in theory. One of methods of evaluating landfill gas mixture diffusion coefficients is to be introduced over here.

6.1 Maxwell-Stefan Equations

As Maxwell quoted earlier that diffusion and convection always occur together. However, for the dilute solutions, the diffusion of constituent φ^α can be described by Maxwell-Stefan equations simply, which developed by Maxwell [88] and Stefan [89]. In an ideal gas system at constant temperature and pressure, driving force may be related to velocity difference between constituents. Therefore, definition of convection in a sigle phase could be carefully avoid.

6.1.1 Binary systems

Normally, the driving force of constituent φ^α is equal to the composition gradient grad n^α_{mol} at constant pressure. And in a system, driving forces are restricted to a condition:

$$\sum_{\alpha=1}^{n} \mathrm{grad}\ \mathrm{n}^\alpha_{mol} = 0. \tag{6.1}$$

Thus, the binary diffusion of constituent φ^α may be written as:

$$\mathrm{grad}\ \mathrm{n}^\alpha_{mol} = -\frac{\mathrm{n}^\alpha_{mol}\mathrm{n}^\beta_{mol}(\boldsymbol{u}_\alpha - \boldsymbol{u}_\beta)}{D^{\alpha\beta}}. \tag{6.2}$$

In which, n^α_{mol} is the mole fraction of constituent φ^α, n^β_{mol} is the mole fraction of constituent φ^β; $\boldsymbol{u}_\alpha$ denotes the velocity of constituent φ^α(with respect to a stationary coordinate reference frame) [90], $\boldsymbol{u}_\beta$ denotes the velocity of constituent φ^β, and $D^{\alpha\beta}$ is the Maxwell-Stefan binary diffusion coefficient. Seen from equation 6.1and equation 6.2, the Maxwell-Stefan binary diffusion coefficients are symmetric, that is

$$D^{\alpha\beta} = D^{\beta\alpha}. \tag{6.3}$$

6.1.2 Multicomponent systems

In the ideal gas systems, *n*-multicomponent diffusions are able to be described by Maxwell-Stefan equation as well. The equations are given in terms of the diffusion fluxes J^α:

$$\mathrm{grad}\ \mathrm{n}^\alpha_{mol} = -\sum_{\alpha=1}^{n} \frac{(\mathrm{n}^\alpha_{mol}\mathrm{J}^\beta - \mathrm{n}^\beta_{mol}\mathrm{J}^\alpha)}{\mathrm{c}D^{\alpha\beta}}. \tag{6.4}$$

Where, c is the total molar concentration of multicomponent. It is defined as:

$$\mathrm{c} = \sum_{\alpha=1}^{n} \mathrm{c}^{\alpha}, \tag{6.5}$$

c^{α} is the molar concentration of constituent φ^{α}.

It is noteworthy that in a *n*-multicomponent system, only *n-1* driving forces are independent. Accordingly, the driving force of constituent φ^{α} in nonideal fluids can be given in the term of $\sum_{\alpha=1}^{n-1} \Gamma^{\alpha\beta} \mathrm{grad}\ \mathrm{n}_{mol}^{\alpha}$ with $\Gamma^{\alpha\beta}$ as the thermodynamic factor [90], which defined as:

$$\Gamma^{\alpha\beta} = \delta^{\alpha\beta} + \mathrm{n}_{mol}^{\alpha} \frac{\partial \ln \gamma^{\alpha}}{\partial \mathrm{n}_{mol}^{\beta}}, \tag{6.6}$$

where γ^{α} is the activity coefficient of constituent φ^{α}. $\delta^{\alpha\beta}$ is Kronecker delta, and it can be defined as:

$$\begin{aligned} \delta^{\alpha\beta} &= 1 \quad \text{if } \alpha = \beta \\ \delta^{\alpha\beta} &= 0 \quad \text{if } \alpha \neq \beta. \end{aligned} \tag{6.7}$$

The thermodynamic factor Γ is able to be calculated by Non-Random Two-Liquid (NRTL)equation [91]. The value of γ^{α} is normally given in some references [90] [91].

If the coefficients $B^{\alpha\alpha}$ and $B^{\alpha\beta}$ are defined by:

$$\begin{aligned} B^{\alpha\alpha} &= \frac{\mathrm{n}_{mol}^{\alpha}}{D^{\alpha \mathrm{n}}} + \sum_{\substack{\gamma=1 \\ \alpha \neq \gamma}}^{\mathrm{n}} \frac{\mathrm{n}_{mol}^{\gamma}}{D^{\alpha\gamma}} \\ B^{\alpha\beta} &= -\mathrm{n}_{mol}^{\beta} \left(\frac{1}{D^{\alpha\beta}} - \frac{1}{D^{\alpha \mathrm{n}}} \right), \end{aligned} \tag{6.8}$$

equation 6.4 thus can be written in the form of *n-1*×*n-1* matrix:

$$(\mathrm{J}) = -\mathrm{c}[B]^{-1}[\Gamma](\mathrm{grad}\ \mathrm{n}_{mol}). \tag{6.9}$$

in which, $[B]$ is a square matrix of order *n-1*. For the multicomponent ideal gas mixtures, Maxwell-Stefan diffusion coefficients $D^{\alpha\beta}$ satisfies condition of equation 6.3.

6.2 Fick's law

At around the same time when Maxwell-Stefan diffusion developed, another diffusion equation was studied by series of experiments [92], named Fick's law [93].

6.2.1 Flux

The one-dimensional flux was defined as:

$$\mathrm{J}^{\alpha} = -\mathrm{D}_{Fick}^{\alpha} \frac{\partial \mathrm{c}^{\alpha}}{\partial \mathrm{z}} \tag{6.10}$$

where J^{α} is the flux per unit area, $D^{\alpha\beta}_{Fick}$ is diffusion coefficient of substance φ^{α}, and z is distance. This equation describes the steady diffusion in a one substance system.

In practice, some mass transfer phenomena, like adsorption and distillation, are more complicated. The flux is combined with diffusion and convective flow. If N_{α} denotes the molar flux of constituent φ^{α}, it can be defined by:

$$N_{\alpha} = c^{\alpha} u_{\alpha}. \tag{6.11}$$

In a one-phase system, which comprised of *n* constitutes, the molar average velocity *u* would be calculated as:

$$u = \sum_{\alpha=1}^{n} n^{\alpha}_{mol} u_{\alpha}. \tag{6.12}$$

where n^{α}_{mol} is the mole fraction of φ^{α}.

As mentioned above, the total flux is related to diffusion flux and convective flow. If the molar average velocity *u* is chosen as the reference velocity, the molar diffusion flux of constituent φ^{α} would be:

$$J^{\alpha} = c^{\alpha}(u_{\alpha} - u), \tag{6.13}$$

and in a system, J^{α} should satisfy conditions:

$$\sum_{\alpha=1}^{n} J^{\alpha} = 0. \tag{6.14}$$

In a two-phase (phase a and phase b) system including a phase interface, a boundary condition must be satisfied at the interface:

$$c^{\alpha}_{a}(u_{\alpha a} - u) = c^{\alpha}_{b}(u_{\alpha b} - u), \tag{6.15}$$

where reference velocity *u* is that of interface, c^{α}_{a} and c^{α}_{b} are the molar concentration of constituent φ^{α} in phase a and phase b respectively. That is, the flux of constituent φ^{α} with respect to the interface should go through the phase boundary continuously.

Furthermore, the molar flux N_{α} of constituent φ^{α} could be divided into two terms:

$$N^{\alpha} = c^{\alpha}(u_{\alpha} - u) + c^{\alpha} u = J^{\alpha} + c^{\alpha} u, \tag{6.16}$$

where J^{α} is diffusion flux which has been introduced above, and the term of $c^{\alpha}u$ describes the convection. In the same way, mass diffusion flux can be calculated by mass average velocity and mass flux.

6.2.2 Binary diffusion

In order to simplify the following diffusion equations, the partial molar volumes are assumed as constant. In binary mixtures, the diffusion flux J^{α} is normally related to the mole fraction

gradient, that is:

$$\mathrm{J}^{\alpha} = \mathrm{c}^{\alpha}(u_{\alpha} - u) = -\mathrm{cD}^{\alpha\beta}_{\mathbf{Fick}}\ \mathrm{grad}\ \mathrm{n}^{\alpha}_{\mathbf{mol}} \tag{6.17}$$

in which, c is the total molar concentration of binary mixtures, $\mathrm{D}^{\alpha\beta}_{Fick}$ is the Fick diffusion coefficient.

Diffusion flux J^{β} would be given as analogous relate:

$$\mathrm{J}^{\beta} = \mathrm{c}^{\beta}(u_{\beta} - u) = -\mathrm{cD}^{\beta\alpha}_{\mathbf{Fick}}\ \mathrm{grad}\ \mathrm{n}^{\beta}_{\mathbf{mol}}. \tag{6.18}$$

Obviously, diffusions flux and mole fractions should satisfy

$$\begin{aligned} \mathrm{J}^{\alpha} + \mathrm{J}^{\beta} &= 0 \\ \mathrm{n}^{\alpha}_{mol} + \mathrm{n}^{\beta}_{mol} &= 1. \end{aligned} \tag{6.19}$$

Thus, there is only one diffusion coefficient relative to molecular diffusion in a binary system. That is,

$$\mathrm{D}^{\alpha\beta}_{Fick} = \mathrm{D}^{\beta\alpha}_{Fick}. \tag{6.20}$$

Actually, there is only one independent diffusion flux J^{α} and gradient of mole fraction grad $\mathrm{n}^{\alpha}_{mol}$ in binary mixtures.

6.2.3 Multicomponent diffusion

According to the given condition of equation 6.14, there are two independent diffusion fluxes and mole fraction gradients in ternary mixtures. Assuming the relation between fluxes and fraction gradients is linear, the diffusion fluxes may be written as:

$$\begin{aligned} \mathrm{J}^{\alpha} &= -\mathrm{CD}^{\alpha\alpha}_{multi}\ \mathrm{grad}\ \mathrm{n}^{\alpha}_{mol} - \mathrm{CD}^{\alpha\beta}_{multi}\ \mathrm{grad}\ \mathrm{n}^{\beta}_{mol} \\ \mathrm{J}^{\beta} &= -\mathrm{CD}^{\beta\alpha}_{multi}\ \mathrm{grad}\ \mathrm{n}^{\alpha}_{mol} - \mathrm{CD}^{\beta\beta}_{multi}\ \mathrm{grad}\ \mathrm{n}^{\beta}_{mol}. \end{aligned} \tag{6.21}$$

$\mathrm{D}^{\beta\alpha}_{multi}$ is the multicomponent diffusion coefficient. It is noteworthy, the diffusion coefficient $\mathrm{D}^{\beta\alpha}_{multi} \neq \mathrm{D}^{\alpha\beta}_{multi}$. The values of multicomponent diffusion coefficients depend on the choice of constituent φ^{α} in a system.

In a *n*-component system, there are *n-1* independent diffusion flux. The Fick's law is therefore defined as:

$$\mathrm{J}^{\alpha} = -\mathrm{c}\sum_{\beta=1}^{n-1} \mathrm{D}^{\alpha\beta}_{multi}\ \mathrm{grad}\ \mathrm{n}^{\beta}_{mol}. \tag{6.22}$$

In a *n*-component system, it is a *n-1*×*n-1* matrix. Thus, the diffusion coefficients in Fick's law could be written in the form of a *n-1*×*n-1* matrix

$$[\mathrm{D}]_{Fick} = \begin{bmatrix} \mathrm{D}_{multi}^{11} & \mathrm{D}_{multi}^{12} & \cdots & \mathrm{D}_{multi}^{1,n-1} \\ \mathrm{D}_{multi}^{21} & \mathrm{D}_{multi}^{22} & \cdots & \mathrm{D}_{multi}^{2,n-1} \\ \vdots & & & \vdots \\ \mathrm{D}_{multi}^{n-1,1} & \mathrm{D}_{multi}^{n-1,2} & \cdots & \mathrm{D}_{multi}^{n-1,n-1} \end{bmatrix}. \tag{6.23}$$

The matrix of $[\mathrm{D}]_{Fick}$ is generally nonsymmetrical. The matrix of multicomponenet diffusion coefficients are determined by compositions of the mixtures.

6.3 Diffusion Coefficients in Gases

Some binary and multicomponent Fick diffusion coefficients can be measured by the diffusion apparatus. However, in engineering calculations these experimental data are unusually fulfill the demands of every particular situation. Thus, it is necessary to estimate diffusion coefficients in theories.

6.3.1 Fick and Maxwell-Stefan diffusion coefficients

The relation between Maxwell-Stefan equation and Fick's law are in the form of:

$$\mathrm{D}_{Fick}^{\alpha\beta} = B^{-1}\Gamma = D^{\alpha\beta}\Gamma. \tag{6.24}$$

In ideal conditions, the thermodynamic factor Γ equation is unity. For an ideal binary-gas system, the relation can be given as:

$$\mathrm{D}_{Fick}^{\alpha\beta} = B^{-1}, \tag{6.25}$$

similarly,

$$[\mathrm{D}]_{Fick} = [B]^{-1} \tag{6.26}$$

is valid for ideal gas mixtures.

6.3.2 Chapman-Enskog theory

As has been known, diffusion coefficients can be estimated theoretically. One of common methods is Chapman-Enskog theory [94]. This theory is analyzed based on the assumption that molecular interactions take place in dilute gases. The results of Chapman-Enskog theory can be simplified into the form:

$$D^{\alpha\beta} = 1.883 \times 10^{-2}\theta^{3/2}\frac{\sqrt{\mathrm{M}_{\mathrm{ol}}^{\alpha} + \mathrm{M}_{\mathrm{ol}}^{\beta}}}{P\sigma_{\alpha\beta}^{2}\Omega_{\mathrm{D}}\sqrt{\mathrm{M}_{\mathrm{ol}}^{\alpha}\mathrm{M}_{\mathrm{ol}}^{\beta}}} \tag{6.27}$$

in which, $\mathrm{M}_{\mathrm{ol}}^{\alpha}$ is molar mass of constituent φ^{α}, θ is the absolute temperature, P is pressure.

The collision diameter $\sigma_{\alpha\beta}$ is the arithmetic average of the two constitutes:

$$\sigma_{\alpha\beta} = \frac{1}{2}(\sigma_{\alpha} + \sigma_{\beta}). \tag{6.28}$$

The dimensionless parameter Ω_{D} is the function of temperature and intermolecular potential field. Normally Ω_{D} can be found as the function $k_{\mathrm{B}}\theta/\varepsilon_{\alpha\beta}$, where k_{B} is the Boltzmann constant, $\varepsilon_{\alpha\beta}$ is a geometric average of contributions from the two constitutes:

$$\varepsilon_{\alpha\beta} = \sqrt{\varepsilon_{\alpha}\varepsilon_{\beta}}. \tag{6.29}$$

The physical data of parameters could be obtained from the literatures [92] [95]. In this way, the inverse matrix of binary diffusion coefficient B and Fick diffusion coefficients $\mathrm{D}_{Fick}^{\alpha\beta}$ can be estimated.

6.3.3 Diffusion coefficients in ternary gases system

In the ternary system, elements of matrix $[B]$ can be calculated as:

$$\begin{aligned}
B^{\alpha\alpha} &= \frac{\mathrm{n}_{mol}^{\alpha}}{D^{\alpha\gamma}} + \frac{\mathrm{n}_{mol}^{\beta}}{D^{\alpha\beta}} + \frac{\mathrm{n}_{mol}^{\gamma}}{D^{\alpha\gamma}} \\
B^{\alpha\beta} &= -\mathrm{n}_{mol}^{\alpha}\left(\frac{1}{D^{\alpha\beta}} - \frac{1}{D^{\alpha\gamma}}\right) \\
B^{\beta\alpha} &= -\mathrm{n}_{mol}^{\beta}\left(\frac{1}{D^{\alpha\beta}} - \frac{1}{D^{\beta\gamma}}\right) \\
B^{\beta\beta} &= \frac{\mathrm{n}_{mol}^{\alpha}}{D^{\alpha\beta}} + \frac{\mathrm{n}_{mol}^{\beta}}{D^{\beta\gamma}} + \frac{\mathrm{n}_{mol}^{\gamma}}{D^{\beta\gamma}}.
\end{aligned} \tag{6.30}$$

Thus, the elements of matrix $[\mathrm{D}]_{Fick}$ are:

$$\begin{aligned}
\mathrm{D}_{multi}^{\alpha\alpha} &= \frac{D^{\alpha\gamma}(\mathrm{n}_{mol}^{\alpha}D^{\beta\gamma} + (1-\mathrm{n}_{mol}^{\alpha})D^{\alpha\beta})}{\mathrm{n}_{mol}^{\alpha}D^{\beta\gamma} + \mathrm{n}_{mol}^{\beta}D^{\alpha\gamma} + \mathrm{n}_{mol}^{\gamma}D^{\alpha\beta}} \\
\mathrm{D}_{multi}^{\alpha\beta} &= \frac{\mathrm{n}_{mol}^{\alpha}D^{\beta\gamma}(D^{\alpha\gamma} - D^{\alpha\beta})}{\mathrm{n}_{mol}^{\alpha}D^{\beta\gamma} + \mathrm{n}_{mol}^{\beta}D^{\alpha\gamma} + \mathrm{n}_{mol}^{\gamma}D^{\alpha\beta}} \\
\mathrm{D}_{multi}^{\beta\alpha} &= \frac{\mathrm{n}_{mol}^{\beta}D^{\alpha\gamma}(D^{\beta\gamma} - D^{\alpha\beta})}{\mathrm{n}_{mol}^{\alpha}D^{\beta\gamma} + \mathrm{n}_{mol}^{\beta}D^{\alpha\gamma} + \mathrm{n}_{mol}^{\gamma}D^{\alpha\beta}} \\
\mathrm{D}_{multi}^{\beta\beta} &= \frac{D^{\beta\gamma}(\mathrm{n}_{mol}^{\beta}D^{\alpha\gamma} + (1-\mathrm{n}_{mol}^{\beta})D^{\alpha\beta})}{\mathrm{n}_{mol}^{\alpha}D^{\beta\gamma} + \mathrm{n}_{mol}^{\beta}D^{\alpha\gamma} + \mathrm{n}_{mol}^{\gamma}D^{\alpha\beta}}.
\end{aligned} \tag{6.31}$$

In the processes of landfill gas adsorption, the gas phase was actually a ternary-gases mixture. Therefore, the Fick diffusion coefficients of CO_2-CH_4-N_2 could be estimated in theories. Giving the input flow rate was 2.143 L·min^{-1}, landfill gas diffusion coefficients in gases could be calculated at 298.15K. The Maxwell-Stefan diffusion coefficients could be calculated according to

Table 6-1: **Maxwell-Stefan Diffusion Coefficients**

No.	**Constituent**	σ **[Å]**	$\varepsilon_{\alpha\beta}/k_{\mathrm{B}}\theta$ **[K]**	$\mathbf{D}^{12}$ **[cm^2·sec^{-1}]**	$\mathbf{D}^{13}$ **[cm^2·sec^{-1}]**	$\mathbf{D}^{32}$ **[cm^2·sec^{-1}]**
1	CO_2	3.941	195.2			
2	CH_4	3.758	148.6	0.1601	0.1474	0.2105
3	N_2	3.798	71.4			
Note: parameters were selected from works of E. L. Cussler [92]						

Table 6-2: **Fick Diffusion Coefficients**

No.	**Constituent**	$\mathbf{n}_{mol}$	$\mathbf{D}^{11}_{multi}$ **[cm^2·sec^{-1}]**	$\mathbf{D}^{12}_{multi}$ **[cm^2·sec^{-1}]**	$\mathbf{D}^{21}_{multi}$ **[cm^2·sec^{-1}]**	$\mathbf{D}^{22}_{multi}$ **[cm^2·sec^{-1}]**
1	CO_2	0.1376				
2	CH_4	0.0890	0.1483	-0.0022	0.0043	0.2016
3	N_2	0.7734				

Chapman-Enskog theory. The parameters and results were listed in table 6-1. The Fick diffusion coefficients were estimated based on equation 6.31, and the results were listed in table 6-2.

6.4 Conclusions

In gases mixed system, diffusion occurs frequently. However, the experimental values of multicomponent diffusion coefficients are fragmentary. For the purpose of engineering calculation, estimation of diffusion coefficients becomes important. Multicomponent diffusion can be described by Maxwell-Stefan equation and Fick's law. These thermodynamics treatments provide some useful methods in diffusion coefficients calculation. In this section, Chapman-Enskog theory is introduced and used to estimate diffusion coefficients of landfill gas systems.

7 Modelling and Simulation on Landfill Gas Adsorption

The experiments on landfill gas adsorption by bottom ash have been discussed previously. For the purpose of engineering, design of multicomponent adsorption columns is a fascinating project. Therefore, the modeling of adsorption phenomena and the use of these models in the simulation is a cost-effective and time-saving approach.

As the elements of the mixture theory described, the porous media can be treated as "smeared" substitute continua with reduced densities for the solid and fluid phases arise [96]. In the 1970s, with the development in combination of the volume fraction concept and the elements of the mixture theory [97], the balance equation of equilibrated forces and of equilibrated inertia was supplemented with continuum mechanics [98]. Then, Lagrange multipliers were introduced to the entropy-inequality and volume fraction condition was considered as a constraint, in order to gain restrictions for the constitutive relations [99]. In the early 1990s, the developed porous media models were implanted into numerical methods, and the study in the saturated and empty porous solids' behavior was of interest [100]. Recently, to improve the fundamentals of the porous media theory become new attempt again. Especially, the theory on multi-component [101] and compressibility of porous solid [102] have been worked out.

Landfill gas adsorption with bottom ash is actually the phenomena of multiphase flow and transport through porous media. As the porous media, solids can contain closed and open pores so that it can be filled with fluids. However, the exact description of location of pores and solid material is nearly impossible. In the study of porous media, the pore space within the solid generally is assumed to be continuous, and thus fluid is able to flow through the porous media continuously. In the present of multiphase flow, the focus is not only on the behaviors of each phase, the mechanical interactions between the phases are to be taken into account as well.

The mass balance and momentum balance are the fundamental concepts of mass transfer [103]. Based on these principles, various experimental phenomena can be expressed as mathematical equations. However, the equations can not be used to describe the system behaviors alone. In fact, the number of unknowns in system is greater than that of balance equations. Some functions of system dynamics will be supplemented hence. The governing equations and constitutive relations among system variables can be developed into the model systems of interest. With application of simulation models, the system behaviors will be predicted under different conditions.

7.1 Phase and Porous Media

A phase is a liquid, solid, or gas within which all physical properties are essentially uniform. In multiphase models, each of the phases is considered to have a separately defined volume fraction and velocity. The behaviour of each constituents in a phase can be described by balance equations respectively. In addition, mass, momentum and energy transfer may occur between phases. Thus, the sharp discontinuities in composition or temperature may exist at the interfaces between phases.

Porous media are materials containing pores. The sets of physical attributes distinguished them from the general multiphase systems. In a specified control volume, the porous media generally include a solid phase and at least a fluid phase. In order to formulate porous media flow modeling, the solid phase is assumed to contain the multiply-connected spaces so that fluid phase is

able to flow within the systems. Furthermore, the pores of porous media are considered to distribute statistically, and an arbitrary volume element in the reference and the actual placement is composed of the volume elements of the real constituents.

Provided that there is a porous medium, which is comprised of a porous solid phase B_S with the boundary $\partial \mathrm{B}_S$, and κ individual constituents φ^α with real volumes v^α, in the actual placement. It can be described by volume fraction. This fraction of constituent φ^α can be formulated as:

$$\mathrm{n}^\alpha(\mathrm{x}, t) = \frac{\mathrm{d}v^\alpha}{\mathrm{d}v}, \tag{7.1}$$

in which, n^α(x,*t*) is the volume fraction of constituent φ^α at position x and time t, dv^α and dv are the partial volume element of φ^α and the total volume respectively.

The volume fractions satisfy the volume fraction condition for κ constituents φ^α,

$$\sum_{\alpha=1}^{\kappa} \mathrm{n}^\alpha = 1. \tag{7.2}$$

The concept of volume fraction is actually an important part theory in balance equations and constitutive relations. With the help of fraction concept, all geometric and physical quantities, motion, and stress, for instance, are defined in the total control space, can be introduced as the statistical average values of the real quantities [96] [104].

7.2 The Mass Balance

In the model of landfill gas adsorption, porous media system comprises an incompressible solid phase, a compressible gas phase, which consisted of three kinds of gas (represented by A, B, C respectively). This model belongs to the hybrid model of second type [105]. n^S,n^G,n^A,n^B, and n^C, are defined as volume fraction of each phase. The sum of volume fraction is restricted to $\sum_{\alpha=1}^{k} \mathrm{n}^\alpha$=1. As for solid and gas phase, we defined

$$\mathrm{M}^\alpha = \int_{\mathrm{Bs}} \rho^\alpha \mathrm{dv} = \int_{\mathrm{Bs}} \rho^{\alpha\mathrm{R}} \mathrm{dv}^\alpha \tag{7.3}$$

in the actual placement, in which ρ^α and $\rho^{\alpha\mathrm{R}}$ are partial densities and realistic densities. They are connected with volume fraction

$$\rho^\alpha = \mathrm{n}^\alpha \rho^{\alpha\mathrm{R}} \tag{7.4}$$

in the actual placement.

For each kind of gas, the partial density can be replaced by molar concentration, which is related to volume fraction of gas phase. So that, molar concentration of gas A is defined as

$$\rho^\mathrm{A} = \mathrm{n}^\mathrm{G} \mathrm{M}^\mathrm{A}_\mathrm{ol} \mathrm{c}^\mathrm{A} \tag{7.5}$$

in the actual placement. $\mathrm{M}^\mathrm{A}_\mathrm{ol}$ is the molar mass of constituent φ^α. The molar concentration c^B and c^C are given in the same way.

The mass balance in the local form is described as

$$(\rho^{\alpha})'_{\alpha} + \rho^{\alpha}\mathrm{div}\mathbf{x}'_{\alpha} = \hat{\rho}^{\alpha}, \tag{7.6}$$

at position x and time t. The term of $\hat{\rho}^{\alpha}$ represents the local mass supply of constituent φ^{α}, and mass supplies fulfill the condition

$$\sum_{\alpha=1}^{\kappa} \hat{\rho}^{\alpha} = 0. \tag{7.7}$$

Inserted with equation 7.4, the mass balance becomes into

$$(\mathrm{n}^{\alpha}\rho^{\alpha\mathrm{R}})'_{\alpha} + \mathrm{n}^{\alpha}\rho^{\alpha\mathrm{R}}\mathrm{div}\mathbf{x}'_{\alpha} = \hat{\rho}^{\alpha}. \tag{7.8}$$

For the incompressible solid phase, the condition of

$$(\rho^{\mathrm{SR}}_{0\mathrm{S}})'_{\mathrm{S}} = (\rho^{\mathrm{SR}})'_{\mathrm{S}} = 0 \tag{7.9}$$

is taken into account.

So, the mass balance equation of incompressible solid phase is

$$(\mathrm{n}^{\mathrm{S}})'_{\mathrm{S}} + \mathrm{n}^{\mathrm{S}}\mathrm{div}\mathbf{x}'_{\mathrm{S}} = \frac{\hat{\rho}^{\mathrm{S}}}{\rho^{\mathrm{SR}}}. \tag{7.10}$$

The mass supply in compressible gas phase is assumed to be zero. Then, the mass balance equation of gas phase is written as

$$(\mathrm{n}^{\mathrm{G}})'_{\mathrm{G}} + \mathrm{n}^{\mathrm{G}}\frac{\rho^{\mathrm{G}}}{\rho^{\mathrm{GR}}} + \mathrm{n}^{\mathrm{G}}\mathrm{div}\mathbf{x}'_{\mathrm{G}} = 0. \tag{7.11}$$

Inserting equation 7.5 into equation 7.6, the mass balance of gas A is

$$(\mathrm{n}^{\mathrm{G}})'_{\mathrm{A}}\mathrm{c}^{\mathrm{A}} + \mathrm{n}^{\mathrm{G}}(\mathrm{c}^{\mathrm{A}})'_{\mathrm{A}} + \mathrm{n}^{\mathrm{G}}\mathrm{c}^{\mathrm{A}}\mathrm{div}\mathbf{x}'_{\mathrm{A}} = \frac{\hat{\rho}^{\mathrm{A}}}{\mathrm{M}^{\mathrm{A}}_{\mathrm{ol}}}. \tag{7.12}$$

This equation also can be applied to the mass balance of gas B and gas C.

The material time derivative of molar concentration c^{A}(**x**,t) is defined as

$$(\mathrm{c}^{\mathrm{A}})'_{\mathrm{A}} = \frac{\partial \mathrm{c}^{\mathrm{A}}}{\partial \mathrm{t}} + \mathrm{gradc}^{\mathrm{A}}\ \mathbf{x}'_{\mathrm{A}}. \tag{7.13}$$

And, the term of $(\mathrm{c}^{\mathrm{A}})'_{\mathrm{S}}$ can be written as

$$(\mathrm{c}^{\mathrm{A}})'_{\mathrm{S}} = \frac{\partial \mathrm{c}^{\mathrm{A}}}{\partial \mathrm{t}} + \mathrm{gradc}^{\mathrm{A}}\ \mathbf{x}'_{\mathrm{S}}. \tag{7.14}$$

From equation 7.13 and equation 7.14, the relation of $(\mathrm{c}^{\mathrm{A}})'_{\mathrm{A}}$ and $(\mathrm{c}^{\mathrm{A}})'_{\mathrm{S}}$ is

$$(\mathrm{c}^{\mathrm{A}})'_{\mathrm{A}} = (\mathrm{c}^{\mathrm{A}})'_{\mathrm{S}} + \mathrm{gradc}^{\mathrm{A}}\ \mathbf{w}_{\mathrm{AS}}, \tag{7.15}$$

in which

$$\mathbf{w}_{\mathrm{AS}} = \mathbf{x}_{\mathrm{A}}^{'} - \mathbf{x}_{\mathrm{S}}^{'}. \tag{7.16}$$

In the same way, the relation of $(\mathrm{n}^{\mathrm{G}})_{\mathrm{A}}^{'}$ and $(\mathrm{n}^{\mathrm{G}})_{\mathrm{S}}^{'}$ is

$$(\mathrm{n}^{\mathrm{G}})_{\mathrm{A}}^{'} = (\mathrm{n}^{\mathrm{G}})_{\mathrm{S}}^{'} + \mathrm{gradn}^{\mathrm{G}}\ \mathbf{w}_{\mathrm{AS}}. \tag{7.17}$$

Inserting equation 7.13, equation 7.14, equation 7.15, equation 7.16 and equation 7.17 into equation 7.12, the equation is written as

$$\begin{aligned} &\mathrm{n}^{\mathrm{G}}[(\mathrm{c}^{\mathrm{A}})_{\mathrm{S}}^{'} + \mathrm{gradc}^{\mathrm{A}}\ \mathbf{w}_{\mathrm{AS}}] + \mathrm{c}^{\mathrm{A}}[(\mathrm{n}^{\mathrm{G}})_{\mathrm{S}}^{'} + \mathrm{gradn}^{\mathrm{G}}\ \mathbf{w}_{\mathrm{AS}}] \\ &+ \mathrm{c}^{\mathrm{A}}\mathrm{n}^{\mathrm{G}}\mathrm{div}\mathbf{w}_{\mathrm{AS}} + \mathrm{c}^{\mathrm{A}}\mathrm{n}^{\mathrm{G}}\mathrm{div}\mathbf{x}_{\mathrm{S}}^{'} - \frac{\hat{\rho}^{\mathrm{A}}}{\mathrm{M}_{\mathrm{ol}}^{\mathrm{A}}} = 0. \end{aligned} \tag{7.18}$$

So that, the mass balance equation of gas A is also in form of

$$\mathrm{n}^{\mathrm{G}}(\mathrm{c}^{\mathrm{A}})_{\mathrm{S}}^{'} + \mathrm{c}^{\mathrm{A}}(\mathrm{n}^{\mathrm{G}})_{\mathrm{S}}{}' + \mathrm{div}(\mathrm{c}^{\mathrm{A}}\mathrm{n}^{\mathrm{G}}\mathbf{w}_{\mathrm{AS}}) + \mathrm{c}^{\mathrm{A}}\mathrm{n}^{\mathrm{G}}\mathrm{div}\mathbf{x}_{\mathrm{S}}^{'} - \frac{\hat{\rho}^{\mathrm{A}}}{\mathrm{M}_{\mathrm{ol}}^{\mathrm{A}}} = 0. \tag{7.19}$$

The mass balance equations of gas B and gas C can be written in the same way.

7.3 The Momentum Balance

The momentum $\mathbf{l}^{\alpha}$ of constituent φ^{α} [103] is defined as

$$\mathbf{l}^{\alpha} = \int_{\mathrm{B}_{\alpha}} \rho^{\alpha}\mathbf{x}_{\alpha}^{'}\mathrm{dv}. \tag{7.20}$$

Thus, the momentum balance equation can be written as

$$(\mathbf{l}^{\alpha})_{\alpha}^{'} = \mathbf{k}^{\alpha} + \int_{\mathrm{B}_{\alpha}} \hat{\mathbf{p}}^{\alpha}\mathrm{dv}. \tag{7.21}$$

This equation means that the material time derivative of the momentum is equal to the sum of external forces. Where the external forces can be expressed as

$$\mathbf{k}^{\alpha} = \int_{\mathrm{B}_{\alpha}} \rho^{\alpha}\mathbf{b}^{\alpha}\mathrm{dv} + \int_{\partial\mathrm{B}_{\alpha}} \mathbf{t}^{\alpha}\mathrm{da}, \tag{7.22}$$

which are combined with a local volume forces $\rho^{\alpha}\mathbf{b}^{\alpha}$ and the external surface forces $\mathbf{t}^{\alpha}$. AS Cauchy's theorem expresses,

$$\mathbf{t}^{\alpha} = \mathbf{T}^{\alpha}\mathbf{n}, \tag{7.23}$$

in which, $\mathbf{T}^\alpha$ and $\mathbf{n}$ represent Cauchy's stress tensor of the constituent φ^α and the unit normal at the surface of the individual constituent body respectively. Meanwhile, the interaction force $\hat{\mathbf{p}}^\alpha$ is uesed to describ the local supply term of momentum of φ^α as

$$\hat{\mathbf{p}}^\alpha = \hat{\mathbf{p}}^\alpha(\mathbf{x}, \mathrm{t}). \tag{7.24}$$

On the other hand, the material time derivative of the momentum can be written as

$$(\mathbf{l}^\alpha)'_\alpha = \int\limits_{\mathrm{B}_\alpha} (\rho^\alpha \mathbf{x}''_\alpha + \hat{\rho}^\alpha \mathbf{x}'_\alpha)\mathrm{dv} \tag{7.25}$$

as well.

With the divergence theorem

$$\int\limits_{\partial \mathrm{B}_\alpha} \mathbf{T}^\alpha \mathbf{n}\mathrm{da} = \int\limits_{\mathrm{B}_\alpha} \mathrm{div}\mathbf{T}^\alpha \mathrm{dv} \tag{7.26}$$

is taken into account, the balance equation of momentum thus can be written as

$$\int\limits_{\mathrm{B}_\alpha} (\rho^\alpha \mathbf{x}''_\alpha + \hat{\rho}^\alpha \mathbf{x}'_\alpha)\mathrm{dv} = \int\limits_{\mathrm{B}_\alpha} (\mathrm{div}\mathbf{T}^\alpha + \rho^\alpha \mathbf{b}^\alpha)\mathrm{dv} + \int\limits_{\mathrm{B}_\alpha} \hat{\mathbf{p}}^\alpha \mathrm{dv}. \tag{7.27}$$

And, the local momentum balance equation for constituent φ^α is

$$\mathrm{div}\mathbf{T}^\alpha + \rho^\alpha(\mathbf{b}^\alpha - \mathbf{x}''_\alpha) = \hat{\rho}^\alpha \mathbf{x}'_\alpha - \hat{\mathbf{p}}^\alpha. \tag{7.28}$$

Where, $\mathbf{b}^\alpha$ is the external body force. In our case, it is gravity. $\mathbf{T}^\alpha$ is the partial Cauchy stress tensor of constituent φ^α. $\hat{\mathbf{p}}^\alpha$ is the interaction force of constituent φ^α. The interaction force on all of constituents should be satisfied with the condition:

$$\sum_{\alpha=1}^{\kappa} \hat{\mathbf{p}}^\alpha = \mathbf{o} \tag{7.29}$$

7.4 The Energy Balance

Usually, the energy balance of a constituent φ^α states that the sum of material time derivations of the internal energy E^α and kinetic energy K^α equals the sum of changes of the mechanical work W^α, the heat Q^α and the energy supply $\hat{\mathrm{e}}^\alpha$ [106].

The material time derivation of internal energy is

$$(\mathrm{E}^\alpha)'_\alpha = \int\limits_{\mathrm{B}_\alpha} [\rho^\alpha (\varepsilon^\alpha)'_\alpha + \hat{\rho}^\alpha \varepsilon^\alpha]\mathrm{dv}, \tag{7.30}$$

with respect to the specific internal energy ε^α and density ρ^α; and that of kinetic energy is

$$(\mathrm{K}^{\alpha})_{\alpha}^{'} = \int\limits_{\mathrm{B}_{\alpha}} (\rho^{\alpha}\mathbf{x}_{\alpha}^{''} + \frac{1}{2}\hat{\rho}^{\alpha}\mathbf{x}_{\alpha}^{'}) \cdot \mathbf{x}_{\alpha}^{'}\mathrm{dv}. \tag{7.31}$$

Over here,

$$\mathrm{W}^{\alpha} = \int\limits_{\mathrm{B}_{\alpha}} \mathbf{x}_{\alpha}^{'} \cdot \rho^{\alpha}\mathbf{b}^{\alpha}\mathrm{dv} + \int\limits_{\partial\mathrm{B}_{\alpha}} \mathbf{x}_{\alpha}^{'} \cdot \mathbf{T}^{\alpha}\mathrm{d}\mathbf{a} \tag{7.32}$$

is the increment of mechanical work and

$$\mathrm{Q}^{\alpha} = \int\limits_{\mathrm{B}_{\alpha}} \rho^{\alpha}\mathrm{r}^{\alpha}\mathrm{dv} + \int\limits_{\partial\mathrm{B}_{\alpha}} \mathbf{q}^{\alpha} \cdot \mathrm{d}\mathbf{a} \tag{7.33}$$

is the increment of no mechanical work. Where, r^{α}= r^{α}(**x**,t) is the external heat supply, and $\mathbf{q}^{\alpha}$= $\mathbf{q}^{\alpha}$(**x**,t) is the heat influx vector.

Introducing the Helmholtz free energy ψ^{α}= ψ^{α}(**x**,t) into the internal energy term, the local form of energy balance is:

$$\begin{aligned} &\rho^{\alpha}[(\psi^{\alpha})_{\alpha}^{'} + (\theta^{\alpha})_{\alpha}^{'} + \theta^{\alpha}(\eta^{\alpha})_{\alpha}^{'}] - \mathbf{T}^{\alpha} \cdot \mathbf{D}_{\alpha} - \rho^{\alpha}\mathrm{r}^{\alpha} + \mathrm{div}\mathbf{q}^{\alpha} \\ &= \hat{e}^{\alpha} - \hat{\mathbf{p}}^{\alpha} \cdot \mathbf{x}_{\alpha}^{'} - \hat{\rho}^{\alpha}(\psi^{\alpha} + \theta^{\alpha}\eta^{\alpha} - \frac{1}{2}\mathbf{x}_{\alpha}^{'}\mathbf{x}_{\alpha}^{'}). \end{aligned} \tag{7.34}$$

In which, η^{α}= η^{α}(**x**,t) denotes the specific entropy of the constituent φ^{α}. θ^{α}= θ^{α}(**x**,t) denotes the local absolute temperature. The relations among ε^{α}, η^{α}, θ^{α} and ψ^{α} can be obtained by Helmholtz function:

$$\psi^{\alpha} = \varepsilon^{\alpha} - \theta^{\alpha}\eta^{\alpha} \tag{7.35}$$

7.5 The Entropy Inequality

As the second law of thermodynamics states that the entropy of a closed system always increases or remains constant. The entropy inequality is a useful way to restrict constitutive modelling conditions. For every individual constituent φ^{α}, the entropy inequality is

$$\sum_{\alpha=1}^{\kappa}(\mathbf{H}^{\alpha})_{\alpha}^{'} \geq \sum_{\alpha=1}^{\kappa}\int\limits_{\mathrm{B}_{\alpha}} \frac{1}{\theta^{\alpha}}\rho^{\alpha}\mathrm{r}^{\alpha}\mathrm{dv} - \sum_{\alpha=1}^{\kappa}\int\limits_{\partial\mathrm{B}_{\alpha}} \frac{1}{\theta^{\alpha}}\mathbf{q}^{\alpha} \cdot \mathrm{d}\mathbf{a}, \tag{7.36}$$

with the entropy of the constituent φ^{α} defined as

$$\mathbf{H}^{\alpha} = \int\limits_{\mathrm{B}_{\alpha}} \rho^{\alpha}\eta^{\alpha}\mathrm{dv}. \tag{7.37}$$

Thus, the entropy material time derivative form can be obtained

$$\sum_{\alpha=1}^{\kappa}(\mathbf{H}^{\alpha})'_{\alpha}=\sum_{\alpha=1}^{\kappa}\int_{\mathrm{B}_{\alpha}}[\rho^{\alpha}(\eta^{\alpha})'_{\alpha}+\hat{\rho}^{\alpha}\eta^{\alpha}]\mathrm{dv}\geq\sum_{\alpha=1}^{\kappa}\int_{\mathrm{B}_{\alpha}}[\frac{1}{\theta^{\alpha}}\rho^{\alpha}\mathrm{r}^{\alpha}-\mathrm{div}(\frac{1}{\theta^{\alpha}}\mathbf{q}^{\alpha})]\mathrm{dv}, \tag{7.38}$$

with the relation of

$$\int_{\partial\mathrm{B}_{\alpha}}\frac{1}{\theta^{\alpha}}\mathbf{q}^{\alpha}\cdot\mathrm{d}\mathbf{a}=\int_{\mathrm{B}_{\alpha}}\mathrm{div}(\frac{1}{\theta^{\alpha}}\mathbf{q}^{\alpha})\mathrm{dv}. \tag{7.39}$$

In addition, considering the relation

$$\mathrm{div}(\frac{1}{\theta^{\alpha}}\mathbf{q}^{\alpha})=\frac{1}{\theta^{\alpha}}(-\frac{1}{\theta^{\alpha}}\mathrm{grad}\theta^{\alpha}\cdot\mathbf{q}^{\alpha}+\mathrm{div}\mathbf{q}^{\alpha}) \tag{7.40}$$

and the local form of energy balance equation 7.34, the local entropy inequality [105] in the porous media, is given as:

$$\begin{aligned}\sum_{\alpha=1}^{\kappa}\frac{1}{\theta^{\alpha}}\{&-\rho^{\alpha}[(\psi^{\alpha})'_{\alpha}+(\theta^{\alpha})'_{\alpha}\eta^{\alpha}]-\hat{\rho}^{\alpha}(\psi^{\alpha}-\frac{1}{2}\mathbf{x}'_{\alpha}\cdot\mathbf{x}'_{\alpha})\\&+\mathbf{T}^{\alpha}\cdot\mathbf{D}_{\alpha}-\hat{\mathbf{p}}^{\alpha}\cdot\mathbf{x}'_{\alpha}-\frac{1}{\theta^{\alpha}}\mathbf{q}^{\alpha}\cdot\mathrm{grad}\theta^{\alpha}+\hat{\mathrm{e}}^{\alpha}\}\geq 0.\end{aligned} \tag{7.41}$$

7.6 The Chemical Potential

Chemical potential μ^{α} is a major parameter in the multi-constituent systems. Under different conditions, it can be defined as the partial derivative of internal energy E^{α}, Helmholtz free energy ψ^{α}= ψ^{α}(x,t), Gibbs energy G, which defined as

$$\mathrm{G}=\mathrm{E}-\theta\mathrm{H}+\mathrm{pV}, \tag{7.42}$$

and Enthalpy S which defined as

$$\mathrm{S}=\mathrm{E}+\mathrm{pV}, \tag{7.43}$$

to the number of particles of φ^{α} [107]. In equation 7.42, θ is absolute temperature, p is pressure and V is volume.

In our case, the gas mixtures are assumed to be in ideal states. It would be more convenient to define chemical potential μ^{α} [108]as related to the derivative of Helmholtz free energy ψ^{α}= ψ^{α}(x,t) to molar concentration of constituent φ^{α}. So that, the chemical potential μ^{α} is given as:

$$\mu^{\alpha}=\mu_{0}^{\alpha}+\frac{\mathrm{R}\theta}{\mathrm{M_{ol}}}\ln\frac{\mathrm{c}^{\alpha}}{\mathrm{c}_{0}^{\alpha}}, \tag{7.44}$$

where R is gas constant; μ_{0}^{α} and c_{0}^{α} are the reference chemical potential and molar concentration of constituent φ^{α}, respectively. This equation can be applied to chemical potential of gas A, B and C.

7.7 Governing Equations of the Calculation Concept

Seen from the balance of mass on solid and gas phase (equation 7.6, 2 equations), balance of momentum (equation 7.28, 6 equations) and physical constraints (equation 7.2, 7.7, 7.29; 1+1+3 equations), there are 13 scalar valued relations to describe this biphasic model. Taken account of the basic constitutive relations of the hybrid type II, the set of unknown quantities of the hybrid type II $\mathcal{U}_{\mathrm{hII}}$, the set of unknown quantities $\mathcal{U}$ in our case, and the set of needed constitutive quantities $\mathcal{C}$ are listed as follows:

$$\begin{aligned} \mathcal{U}_{\mathrm{hII}} = &\ \{\mathbf{X}_\alpha,\ \mathrm{n}^\alpha,\ \rho^{\mathrm{GR}},\ \theta,\ \hat{\mathbf{p}}^{\mathrm{S}},\ \hat{\rho}^{\mathrm{G}},\ \hat{\mathrm{e}}^{\mathrm{G}}\} \quad \Rightarrow \quad \nu^{14} \quad , \\ \mathcal{U} = &\ \{\mathbf{X}_\alpha,\ \mathrm{n}^\alpha,\ \rho^{\mathrm{GR}},\ \hat{\mathbf{p}}^{\mathrm{S}},\ \hat{\rho}^{\mathrm{G}}\} \quad \Rightarrow \quad \nu^{12} \quad , \\ \mathcal{C} = &\ \{\mathbf{T}^\alpha,\ \mathbf{q}^\alpha,\ \hat{\mathbf{p}}^{\mathrm{G}},\ \hat{\rho}^{\mathrm{S}},\ \psi^\alpha\} \quad \Rightarrow \quad \nu^{24} \quad . \end{aligned} \tag{7.45}$$

In equation 7.45, $\mathbf{X}_\alpha$ is the motion function. And, the balance equation of moment of momentum $\mathbf{T}^\alpha = (\mathbf{T}^\alpha)^{\mathrm{T}}$ is considered, thus it leads to a symmetric tensor with six unknown quantities included.

7.8 Interaction Conditions

As equation 7.29 shows, the sum of interaction force of all of constituents is zero. The term $\sum_{\alpha=1}^{\kappa}\{-\hat{\mathbf{p}}^\alpha \cdot \mathbf{x}_\alpha^{'}\}$ can be expressed as:

$$\begin{aligned} &\sum_{\alpha=1}^{\kappa}\{-\hat{\mathbf{p}}^\alpha \cdot \mathbf{x}_\alpha^{'}\} \\ &= -\hat{\mathbf{p}}^{\mathrm{S}} \cdot \mathbf{x}_{\mathrm{S}}^{'} - \hat{\mathbf{p}}^{\mathrm{G}} \cdot \mathbf{x}_{\mathrm{G}}^{'} - \hat{\mathbf{p}}^{\mathrm{A}} \cdot \mathbf{x}_{\mathrm{A}}^{'} - \hat{\mathbf{p}}^{\mathrm{B}} \cdot \mathbf{x}_{\mathrm{B}}^{'} - \hat{\mathbf{p}}^{\mathrm{C}} \cdot \mathbf{x}_{\mathrm{C}}^{'} \\ &= (\hat{\mathbf{p}}^{\mathrm{G}} + \hat{\mathbf{p}}^{\mathrm{A}} + \hat{\mathbf{p}}^{\mathrm{B}} + \hat{\mathbf{p}}^{\mathrm{C}}) \cdot \mathbf{x}_{\mathrm{S}}^{'} - \hat{\mathbf{p}}^{\mathrm{G}} \cdot \mathbf{x}_{\mathrm{G}}^{'} - \hat{\mathbf{p}}^{\mathrm{A}} \cdot \mathbf{x}_{\mathrm{A}}^{'} - \hat{\mathbf{p}}^{\mathrm{B}} \cdot \mathbf{x}_{\mathrm{B}}^{'} - \hat{\mathbf{p}}^{\mathrm{C}} \cdot \mathbf{x}_{\mathrm{C}}^{'} \\ &= -\hat{\mathbf{p}}^{\mathrm{G}} \cdot (\mathbf{x}_{\mathrm{G}}^{'} - \mathbf{x}_{\mathrm{S}}^{'}) - \hat{\mathbf{p}}^{\mathrm{A}} \cdot (\mathbf{x}_{\mathrm{A}}^{'} - \mathbf{x}_{\mathrm{S}}^{'}) - \hat{\mathbf{p}}^{\mathrm{B}} \cdot (\mathbf{x}_{\mathrm{B}}^{'} - \mathbf{x}_{\mathrm{S}}^{'}) - \hat{\mathbf{p}}^{\mathrm{C}} \cdot (\mathbf{x}_{\mathrm{C}}^{'} - \mathbf{x}_{\mathrm{S}}^{'}) \\ &= -\hat{\mathbf{p}}^{\mathrm{G}} \cdot \mathbf{w}_{\mathrm{GS}} - \hat{\mathbf{p}}^{\mathrm{A}} \cdot \mathbf{w}_{\mathrm{AG}} - \hat{\mathbf{p}}^{\mathrm{A}} \cdot \mathbf{w}_{\mathrm{GS}} - \hat{\mathbf{p}}^{\mathrm{B}} \cdot \mathbf{w}_{\mathrm{BG}} - \hat{\mathbf{p}}^{\mathrm{B}} \cdot \mathbf{w}_{\mathrm{GS}} \\ &\quad - \hat{\mathbf{p}}^{\mathrm{C}} \cdot \mathbf{w}_{\mathrm{CG}} - \hat{\mathbf{p}}^{\mathrm{C}} \cdot \mathbf{w}_{\mathrm{GS}} \\ &= (-\hat{\mathbf{p}}^{\mathrm{G}} - \hat{\mathbf{p}}^{\mathrm{A}} - \hat{\mathbf{p}}^{\mathrm{B}} - \hat{\mathbf{p}}^{\mathrm{C}}) \cdot \mathbf{w}_{\mathrm{GS}} - \hat{\mathbf{p}}^{\mathrm{A}} \cdot \mathbf{w}_{\mathrm{AG}} - \hat{\mathbf{p}}^{\mathrm{B}} \cdot \mathbf{w}_{\mathrm{BG}} - \hat{\mathbf{p}}^{\mathrm{C}} \cdot \mathbf{w}_{\mathrm{CG}}, \end{aligned} \tag{7.46}$$

with

$$\mathbf{w}_{\mathrm{AS}} = \mathbf{w}_{\mathrm{AG}} + \mathbf{w}_{\mathrm{GS}}, \tag{7.47}$$

$$\mathbf{w}_{\mathrm{BS}} = \mathbf{w}_{\mathrm{BG}} + \mathbf{w}_{\mathrm{GS}}, \tag{7.48}$$

and

$$\mathbf{w}_{\mathrm{CS}} = \mathbf{w}_{\mathrm{CG}} + \mathbf{w}_{\mathrm{GS}}. \tag{7.49}$$

7.9 Saturation Conditions

The volume fraction of solid, gas phase and all kinds of gases is constrained by a condition

$$\mathrm{n^S} + \mathrm{n^G} + \mathrm{n^A} + \mathrm{n^B} + \mathrm{n^C} = 1. \tag{7.50}$$

Therefore, the material time derivative of equation 7.50 with respected to the motion of solid phase is:

$$(\mathrm{n^S})'_\mathrm{S} + (\mathrm{n^G})'_\mathrm{S} + (\mathrm{n^A})'_\mathrm{S} + (\mathrm{n^B})'_\mathrm{S} + (\mathrm{n^C})'_\mathrm{S} = 0. \tag{7.51}$$

The relation of $(\mathrm{n^G})'_\mathrm{S}$ and $(\mathrm{n^G})'_\mathrm{G}$ is

$$\begin{aligned}(\mathrm{n^G})'_\mathrm{S} &= (\mathrm{n^G})'_\mathrm{G} - \mathrm{gradn^G} \cdot (\mathbf{x}'_\mathrm{G} - \mathbf{x}'_\mathrm{S}) \\ &= (\mathrm{n^G})'_\mathrm{G} - \mathrm{gradn^G} \cdot \mathbf{w}_\mathrm{GS}.\end{aligned} \tag{7.52}$$

For gas A, $(\mathrm{n^A})'_\mathrm{S}$ can be written as:

$$\begin{aligned}(\mathrm{n^A})'_\mathrm{S} &= \frac{\mathrm{M^A_{ol}}}{\rho^\mathrm{AR}}(\mathrm{c^A n^G})'_\mathrm{S} \\ &= \frac{\mathrm{M^A_{ol}}}{\rho^\mathrm{AR}}[(\mathrm{c^A})'_\mathrm{S}\mathrm{n^G} + \mathrm{c^A}(\mathrm{n^G})'_\mathrm{S}].\end{aligned} \tag{7.53}$$

Inserting equation 7.15 into equation 7.53, the final form of $(\mathrm{n^A})'_\mathrm{S}$ will be

$$(\mathrm{n^A})'_\mathrm{S} = \frac{\mathrm{M^A_{ol}}}{\rho^\mathrm{AR}}[\mathrm{n^G}(\mathrm{c^A})'_\mathrm{A} - \mathrm{n^G gradc^A} \cdot \mathbf{w}_\mathrm{AS} + \mathrm{c^A}(\mathrm{n^G})'_\mathrm{G} - \mathrm{c^A gradn^G} \cdot \mathbf{w}_\mathrm{GS}]. \tag{7.54}$$

For gas B and C, $(\mathrm{n^B})'_\mathrm{S}$ and $(\mathrm{n^C})'_\mathrm{S}$ can be written in the same way. So that, the change of saturation condition becomes into

$$\begin{aligned}&(\mathrm{n^S})'_\mathrm{S} + (\mathrm{n^G})'_\mathrm{G} - \mathrm{gradn^G} \cdot \mathbf{w}_\mathrm{GS} \\ &+ \frac{\mathrm{M^A_{ol}}}{\rho^\mathrm{AR}}[\mathrm{n^G}(\mathrm{c^A})'_\mathrm{A} - \mathrm{n^G gradc^A} \cdot \mathbf{w}_\mathrm{AS} + \mathrm{c^A}(\mathrm{n^G})'_\mathrm{G} - \mathrm{c^A gradn^G} \cdot \mathbf{w}_\mathrm{GS}] \\ &+ \frac{\mathrm{M^B_{ol}}}{\rho^\mathrm{BR}}[\mathrm{n^G}(\mathrm{c^B})'_\mathrm{B} - \mathrm{n^G gradc^B} \cdot \mathbf{w}_\mathrm{BS} + \mathrm{c^B}(\mathrm{n^G})'_\mathrm{G} - \mathrm{c^B gradn^G} \cdot \mathbf{w}_\mathrm{GS}] \\ &+ \frac{\mathrm{M^C_{ol}}}{\rho^\mathrm{CR}}[\mathrm{n^G}(\mathrm{c^C})'_\mathrm{C} - \mathrm{n^G gradc^C} \cdot \mathbf{w}_\mathrm{CS} + \mathrm{c^C}(\mathrm{n^G})'_\mathrm{G} - \mathrm{c^C gradn^G} \cdot \mathbf{w}_\mathrm{GS}] \\ &= 0.\end{aligned} \tag{7.55}$$

7.10 Lagrange Multipliers

In this case, Lagrange multipliers [109] are used to eliminate the dependencies of the process variable. Thus, mass balance equation of solid, gas A, B and C can be multiplied by λ^{S}, λ^{A}, λ^{B} and λ^{C} respectively. These equations will be introduced into entropy inequality as constraints. For the solid phase, the relation is:

$$\frac{1}{\theta^{\mathrm{S}}}\lambda^{\mathrm{S}}[(\mathrm{n}^{\mathrm{S}})'_{\mathrm{S}} + \mathrm{n}^{\mathrm{S}}\mathrm{div}\mathbf{x}'_{\mathrm{S}} - \frac{\hat{\rho}^{\mathrm{S}}}{\rho^{\mathrm{SR}}}] = 0, \tag{7.56}$$

and the relation to gas A is given as

$$\frac{1}{\theta^{\mathrm{A}}}\lambda^{\mathrm{A}}[(\mathrm{n}^{\mathrm{G}})'_{\mathrm{A}}\mathrm{c}^{\mathrm{A}} + \mathrm{n}^{\mathrm{G}}(\mathrm{c}^{\mathrm{A}})'_{\mathrm{A}} + \mathrm{n}^{\mathrm{G}}\mathrm{c}^{\mathrm{A}}\mathrm{div}\mathbf{x}'_{\mathrm{A}} - \frac{\hat{\rho}^{\mathrm{A}}}{\mathrm{M}^{\mathrm{A}}_{\mathrm{ol}}}] = 0. \tag{7.57}$$

In our case, Lagrange multipliers with gas B and C are given in the same form.

Besides these constraints, the impact of saturation condition will be taken into account. In equation 7.55, the 4$^{\mathrm{th}}$, 5$^{\mathrm{th}}$ and 6$^{\mathrm{th}}$ terms are more less than 1. Therefore, these terms will be ignored as a constraint for entropy inequality. Thus, another Lagrange multiplier λ is introduced as

$$\frac{1}{\theta^{\mathrm{ref}}}\lambda[(\mathrm{n}^{\mathrm{S}})'_{\mathrm{S}} + (\mathrm{n}^{\mathrm{G}})'_{\mathrm{G}} - \mathrm{gradn}^{\mathrm{G}} \cdot \mathbf{w}_{\mathrm{GS}}] = 0, \tag{7.58}$$

with

$$\frac{1}{\theta^{\mathrm{ref}}} = \frac{1}{2}\,\frac{\theta^{\mathrm{S}} + \theta^{\mathrm{G}}}{\theta^{\mathrm{S}}\theta^{\mathrm{G}}}. \tag{7.59}$$

7.11 Evaluation of Entropy Inequality

For simplification, only the isothermal equations on porous media are discussed over here. Thus, the term of $\frac{1}{\theta^{\alpha}}$, $\frac{1}{\theta^{\alpha}}\mathbf{q}^{\alpha} \cdot \mathrm{grad}\theta^{\alpha}$ and $\hat{\mathrm{e}}^{\alpha}$ will to be ignored. The constitutive assumptions for entropy inequality are listed as following:

$$\begin{gathered}\psi^{\mathrm{S}} = \psi^{\mathrm{S}}(\mathbf{c}_{\mathrm{S}}, \mathrm{n}^{\mathrm{S}}),\ \psi^{\mathrm{G}} = \psi^{\mathrm{G}}(\rho^{\mathrm{GR}}),\ \psi^{\mathrm{A}} = \psi^{\mathrm{A}}(\mathrm{c}^{\mathrm{A}}),\\ \psi^{\mathrm{B}} = \psi^{\mathrm{B}}(\mathrm{c}^{\mathrm{B}}),\ \psi^{\mathrm{c}} = \psi^{\mathrm{c}}(\mathrm{c}^{\mathrm{C}}).\end{gathered} \tag{7.60}$$

Therefore, the term of $\rho^{\alpha}(\psi^{\alpha})'_{\alpha}$ can be expressed as:

$$
\begin{aligned}
\rho^{\mathrm{S}}(\psi^{\mathrm{S}})'_{\mathrm{S}} &= 2\rho^{\mathrm{S}}\mathbf{F}_{\mathrm{S}}\frac{\partial\psi^{\mathrm{S}}}{\partial\mathbf{C}_{\mathrm{S}}}\mathbf{F}_{\mathrm{S}}^{\mathbf{T}}\cdot\mathbf{D}_{\mathrm{S}} + \rho^{\mathrm{S}}\frac{\partial\psi^{\mathrm{S}}}{\partial \mathrm{n}^{\mathrm{S}}}(\mathrm{n}^{\mathrm{S}})'_{\mathrm{S}},\\
\rho^{\mathrm{G}}(\psi^{\mathrm{G}})'_{\mathrm{G}} &= \rho^{\mathrm{G}}\frac{\partial\psi^{\mathrm{G}}}{\partial\rho^{\mathrm{GR}}}(\rho^{\mathrm{GR}})'_{\mathrm{G}},\\
\rho^{\mathrm{A}}(\psi^{\mathrm{A}})'_{\mathrm{A}} &= \rho^{\mathrm{A}}\frac{\partial\psi^{\mathrm{A}}}{\partial \mathrm{c}^{\mathrm{A}}}(\mathrm{c}^{\mathrm{A}})'_{\mathrm{A}},\\
\rho^{\mathrm{B}}(\psi^{\mathrm{B}})'_{\mathrm{B}} &= \rho^{\mathrm{B}}\frac{\partial\psi^{\mathrm{B}}}{\partial \mathrm{c}^{\mathrm{B}}}(\mathrm{c}^{\mathrm{B}})'_{\mathrm{B}},\\
\rho^{\mathrm{C}}(\psi^{\mathrm{C}})'_{\mathrm{C}} &= \rho^{\mathrm{C}}\frac{\partial\psi^{\mathrm{C}}}{\partial \mathrm{c}^{\mathrm{C}}}(\mathrm{c}^{\mathrm{C}})'_{\mathrm{C}},
\end{aligned}
\tag{7.61}
$$

With equations on mass balance, interaction conditions, saturation conditions and Lagrange multipliers, the entropy inequality on porous media is written as

$$
\begin{aligned}
&- 2\rho^{\mathrm{S}}\mathbf{F}_{\mathrm{S}}\frac{\partial\psi^{\mathrm{S}}}{\partial\mathbf{C}_{\mathrm{S}}}\mathbf{F}_{\mathrm{S}}^{\mathbf{T}}\cdot\mathbf{D}_{\mathrm{S}} - \rho^{\mathrm{S}}\frac{\partial\psi^{\mathrm{S}}}{\partial\mathrm{n}^{\mathrm{S}}}(\mathrm{n}^{\mathrm{S}})'_{\mathrm{S}} \\
&- \rho^{\mathrm{G}}\frac{\partial\psi^{\mathrm{G}}}{\partial\rho^{\mathrm{GR}}}(\rho^{\mathrm{GR}})'_{\mathrm{G}} - \rho^{\mathrm{A}}\frac{\partial\psi^{\mathrm{A}}}{\partial\mathrm{c}^{\mathrm{A}}}(\mathrm{c}^{\mathrm{A}})'_{\mathrm{A}} - \rho^{\mathrm{B}}\frac{\partial\psi^{\mathrm{B}}}{\partial\mathrm{c}^{\mathrm{B}}}(\mathrm{c}^{\mathrm{B}})'_{\mathrm{B}} - \rho^{\mathrm{C}}\frac{\partial\psi^{\mathrm{C}}}{\partial\mathrm{c}^{\mathrm{C}}}(\mathrm{c}^{\mathrm{C}})'_{\mathrm{C}} \\
&- \hat{\rho}^{\mathrm{S}}(\psi^{\mathrm{S}} - \frac{1}{2}\mathbf{x}'_{\mathrm{S}}\cdot\mathbf{x}'_{\mathrm{S}}) - \hat{\rho}^{\mathrm{A}}(\psi^{\mathrm{A}} - \frac{1}{2}\mathbf{x}'_{\mathrm{A}}\cdot\mathbf{x}'_{\mathrm{A}}) - \hat{\rho}^{\mathrm{B}}(\psi^{\mathrm{B}} - \frac{1}{2}\mathbf{x}'_{\mathrm{B}}\cdot\mathbf{x}'_{\mathrm{B}}) \\
&- \hat{\rho}^{\mathrm{C}}(\psi^{\mathrm{C}} - \frac{1}{2}\mathbf{x}'_{\mathrm{C}}\cdot\mathbf{x}'_{\mathrm{C}}) \\
&+ \mathbf{T}^{\mathrm{S}}\cdot\mathbf{D}_{\mathrm{S}} + \mathbf{T}^{\mathrm{G}}\cdot\mathbf{D}_{\mathrm{G}} + \mathbf{T}^{\mathrm{A}}\cdot\mathbf{D}_{\mathrm{A}} + \mathbf{T}^{\mathrm{B}}\cdot\mathbf{D}_{\mathrm{B}} + \mathbf{T}^{\mathrm{C}}\cdot\mathbf{D}_{\mathrm{C}} \\
&- \mathbf{w}_{\mathrm{GS}}\cdot(\hat{\mathbf{p}}^{\mathrm{G}} + \hat{\mathbf{p}}^{\mathrm{A}} + \hat{\mathbf{p}}^{\mathrm{B}} + \hat{\mathbf{p}}^{\mathrm{C}}) - \mathbf{w}_{\mathrm{AG}}\cdot\hat{\mathbf{p}}^{\mathrm{A}} - \mathbf{w}_{\mathrm{BG}}\cdot\hat{\mathbf{p}}^{\mathrm{B}} - \mathbf{w}_{\mathrm{CG}}\cdot\hat{\mathbf{p}}^{\mathrm{C}} \\
&+ \lambda^{\mathrm{S}}[(\mathrm{n}^{\mathrm{S}})'_{\mathrm{S}} + \mathrm{n}^{\mathrm{S}}\mathrm{div}\mathbf{x}'_{\mathrm{S}} - \frac{\hat{\rho}^{\mathrm{A}}}{\rho^{\mathrm{SR}}}] \\
&+ \lambda^{\mathrm{A}}[-\mathrm{n}^{\mathrm{G}}\mathrm{c}^{\mathrm{A}}\frac{(\rho^{\mathrm{GR}})'_{\mathrm{G}}}{\rho^{\mathrm{GR}}} - \mathrm{n}^{\mathrm{G}}\mathrm{c}^{\mathrm{A}}\mathrm{div}\mathbf{x}'_{\mathrm{G}} + \mathrm{c}^{\mathrm{A}}\mathrm{gradn}^{\mathrm{G}}\cdot\mathbf{w}_{\mathrm{AG}} + \mathrm{n}^{\mathrm{G}}(\mathrm{c}^{\mathrm{A}})'_{\mathrm{A}} \\
&\qquad + \mathrm{n}^{\mathrm{G}}\mathrm{c}^{\mathrm{A}}\mathrm{div}\mathbf{x}'_{\mathrm{A}} - \frac{\hat{\rho}^{\mathrm{A}}}{\mathrm{M}^{\mathrm{A}}_{\mathrm{ol}}}] \\
&+ \lambda^{\mathrm{B}}[-\mathrm{n}^{\mathrm{G}}\mathrm{c}^{\mathrm{B}}\frac{(\rho^{\mathrm{GR}})'_{\mathrm{G}}}{\rho^{\mathrm{GR}}} - \mathrm{n}^{\mathrm{G}}\mathrm{c}^{\mathrm{B}}\mathrm{div}\mathbf{x}'_{\mathrm{G}} + \mathrm{c}^{\mathrm{B}}\mathrm{gradn}^{\mathrm{G}}\cdot\mathbf{w}_{\mathrm{BG}} + \mathrm{n}^{\mathrm{G}}(\mathrm{c}^{\mathrm{B}})'_{\mathrm{B}} \\
&\qquad + \mathrm{n}^{\mathrm{G}}\mathrm{c}^{\mathrm{B}}\mathrm{div}\mathbf{x}'_{\mathrm{B}} - \frac{\hat{\rho}^{\mathrm{B}}}{\mathrm{M}^{\mathrm{B}}_{\mathrm{ol}}}] \\
&+ \lambda^{\mathrm{C}}[-\mathrm{n}^{\mathrm{G}}\mathrm{c}^{\mathrm{C}}\frac{(\rho^{\mathrm{GR}})'_{\mathrm{G}}}{\rho^{\mathrm{GR}}} - \mathrm{n}^{\mathrm{G}}\mathrm{c}^{\mathrm{C}}\mathrm{div}\mathbf{x}'_{\mathrm{G}} + \mathrm{c}^{\mathrm{C}}\mathrm{gradn}^{\mathrm{G}}\cdot\mathbf{w}_{\mathrm{CG}} + \mathrm{n}^{\mathrm{G}}(\mathrm{c}^{\mathrm{C}})'_{\mathrm{C}} \\
&\qquad + \mathrm{n}^{\mathrm{G}}\mathrm{c}^{\mathrm{C}}\mathrm{div}\mathbf{x}'_{\mathrm{C}} - \frac{\hat{\rho}^{\mathrm{C}}}{\mathrm{M}^{\mathrm{C}}_{\mathrm{ol}}}] \\
&- \lambda[(\mathrm{n}^{\mathrm{S}})'_{\mathrm{S}} - \mathrm{n}^{\mathrm{G}}\frac{(\rho^{\mathrm{GR}})'_{\mathrm{G}}}{\rho^{\mathrm{GR}}} - \mathrm{n}^{\mathrm{G}}\mathrm{div}\mathbf{x}'_{\mathrm{G}} - \mathrm{gradn}^{\mathrm{G}}\cdot\mathbf{w}_{\mathrm{GS}}] \geq 0.
\end{aligned}
\tag{7.62}
$$

The entropy inequality can be transferred into

$$
\begin{aligned}
&\mathbf{D}_{\mathrm{S}} \cdot \{-2\rho^{\mathrm{S}}\mathbf{F}_{\mathrm{S}}\frac{\partial\psi^{\mathrm{S}}}{\partial\mathbf{C}_{\mathrm{S}}}\mathbf{F}_{\mathrm{S}}^{\mathbf{T}} + \mathbf{T}^{\mathrm{S}} + \lambda^{\mathrm{S}}\mathrm{n}^{\mathrm{S}}\} \\
&+ \mathbf{D}_{\mathrm{G}} \cdot \{\mathbf{T}^{\mathrm{G}} - \lambda^{\mathrm{A}}\mathrm{n}^{\mathrm{G}}\mathrm{c}^{\mathrm{A}}\mathbf{I} - \lambda^{\mathrm{B}}\mathrm{n}^{\mathrm{G}}\mathrm{c}^{\mathrm{B}}\mathbf{I} - \lambda^{\mathrm{C}}\mathrm{n}^{\mathrm{G}}\mathrm{c}^{\mathrm{C}}\mathbf{I} + \lambda\mathrm{n}^{\mathrm{G}}\mathbf{I}\} \\
&+ \mathbf{D}_{\mathrm{A}} \cdot \{\mathbf{T}^{\mathrm{A}} + \lambda^{\mathrm{A}}\mathrm{n}^{\mathrm{G}}\mathrm{c}^{\mathrm{A}}\mathbf{I}\} \\
&+ \mathbf{D}_{\mathrm{B}} \cdot \{\mathbf{T}^{\mathrm{B}} + \lambda^{\mathrm{B}}\mathrm{n}^{\mathrm{G}}\mathrm{c}^{\mathrm{B}}\mathbf{I}\} \\
&+ \mathbf{D}_{\mathrm{C}} \cdot \{\mathbf{T}^{\mathrm{C}} + \lambda^{\mathrm{C}}\mathrm{n}^{\mathrm{G}}\mathrm{c}^{\mathrm{C}}\mathbf{I}\} \\
&+ (\mathrm{n}^{\mathrm{S}})'_{\mathrm{S}}\{-\rho^{\mathrm{S}}\frac{\partial\psi^{\mathrm{S}}}{\partial\mathrm{n}^{\mathrm{S}}} + \lambda^{S} - \lambda\} \\
&+ (\rho^{\mathrm{GR}})'_{\mathrm{G}}\{\lambda\mathrm{n}^{\mathrm{G}}\frac{1}{\rho^{\mathrm{GR}}} - \lambda^{\mathrm{A}}\mathrm{n}^{\mathrm{G}}\mathrm{c}^{\mathrm{A}}\frac{1}{\rho^{\mathrm{GR}}} - \lambda^{\mathrm{B}}\mathrm{n}^{\mathrm{G}}\mathrm{c}^{\mathrm{B}}\frac{1}{\rho^{\mathrm{GR}}} - \lambda^{\mathrm{C}}\mathrm{n}^{\mathrm{G}}\mathrm{c}^{\mathrm{C}}\frac{1}{\rho^{\mathrm{GR}}} - \rho^{\mathrm{G}}\frac{\partial\psi^{\mathrm{G}}}{\partial\rho^{\mathrm{GR}}}\} \\
&+ (\mathrm{c}^{\mathrm{A}})'_{\mathrm{A}}\{-\rho^{\mathrm{A}}\frac{\partial\psi^{\mathrm{A}}}{\partial\mathrm{c}^{\mathrm{A}}} + \lambda^{\mathrm{A}}\mathrm{n}^{\mathrm{G}}\} \\
&+ (\mathrm{c}^{\mathrm{B}})'_{\mathrm{B}}\{-\rho^{\mathrm{B}}\frac{\partial\psi^{\mathrm{B}}}{\partial\mathrm{c}^{\mathrm{B}}} + \lambda^{\mathrm{B}}\mathrm{n}^{\mathrm{G}}\} \\
&+ (\mathrm{c}^{\mathrm{C}})'_{\mathrm{C}}\{-\rho^{\mathrm{C}}\frac{\partial\psi^{\mathrm{C}}}{\partial\mathrm{c}^{\mathrm{C}}} + \lambda^{\mathrm{C}}\mathrm{n}^{\mathrm{G}}\} \\
&- \hat{\rho}^{\mathrm{S}}\{\psi^{\mathrm{S}} - \frac{1}{2}\mathbf{x}'_{\mathrm{S}} \cdot \mathbf{x}'_{\mathrm{S}} + \lambda^{\mathrm{S}}\frac{1}{\rho^{\mathrm{SR}}}\} \\
&- \hat{\rho}^{\mathrm{A}}\{\psi^{\mathrm{A}} - \frac{1}{2}\mathbf{x}'_{\mathrm{A}} \cdot \mathbf{x}'_{\mathrm{A}} + \lambda^{\mathrm{A}}\frac{1}{\mathrm{M}^{\mathrm{A}}_{\mathrm{ol}}}\} \\
&- \hat{\rho}^{\mathrm{B}}\{\psi^{\mathrm{B}} - \frac{1}{2}\mathbf{x}'_{\mathrm{B}} \cdot \mathbf{x}'_{\mathrm{B}} + \lambda^{\mathrm{B}}\frac{1}{\mathrm{M}^{\mathrm{B}}_{\mathrm{ol}}}\} \\
&- \hat{\rho}^{\mathrm{C}}\{\psi^{\mathrm{C}} - \frac{1}{2}\mathbf{x}'_{\mathrm{C}} \cdot \mathbf{x}'_{\mathrm{C}} + \lambda^{\mathrm{C}}\frac{1}{\mathrm{M}^{\mathrm{C}}_{\mathrm{ol}}}\} \\
&- \mathbf{w}_{\mathrm{GS}}\{\hat{\mathbf{p}}^{\mathrm{G}} + \hat{\mathbf{p}}^{\mathrm{A}} + \hat{\mathbf{p}}^{\mathrm{B}} + \hat{\mathbf{p}}^{\mathrm{C}} - \lambda\mathrm{gradn}^{\mathrm{G}}\} \\
&- \mathbf{w}_{\mathrm{AG}}\{\hat{\mathbf{p}}^{\mathrm{A}} - \lambda^{\mathrm{A}}\mathrm{c}^{\mathrm{A}}\mathrm{gradn}^{\mathrm{G}}\} \\
&- \mathbf{w}_{\mathrm{BG}}\{\hat{\mathbf{p}}^{\mathrm{B}} - \lambda^{\mathrm{B}}\mathrm{c}^{\mathrm{B}}\mathrm{gradn}^{\mathrm{G}}\} \\
&- \mathbf{w}_{\mathrm{CG}}\{\hat{\mathbf{p}}^{\mathrm{C}} - \lambda^{\mathrm{C}}\mathrm{c}^{\mathrm{C}}\mathrm{gradn}^{\mathrm{G}}\} \geq 0.
\end{aligned}
\tag{7.63}
$$

As shown in entropy inequality of equation 7.41, the dissipation mechanism reads

$$\begin{aligned} D = &- \mathbf{w}_{\mathrm{GS}}\{\hat{\mathbf{p}}^{\mathrm{G}} + \hat{\mathbf{p}}^{\mathrm{A}} + \hat{\mathbf{p}}^{\mathrm{B}} + \hat{\mathbf{p}}^{\mathrm{C}} - \lambda \mathrm{gradn}^{\mathrm{G}}\} \\ &- \mathbf{w}_{\mathrm{AG}}\{\hat{\mathbf{p}}^{\mathrm{A}} - \lambda^{\mathrm{A}}\mathrm{c}^{\mathrm{A}}\mathrm{gradn}^{\mathrm{G}}\} \\ &- \mathbf{w}_{\mathrm{BG}}\{\hat{\mathbf{p}}^{\mathrm{B}} - \lambda^{\mathrm{B}}\mathrm{c}^{\mathrm{B}}\mathrm{gradn}^{\mathrm{G}}\} \\ &- \mathbf{w}_{\mathrm{CG}}\{\hat{\mathbf{p}}^{\mathrm{C}} - \lambda^{\mathrm{C}}\mathrm{c}^{\mathrm{C}}\mathrm{gradn}^{\mathrm{G}}\} \geq 0. \end{aligned} \tag{7.64}$$

The structure of dissipation shows that the irreversibility of processes is connected with the seepage velocities $\mathbf{w}_{\mathrm{GS}}$, $\mathbf{w}_{\mathrm{AG}}$, $\mathbf{w}_{\mathrm{BG}}$ and $\mathbf{w}_{\mathrm{CG}}$.

To obtain the constitutive relations for interaction force $\hat{\mathbf{p}}^{\alpha}$ of φ^{α}, for Cauchy stress tensor $\mathbf{T}^{\alpha}$, the quantity of λ and seepage velocities, some necessary conditions will be taken into account.

7.11.1 Evaluation of Lagrange multipliers

With the condition

$$-\rho^{\alpha}\frac{\partial \psi^{\alpha}}{\partial \mathrm{c}^{\alpha}} + \lambda^{\alpha}\mathrm{n}^{\mathrm{G}} = 0 \tag{7.65}$$

for gas A, B, C and equation 7.44 on chemical potential, the quantities of λ^{α} and λ are

$$\begin{aligned} \lambda^{\mathrm{A}} &= \frac{\rho^{\mathrm{A}}}{\mathrm{n}^{\mathrm{G}}}\frac{\partial \psi^{\mathrm{A}}}{\partial \mathrm{c}^{\mathrm{A}}} = \mathrm{c}^{\mathrm{A}}\mathrm{M}^{\mathrm{A}}_{\mathrm{ol}}\frac{\partial \psi^{\mathrm{A}}}{\partial \mathrm{c}^{\mathrm{A}}} = \frac{1}{\mathrm{c}^{\mathrm{A}}}\mu^{\mathrm{A}}, \\ \lambda^{\mathrm{B}} &= \frac{\rho^{\mathrm{B}}}{\mathrm{n}^{\mathrm{G}}}\frac{\partial \psi^{\mathrm{B}}}{\partial \mathrm{c}^{\mathrm{B}}} = \mathrm{c}^{\mathrm{B}}\mathrm{M}^{\mathrm{B}}_{\mathrm{ol}}\frac{\partial \psi^{\mathrm{B}}}{\partial \mathrm{c}^{\mathrm{B}}} = \frac{1}{\mathrm{c}^{\mathrm{B}}}\mu^{\mathrm{B}}, \\ \lambda^{\mathrm{C}} &= \frac{\rho^{\mathrm{C}}}{\mathrm{n}^{\mathrm{G}}}\frac{\partial \psi^{\mathrm{C}}}{\partial \mathrm{c}^{\mathrm{C}}} = \mathrm{c}^{\mathrm{C}}\mathrm{M}^{\mathrm{C}}_{\mathrm{ol}}\frac{\partial \psi^{\mathrm{C}}}{\partial \mathrm{c}^{\mathrm{C}}} = \frac{1}{\mathrm{c}^{\mathrm{C}}}\mu^{\mathrm{C}}. \end{aligned} \tag{7.66}$$

Thus,

$$\lambda = (\rho^{\mathrm{GR}})^2\frac{\partial \psi^{\mathrm{G}}}{\partial \rho^{\mathrm{GR}}} + \mu^{\mathrm{A}} + \mu^{\mathrm{B}} + \mu^{\mathrm{C}} \tag{7.67}$$

and

$$\lambda^{\mathrm{S}} = \lambda + \rho^{\mathrm{S}}\frac{\partial \psi^{\mathrm{S}}}{\partial \mathrm{n}^{\mathrm{S}}}. \tag{7.68}$$

7.11.2 Evaluation of Cauchy stress tensors

As entropy inequality shows, the 1^{st} to 5^{th} terms are zero. Thus, the Cauchy stress tensors are

$$\begin{aligned}
\mathbf{T}^{\mathrm{S}} &= -\lambda^{\mathrm{S}}\mathrm{n}^{\mathrm{S}} + 2\rho^{\mathrm{S}}\mathbf{F}_{\mathrm{S}}\frac{\partial\psi^{\mathrm{S}}}{\partial\mathbf{C}_{\mathrm{S}}}\mathbf{F}_{\mathrm{S}}^{\mathbf{T}}, \\
\mathbf{T}^{\mathrm{G}} &= \lambda^{\mathrm{A}}\mathrm{n}^{\mathrm{G}}\mathrm{c}^{\mathrm{A}}\mathbf{I} + \lambda^{\mathrm{B}}\mathrm{n}^{\mathrm{G}}\mathrm{c}^{\mathrm{B}}\mathbf{I} + \lambda^{\mathrm{C}}\mathrm{n}^{\mathrm{G}}\mathrm{c}^{\mathrm{C}}\mathbf{I} - \lambda\mathrm{n}^{\mathrm{G}}\mathbf{I} \\
&= -\mathrm{n}^{\mathrm{G}}(\rho^{\mathrm{GR}})^2\frac{\partial\psi^{\mathrm{G}}}{\partial\rho^{\mathrm{GR}}} \\
&= -\mathrm{n}^{\mathrm{G}}\mathrm{p}^{\mathrm{GR}}\mathbf{I}, \\
\mathbf{T}^{\mathrm{A}} &= -\lambda^{\mathrm{A}}\mathrm{n}^{\mathrm{G}}\mathrm{c}^{\mathrm{A}}\mathbf{I} = -\mathrm{n}^{\mathrm{G}}\mu^{\mathrm{A}}\mathbf{I}, \\
\mathbf{T}^{\mathrm{B}} &= -\lambda^{\mathrm{B}}\mathrm{n}^{\mathrm{G}}\mathrm{c}^{\mathrm{B}}\mathbf{I} = -\mathrm{n}^{\mathrm{G}}\mu^{\mathrm{B}}\mathbf{I}, \\
\mathbf{T}^{\mathrm{C}} &= -\lambda^{\mathrm{C}}\mathrm{n}^{\mathrm{G}}\mathrm{c}^{\mathrm{C}}\mathbf{I} = -\mathrm{n}^{\mathrm{G}}\mu^{\mathrm{C}}\mathbf{I}.
\end{aligned} \tag{7.69}$$

where p^{GR} is the pressure of gas phase.

7.11.3 Evaluation of molar concentration

The definition of chemical potential has been given in equation 7.44. Assumed

$$\bar{\mu}^{\alpha} = \mu^{\alpha} - \mu_0^{\alpha}, \tag{7.70}$$

and

$$\theta = \theta^{\mathrm{A}} = \theta^{\mathrm{B}} = \theta^{\mathrm{C}}, \tag{7.71}$$

so that, the molar concentration of gases can be given as

$$\begin{aligned}
\mathrm{c}^{\mathrm{A}} &= \exp(\frac{1}{\mathrm{R}\theta}\bar{\mu}^{\mathrm{A}}\mathrm{M}_{\mathrm{ol}}^{\mathrm{A}})\cdot\mathrm{c}_0^{\mathrm{A}}, \\
\mathrm{c}^{\mathrm{B}} &= \exp(\frac{1}{\mathrm{R}\theta}\bar{\mu}^{\mathrm{B}}\mathrm{M}_{\mathrm{ol}}^{\mathrm{B}})\cdot\mathrm{c}_0^{\mathrm{B}}, \\
\mathrm{c}^{\mathrm{C}} &= \exp(\frac{1}{\mathrm{R}\theta}\bar{\mu}^{\mathrm{C}}\mathrm{M}_{\mathrm{ol}}^{\mathrm{C}})\cdot\mathrm{c}_0^{\mathrm{C}}.
\end{aligned} \tag{7.72}$$

Thus, the derivative forms of molar concentration are written as

$$
\begin{aligned}
(\mathrm{c}^{\mathrm{A}})'_{\mathrm{S}} &= \frac{\partial \mathrm{c}^{\mathrm{A}}}{\partial \mu^{\mathrm{A}}}(\bar{\mu^{\mathrm{A}}})'_{\mathrm{S}} = \frac{\mathrm{M}^{\mathrm{A}}_{\mathrm{ol}}}{\mathrm{R}\theta}\mathrm{c}^{\mathrm{A}}_{0}\exp(\frac{\bar{\mu}^{\mathrm{A}}\mathrm{M}^{\mathrm{A}}_{\mathrm{ol}}}{\mathrm{R}\theta})\cdot(\mu^{\mathrm{A}})'_{\mathrm{S}},\\
(\mathrm{c}^{\mathrm{B}})'_{\mathrm{S}} &= \frac{\partial \mathrm{c}^{\mathrm{B}}}{\partial \mu^{\mathrm{B}}}(\bar{\mu^{\mathrm{B}}})'_{\mathrm{S}} = \frac{\mathrm{M}^{\mathrm{B}}_{\mathrm{ol}}}{\mathrm{R}\theta}\mathrm{c}^{\mathrm{B}}_{0}\exp(\frac{\bar{\mu}^{\mathrm{B}}\mathrm{M}^{\mathrm{B}}_{\mathrm{ol}}}{\mathrm{R}\theta})\cdot(\mu^{\mathrm{B}})'_{\mathrm{S}},\\
(\mathrm{c}^{\mathrm{C}})'_{\mathrm{S}} &= \frac{\partial \mathrm{c}^{\mathrm{C}}}{\partial \mu^{\mathrm{C}}}(\bar{\mu^{\mathrm{C}}})'_{\mathrm{S}} = \frac{\mathrm{M}^{\mathrm{C}}_{\mathrm{ol}}}{\mathrm{R}\theta}\mathrm{c}^{\mathrm{C}}_{0}\exp(\frac{\bar{\mu}^{\mathrm{C}}\mathrm{M}^{\mathrm{C}}_{\mathrm{ol}}}{\mathrm{R}\theta})\cdot(\mu^{\mathrm{C}})'_{\mathrm{S}}.
\end{aligned}
\tag{7.73}
$$

7.11.4 Evaluation of seepage velocities

Tracing back to equation 7.19 of mass balance, the 3^{rd} term is the definition of flux

$$
\mathrm{J}^{\alpha} = \mathrm{c}^{\alpha}\mathrm{n}^{\mathrm{G}}\mathbf{w}_{\alpha\mathrm{S}}. \tag{7.74}
$$

Actually, the flux can be expressed by Fick's law. Thus, the seepage velocities of gas A, B and C are

$$
\begin{aligned}
\mathbf{w}_{\mathrm{AS}} &= \mathrm{D}_{\mathrm{AG}}(-\mathrm{n}^{\mathrm{G}}\mathrm{grad}\mu^{\mathrm{A}}),\\
\mathbf{w}_{\mathrm{BS}} &= \mathrm{D}_{\mathrm{BG}}(-\mathrm{n}^{\mathrm{G}}\mathrm{grad}\mu^{\mathrm{B}}),\\
\mathbf{w}_{\mathrm{CS}} &= \mathrm{D}_{\mathrm{CG}}(-\mathrm{n}^{\mathrm{G}}\mathrm{grad}\mu^{\mathrm{C}}),
\end{aligned}
\tag{7.75}
$$

where D_{AG}, D_{BG} and D_{CG} are the Fick's diffusion coefficients of gas A, B, C in gas phase.

Taking the term of $\mathbf{T}^{\mathrm{G}}$ into momentum balance equation and assumed acceleration $\mathbf{x}'' = 0$, the momentum balance equation for gas phase is

$$
-\mathrm{n}^{\mathrm{G}}\mathrm{gradp}^{\mathrm{GR}} + \rho^{\mathrm{G}}\mathrm{b} + \alpha_{\mathrm{AG}}\mathbf{w}_{\mathrm{AG}} + \alpha_{\mathrm{BG}}\mathbf{w}_{\mathrm{BG}} + \alpha_{\mathrm{CG}}\mathbf{w}_{\mathrm{CG}} - \alpha_{\mathrm{GS}}\mathbf{w}_{\mathrm{GS}} = 0. \tag{7.76}
$$

So that, the seepage velocity $\mathbf{w}_{\mathrm{GS}}$ is evaluated

$$
\mathbf{w}_{\mathrm{GS}} = \frac{1}{\alpha_{\mathrm{GS}}}(-\mathrm{n}^{\mathrm{G}}\mathrm{gradp}^{\mathrm{GR}} + \rho^{\mathrm{G}}\mathrm{b} + \alpha_{\mathrm{AG}}\mathbf{w}_{\mathrm{AG}} + \alpha_{\mathrm{BG}}\mathbf{w}_{\mathrm{BG}} + \alpha_{\mathrm{CG}}\mathbf{w}_{\mathrm{CG}}), \tag{7.77}
$$

in which, α_{GS}=$\frac{1}{\mathrm{D}_{\mathrm{GS}}}$, α_{AG}=$\frac{1}{\mathrm{D}_{\mathrm{AG}}}$, α_{BG}=$\frac{1}{\mathrm{D}_{\mathrm{BG}}}$ and α_{CG}=$\frac{1}{\mathrm{D}_{\mathrm{CG}}}$.

7.11.5 Evaluation of interaction forces

The interaction forces among gases are postulated as

$$\begin{aligned}
\hat{\mathbf{p}}^{\mathrm{A}} &= \mu^{\mathrm{A}}\mathrm{gradn}^{\mathrm{G}} - \alpha_{\mathrm{AG}}\mathbf{w}_{\mathrm{AG}},\\
\hat{\mathbf{p}}^{\mathrm{B}} &= \mu^{\mathrm{B}}\mathrm{gradn}^{\mathrm{G}} - \alpha_{\mathrm{BG}}\mathbf{w}_{\mathrm{BG}},\\
\hat{\mathbf{p}}^{\mathrm{C}} &= \mu^{\mathrm{C}}\mathrm{gradn}^{\mathrm{G}} - \alpha_{\mathrm{CG}}\mathbf{w}_{\mathrm{CG}},\\
\hat{\mathbf{p}}^{\mathrm{G}} &= \lambda\mathrm{gradn}^{\mathrm{G}} - \hat{\mathbf{p}}^{\mathrm{A}} - \hat{\mathbf{p}}^{\mathrm{B}} - \hat{\mathbf{p}}^{\mathrm{C}} - \alpha_{\mathrm{GS}}\mathbf{w}_{\mathrm{GS}}.
\end{aligned} \tag{7.78}$$

7.12 Weak Forms

In order to determine the mass balance and momentum balance equations, the weak forms will to be set up.

7.12.1 Momentum for mixture

The sum of Cauchy stress tensor of constitutive φ^{α} is

$$\mathbf{T}^{\mathrm{S}} + \mathbf{T}^{\mathrm{G}} + \mathbf{T}^{\mathrm{A}} + \mathbf{T}^{\mathrm{B}} + \mathbf{T}^{\mathrm{C}} = -\lambda\mathbf{I} + 2\rho^{\mathrm{S}}\mathbf{F}_{\mathrm{S}}\frac{\partial\psi^{\mathrm{S}}}{\partial\mathbf{C}_{\mathrm{S}}}\mathbf{F}_{\mathrm{S}}^{\mathbf{T}} = -\lambda\mathbf{I} + \mathbf{T}_{\mathrm{E}}^{\mathrm{S}}. \tag{7.79}$$

Thus, the momentum balance of mixture can be written as

$$\mathrm{div}\{-\lambda\mathbf{I} + \mathbf{T}_{\mathrm{E}}^{\mathrm{S}}\} + (\rho^{\mathrm{S}} + \rho^{\mathrm{G}} + \rho^{\mathrm{A}} + \rho^{\mathrm{B}} + \rho^{\mathrm{C}})\mathbf{b} - \hat{\rho}^{\mathrm{A}}\mathbf{w}_{\mathrm{AS}} - \hat{\rho}^{\mathrm{B}}\mathbf{w}_{\mathrm{BS}} - \hat{\rho}^{\mathrm{C}}\mathbf{w}_{\mathrm{CS}} = 0. \tag{7.80}$$

Considering the relations $\mathrm{dv} = \mathbf{J}_{\mathrm{S}}\mathrm{dV}_{0\mathrm{S}}$ and Jacobian $\mathrm{Lin}\ \mathbf{J}_{\mathrm{S}} = 1 + \mathrm{tr}\varepsilon$, the weak form of momentum balance equation for mixture is

$$\begin{aligned}
\mathrm{G}_{\mathrm{BMM}} = &\sum_{\mathrm{I}}(\delta\mathrm{d}\mathbf{u}_{\mathrm{S}}^{\mathrm{I}})^{\mathrm{T}}\int_{\mathrm{B}_{0\mathrm{S}}}\mathrm{B}_{\mathrm{I}}^{\mathrm{T}}(-\lambda\mathbf{I} + \mathbf{S}_{\mathrm{LIN}}^{\mathrm{E}})\mathrm{dV}_{0\mathrm{S}}\\
&- \sum_{\mathrm{I}}(\delta\mathrm{d}\mathbf{u}_{\mathrm{S}}^{\mathrm{I}})^{\mathrm{T}}\int_{\mathrm{B}_{0\mathrm{S}}}\mathrm{N}_{\mathrm{I}}(\rho^{\mathrm{S}} + \rho^{\mathrm{G}} + \mathrm{c}^{\mathrm{A}}\mathrm{M}_{\mathrm{ol}}^{\mathrm{A}}\mathrm{n}^{\mathrm{G}} + \mathrm{c}^{\mathrm{B}}\mathrm{M}_{\mathrm{ol}}^{\mathrm{B}}\mathrm{n}^{\mathrm{G}} + \mathrm{c}^{\mathrm{C}}\mathrm{M}_{\mathrm{ol}}^{\mathrm{C}}\mathrm{n}^{\mathrm{G}})\mathbf{b}\mathbf{J}_{\mathrm{S}}\mathrm{dV}_{0\mathrm{S}}\\
&+ \sum_{\mathrm{I}}(\delta\mathrm{d}\mathbf{u}_{\mathrm{S}}^{\mathrm{I}})^{\mathrm{T}}\int_{\mathrm{B}_{0\mathrm{S}}}\mathrm{N}_{\mathrm{I}}\hat{\rho}^{\mathrm{A}}\mathbf{w}_{\mathrm{AS}}\mathbf{J}_{\mathrm{S}}\mathrm{dV}_{0\mathrm{S}} + \sum_{\mathrm{I}}(\delta\mathrm{d}\mathbf{u}_{\mathrm{S}}^{\mathrm{I}})^{\mathrm{T}}\int_{\mathrm{B}_{0\mathrm{S}}}\mathrm{N}_{\mathrm{I}}\hat{\rho}^{\mathrm{B}}\mathbf{w}_{\mathrm{BS}}\mathbf{J}_{\mathrm{S}}\mathrm{dV}_{0\mathrm{S}}\\
&+ \sum_{\mathrm{I}}(\delta\mathrm{d}\mathbf{u}_{\mathrm{S}}^{\mathrm{I}})^{\mathrm{T}}\int_{\mathrm{B}_{0\mathrm{S}}}\mathrm{N}_{\mathrm{I}}\hat{\rho}^{\mathrm{C}}\mathbf{w}_{\mathrm{CS}}\mathbf{J}_{\mathrm{S}}\mathrm{dV}_{0\mathrm{S}} - \sum_{\mathrm{I}}(\delta\mathrm{d}\mathbf{u}_{\mathrm{S}}^{\mathrm{I}})^{\mathrm{T}}\int_{\partial\mathrm{B}_{\mathrm{S}}}\mathrm{N}_{\mathrm{I}}(-\lambda\mathbf{I} + \mathbf{S}_{\mathrm{E,LIN}}^{\mathrm{S}})\mathrm{n}_0\mathrm{dA}_{0\mathrm{S}},
\end{aligned} \tag{7.81}$$

in which, $\delta\mathrm{d}\mathbf{u}_{\mathrm{S}}$ is the weight function.

7.12.2 Mass balance equations

For the solid phase, the mass balance equation is multiplied with weight function $\delta \mathrm{n}^{\mathrm{S}}$. Thus the mass balance equation for solid phase is

$$\begin{aligned}
\mathrm{G}_{\mathrm{MBMS}} &= \int_{\mathrm{B}} [\mathrm{div}\mathbf{x}_{\mathrm{S}}^{'} + \mathrm{div}\mathrm{n}^{\mathrm{G}}\mathbf{w}_{\mathrm{GS}} - \mathrm{n}^{\mathrm{G}}\mathrm{div}\mathbf{x}_{\mathrm{G}}^{'} - (\mathrm{n}^{\mathrm{G}})_{\mathrm{G}}^{'} - \frac{\hat{\rho}^{\mathrm{S}}}{\rho_{0\mathrm{S}}^{\mathrm{SR}}}]\mathrm{dn}^{\mathrm{S}}\mathrm{dv} \\
&= \sum_{\mathrm{I}}(\delta \mathrm{dn}^{\mathrm{S}})^{\mathrm{T}} \int_{\mathrm{B}_{0\mathrm{S}}} \mathrm{N}_{\mathrm{I}}\mathrm{tr}\mathbf{D}_{\mathrm{S}}\mathbf{J}_{\mathrm{S}}\mathrm{dV}_{0\mathrm{S}} - \sum_{\mathrm{I}}(\delta \mathrm{dn}^{\mathrm{S}})^{\mathrm{T}} \int_{\mathrm{B}_{0\mathrm{S}}} \mathrm{N}_{\mathrm{I}}\mathrm{n}^{\mathrm{G}}\mathrm{tr}\mathbf{D}_{\mathrm{G}}\mathbf{J}_{\mathrm{S}}\mathrm{dV}_{0\mathrm{S}} \\
&- \sum_{\mathrm{I}}(\delta \mathrm{dn}^{\mathrm{S}})^{\mathrm{T}} \int_{\mathrm{B}_{0\mathrm{S}}} \mathrm{N}_{\mathrm{I}}(\mathrm{n}^{\mathrm{G}})_{\mathrm{G}}^{'}\mathrm{tr}\mathbf{D}_{\mathrm{G}}\mathbf{J}_{\mathrm{S}}\mathrm{dV}_{0\mathrm{S}} - \sum_{\mathrm{I}}(\delta \mathrm{dn}^{\mathrm{S}})^{\mathrm{T}} \int_{\mathrm{B}_{0\mathrm{S}}} \mathrm{N}_{\mathrm{I}}\frac{\hat{\rho}^{\mathrm{S}}}{\rho_{0\mathrm{S}}^{\mathrm{SR}}}\mathbf{J}_{\mathrm{S}}\mathrm{dV}_{0\mathrm{S}} \\
&- \sum_{\mathrm{I}}(\delta \mathrm{dn}^{\mathrm{S}})^{\mathrm{T}} \int_{\mathrm{B}_{0\mathrm{S}}} \mathrm{B}_{\mathrm{I}}^{\mathrm{T}}\mathrm{n}^{\mathrm{G}}\mathbf{w}_{\mathrm{GS}}\mathbf{J}_{\mathrm{S}}\mathrm{dV}_{0\mathrm{S}} + \sum_{\mathrm{I}}(\delta \mathrm{dn}^{\mathrm{S}})^{\mathrm{T}} \int_{\partial \mathrm{B}_{\mathrm{S}}} \mathrm{N}_{\mathrm{I}}\mathrm{n}^{\mathrm{G}}\mathbf{w}_{\mathrm{GS}}\mathrm{n}_0\mathrm{dA}_{0\mathrm{S}}.
\end{aligned} \tag{7.82}$$

For gas A, B and C, the mass balance equations are multiplied by weight function of $\delta\mu^{\alpha}$. Therefore, the mass balance equation of gas A can be written as

$$\begin{aligned}
\mathrm{G}_{\mathrm{MBA}} &= \sum_{\mathrm{I}}(\delta \mathrm{d}\mu^{\mathrm{A}}) \int_{\mathrm{B}_{0\mathrm{S}}} \mathrm{N}_{\mathrm{I}}\mathrm{n}^{\mathrm{G}}\frac{\mathrm{M}_{\mathrm{ol}}^{\mathrm{A}}}{\mathrm{R}\theta}\mathrm{c}_0^{\mathrm{A}}\exp(\frac{\bar{\mu}^{\mathrm{A}}\mathrm{M}_{\mathrm{ol}}^{\mathrm{A}}}{\mathrm{R}\theta})(\mu^{\mathrm{A}})_{\mathrm{S}}^{'}\mathbf{J}_{\mathrm{S}}\mathrm{dV}_{0\mathrm{S}} \\
&- \sum_{\mathrm{I}}(\delta \mathrm{d}\mu^{\mathrm{A}}) \int_{\mathrm{B}_{0\mathrm{S}}} \mathrm{N}_{\mathrm{I}}\mathrm{c}^{\mathrm{A}}(\mathrm{n}^{\mathrm{S}})_{\mathrm{S}}^{'}\mathbf{J}_{\mathrm{S}}\mathrm{dV}_{0\mathrm{S}} - \sum_{\mathrm{I}}(\delta \mathrm{d}\mu^{\mathrm{A}}) \int_{\mathrm{B}_{0\mathrm{S}}} \mathrm{B}_{\mathrm{I}}^{\mathrm{T}}\mathrm{J}^{\mathrm{A}}\mathbf{J}_{\mathrm{S}}\mathrm{dV}_{0\mathrm{S}} \\
&+ \sum_{\mathrm{I}}(\delta \mathrm{d}\mu^{\mathrm{A}}) \int_{\mathrm{B}_{0\mathrm{S}}} \mathrm{N}_{\mathrm{I}}\mathrm{c}^{\mathrm{A}}\mathrm{n}^{\mathrm{G}}\mathrm{tr}\mathbf{D}_{\mathrm{S}}\mathbf{J}_{\mathrm{S}}\mathrm{dV}_{0\mathrm{S}} - \sum_{\mathrm{I}}(\delta \mathrm{d}\mu^{\mathrm{A}}) \int_{\mathrm{B}_{0\mathrm{S}}} \mathrm{N}_{\mathrm{I}}\frac{\hat{\rho}^{\mathrm{A}}}{\mathrm{M}_{\mathrm{ol}}^{\mathrm{A}}}\mathbf{J}_{\mathrm{S}}\mathrm{dV}_{0\mathrm{S}} \\
&+ \sum_{\mathrm{I}}(\delta \mathrm{d}\mu^{\mathrm{A}}) \int_{\partial \mathrm{B}_{\mathrm{S}}} \mathrm{N}_{\mathrm{I}}\mathrm{J}^{\mathrm{A}}\mathrm{n}_0\mathrm{dA}_{0\mathrm{S}},
\end{aligned} \tag{7.83}$$

the mass balance equations on gas B and C can be written in the same way.

7.13 Finite Element Discretization

As to many continuum problems arise in engineering and physics, they are usually posed by appropriate differential equations and boundary conditions to be imposed on the unknown function [110]. This unknown function **u** will satisfiy a certain differential equation set

$$\mathbf{A}(\mathbf{u}) = \left\{ \begin{array}{c} A_1(\mathbf{u}) \\ A_2(\mathbf{u}) \\ \vdots \end{array} \right\} = 0 \tag{7.84}$$

in a domain Ω, together with certain boundary conditions

$$\mathbf{B}(\mathbf{u}) = \left\{ \begin{array}{c} B_1(\mathbf{u}) \\ B_2(\mathbf{u}) \\ \vdots \end{array} \right\} = 0 \tag{7.85}$$

on the boundaries Γ of the domain.

Thus, the finite element process will seek the solution in the approximate form

$$\mathbf{u} \approx \hat{\mathbf{u}} = \sum_{i=1}^{n} \mathbf{N}_i \mathbf{a}_i = \mathbf{N}\mathbf{a} \tag{7.86}$$

where $\mathbf{N}_i$ are shape functions prescribed in terms of independent variables and all or most of the parameters $\mathbf{a}_i$ are unknown.

It is noteworthy that the shape functions are usually defined locally for elements or sudomains, and the properties of discrete systems are recovered if the approximating equations are cast in an integral form.

7.14 Interphase Mass Transfer

Adsorption is in fact the mass transfer between the solid phase and fluid phase. In general, there are two kinds of ways to be used to model the interphase transfer. One of them is so called kinetic formulation model. In this approach, the driving force for mass transfer is expressed as the difference between the actual concentration and some equilibrium concentration. The other one is a set of functions on dissipative mass exchange. This method postulates that the rate of mass transfer is fast. Thus, the concentration of a constituent φ^α is distributed between phases. In order to fill the requirements of simulation, no matter kinetic models or functions on dissipative mass exchange, both of them should describe the equilibrium state of each constituent φ^α.

7.14.1 Kinetic models

In kinetic models, the mass transfer term of constituent φ^α is related to a rate of mass exchange between phases, that is $\hat{\rho}^\alpha = \frac{\partial \bar{\rho}^\alpha}{\partial \mathrm{t}}$, in which $\bar{\rho}^\alpha$ is the average amount adsorbed of constituent φ^α in a phase. In the case of landfill gas adsorption, mass transfer takes place between solid phase and gas phase. Normally, mass transfer in the solid phase could be expressed as:

$$\frac{\partial \bar{\rho}^{\alpha\mathrm{S}}}{\partial \mathrm{t}} = \kappa_{\mathrm{SG}}^{\alpha\mathrm{S}} (\rho^{*\alpha\mathrm{S}} - \bar{\rho}^{\alpha\mathrm{S}}), \tag{7.87}$$

where $\kappa_{\mathrm{SG}}^{\alpha\mathrm{S}}$ is the mass transfer coefficient, and $\rho^{*\alpha\mathrm{S}}$ is the adsorbed density of φ^α in the equilibrium state. The mass transfer coefficient could be a function of the Darcy velocity, dispersion coefficient, constituents concentrations, temperature, and amount of interfacial area between solid and gas phase [111].

Based on the results of landfill gas adsorption experiments, it can be obtained in a form of equilibrium of each constituent φ^α concentrations. As discussed in section 5.3, this kind of

equilibrium concentration is related to the flow rate of input gas. The coefficients of equilibrium model can be determined by fitting to the experimental data.

However, modeling of kinetic models is a complicated proceeding. As to the landfill gas adsorption, three kinds of gases and two kinds of phases are involved for equilibrium state. In addition, the mass transfer coefficient of each constituent are required to be evaluated between solid and gas phases. It means that the simplified models on interphase transfer are needed for the purpose of simulation.

7.14.2 Functions on dissipative mass exchange

Instead of evaluating the transfer equation for each constituent φ^α in each phase, the functions on dissipative mass exchange only need to solve the transfer equation of φ^α in one phase. In this model systems, it is assumed that the mass transferred between phases does not accumulate at the interface. Thus, the terms of mass transfer can be written as:

$$\begin{aligned} \hat{\rho}^{\mathrm{S}} &= -\delta_{\Psi}^{\mathrm{S}}(\Psi^{\mathrm{S}} - \Psi^{\mathrm{G}}), \\ \hat{\rho}^{\mathrm{S}} &= -\hat{\rho}^{\mathrm{G}}, \end{aligned} \tag{7.88}$$

with

$$\Psi^\alpha = \psi^\alpha + \frac{1}{\rho^\alpha}\mathrm{p} + \rho^\alpha \frac{\partial \psi^\alpha}{\partial \rho^\alpha}. \tag{7.89}$$

Where, $\delta_{\Psi}^{\mathrm{S}}$ is a constant for the chemical potential functions Ψ^{S} and Ψ^{G}. Ψ^α is the reduced chemical potential.

Seen from experiments on landfill gas adsorption, the mass exchange mainly depends on the amount of bottom ash, which denoted as solid phase in modeling, and the concentration of CO_2 in gas phase. As the experiments illustrated, the amount of gas concentration in gas phase would reduce as amount of solid increasing, which can be expressed as a function of solid concentration. On the contrary, with the CO_2 concentration increasing, the amount of gas phase will increase before the solid adsorption capacity arrive to maximum.

Therefore, the interphase mass transfer of adsorption can be written as:

$$\hat{\rho}^{\mathrm{G}} = \hat{\rho}_{\rho^{\mathrm{S}}}^{\mathrm{G}} \circ \hat{\rho}_{\rho^{\mathrm{CO_2}}}^{\mathrm{G}}. \tag{7.90}$$

The mass exchange can be defined as a function of solid concentration:

$$\hat{\rho}_{\rho^{\mathrm{S}}} = \exp[\kappa_{\rho^{\mathrm{S}}} \cdot (\rho^{\mathrm{S}})^3], \tag{7.91}$$

where, the constant $\kappa_{\rho^{\mathrm{S}}}$ is related to bottom ash breakthrough capacity $\mathrm{C}_{\max}^{\mathrm{S}}$. The relation between solid concentration and mass exchange can be ploted by figure 7-1.

On the other hand, as figure 7-2 shown, the mass exchange is a function of CO_2 concentration as well:

$$\hat{\rho}_{\rho^{\mathrm{CO_2}}} = 1 - \exp[\kappa_{\rho^{\mathrm{CO_2}}} \cdot (\rho^{\mathrm{CO_2}})^3], \tag{7.92}$$

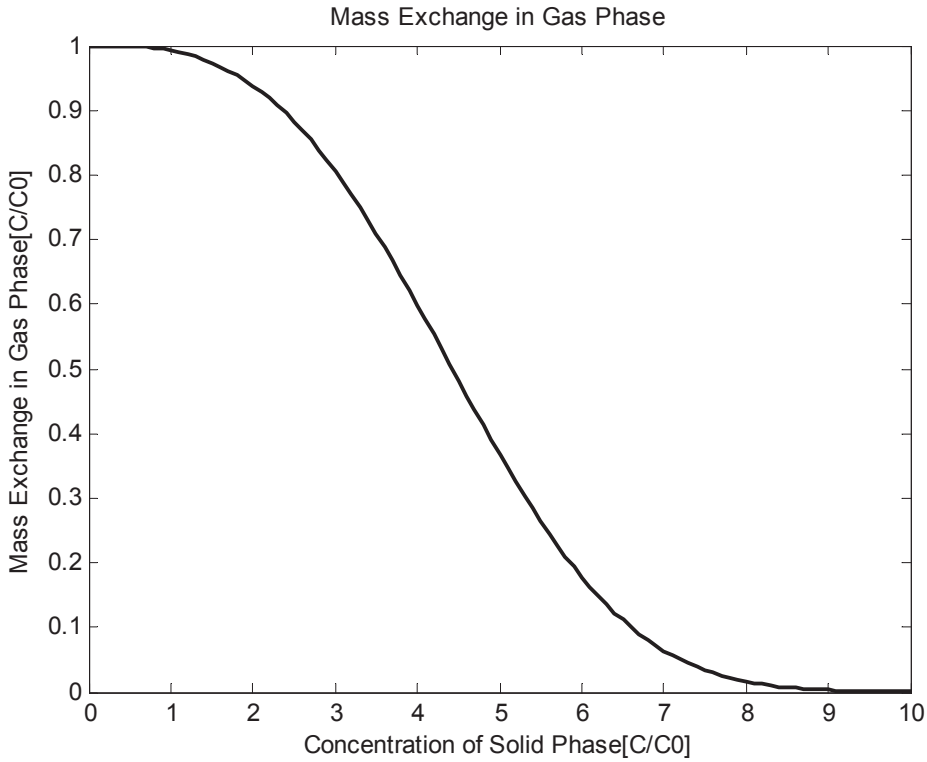

Figure 7-1: The Relation Between Mass Exchange and Solid Concentration.

and $\kappa_{\rho^{\mathrm{CO_2}}}$ is involed with the initial concentration of CO_2 in landfill gas mixtures.

7.15 Initial and Boundary Conditions

Generally, a region of interesting would be chosen in a numerical simulation. It is necessary to specify initial conditions throughout the domain. And, an optional boundary condition must be considered at each point on the boundary. In most cases, the boundary conditions are very important for the processes of simulation. Different boundary conditions may cause quite different simulation results.

Normally, there are three types of boundary conditions to be taken into account. The first type condition is also named as Dirichlet boundary condition. At a point on the boundary $\mathbf{x}_\mathrm{b}$, an unknown solution u(**x**,t) of constituent φ^α can be specified as:

$$\mathrm{u}^\alpha(\mathbf{x}_\mathrm{b}, \mathrm{t}) = \Omega^\alpha(\mathbf{x}_\mathrm{b}, \mathrm{t}). \tag{7.93}$$

That is, the value of a function is imposed on the boundary. In which, Ω^α is the specified distribution of the domain.

The second type condition is named Neumann boundary condition. It specifies the normal derivative values of a function on the surface of the domain. That is written as:

$$(\mathbf{n} \cdot \mathrm{gradu}^\alpha)|_{\mathbf{x}_\mathrm{b}} = \Omega^\alpha(\mathbf{x}_\mathrm{b}, \mathrm{t}). \tag{7.94}$$

Where, **n** denotes the normal to the boundary $\partial\Omega^\alpha$.

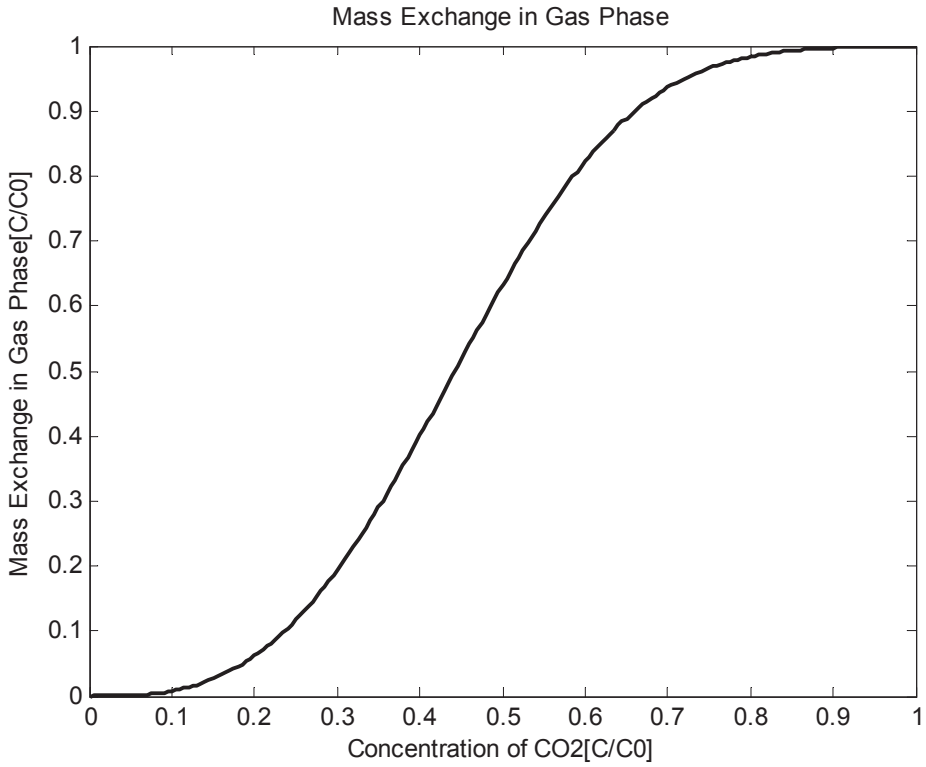

Figure 7-2: The Relation Between CO_2 Concentration and Mass Exchange.

Table 7-1: **Initial Conditions of Simulation**

Sign	Name	Value	Unit
P	Pressure	100.0	[Pa]
$\rho_0^{CO_2}$	CO_2 Initial Concentration	0.383	[g· L^{-1}]
θ	Temperature	298.0	[K]
D^{CO_2}	Diffusion Coefficient	0.16	[m· s^{-1}]
C^S_{max}	Average Breakthrough Capacity	5.42	[g CO_2·(L Solid)$^{-1}$]

The third type condition is Robin boundary conditions. For an unknown solution u^α in a region Ω^α, Robin boundary conditions is used to specify the condition as:

$$a\mathrm{u}^\alpha + b\frac{\partial \mathrm{u}^\alpha}{\partial \mathbf{n}} = \mathrm{U}^\alpha(\mathbf{x}_\mathrm{b}, \mathrm{t}), \tag{7.95}$$

That is, some non-zero values of a and b and a given function $\mathrm{U}^\alpha(\mathbf{x}_\mathrm{b}, \mathrm{t})$ can be defined on $\partial\Omega^\alpha$. In which, a and b may be constants or functions.

In the study of landfill gas adsorption, the interesting region is an open reactor. Within this reactor, the influent and effluent flow would be taken into consideration. Thus, the second type condition can be applied to simulation. At the boundary of domain, flux can be given as the normal gradient. For a situation where no flow occurs at the boundary, the normal gradient will be zero.

If the concentration and velocities of gases are varying with time, the initial conditions must be specified in simulation processes. At the beginning time, t=0, some parts of conditions are list in table 7-1.

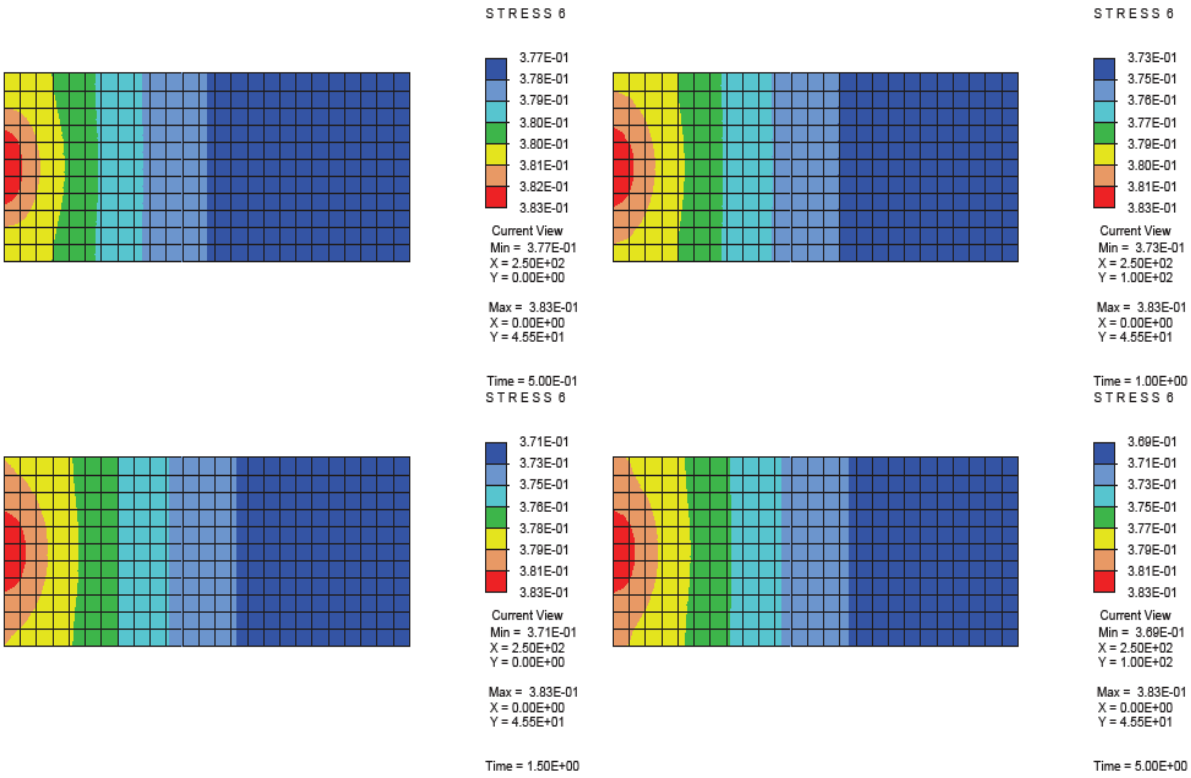

Figure 7-3: CO_2 Concentration in a Two-Dimension Region.

Here, the diffusion coefficient D^{CO_2} is evaluated for CO_2-CH_4-N_2 gas mixtures. It is the effective diffusion coefficients by neglecting the off-diagonal elements of the Fick matrix [112].

7.16 Simulation Results

The landfill gas adsorption models were solved by finite element methods with the Finite Element Analysis Program packages (FEAP). The model simulated adsorption processes in a two-dimension region, and the equations were calculated for every 0.1 time step.

7.16.1 Concentration and chemical potential

As shown in figure 7-3, CO_2 concentration would be adsorbed as gas flowed through the simulated region. The CO_2 concentration diminished gradually from gas inlet to outlet.

On the other hand, the CO_2 chemical potential would decrease continuously until the mass exchange between gas and solid phases get to equilibrium state. Figure 7-4 showed the chemical potential difference between CO_2 in inlet gas mixtures and that of adsorption processes.

7.16.2 Velocities of fluids

Figure 7-5 recorded the velocities of gas phase and CO_2 in processes. As discussed in initial conditions, the outlet of adsorbent bed was connected to surroundings. Thus, there existed a pressure gradient between the simulation region and surroundings. At inlet of simulation region,

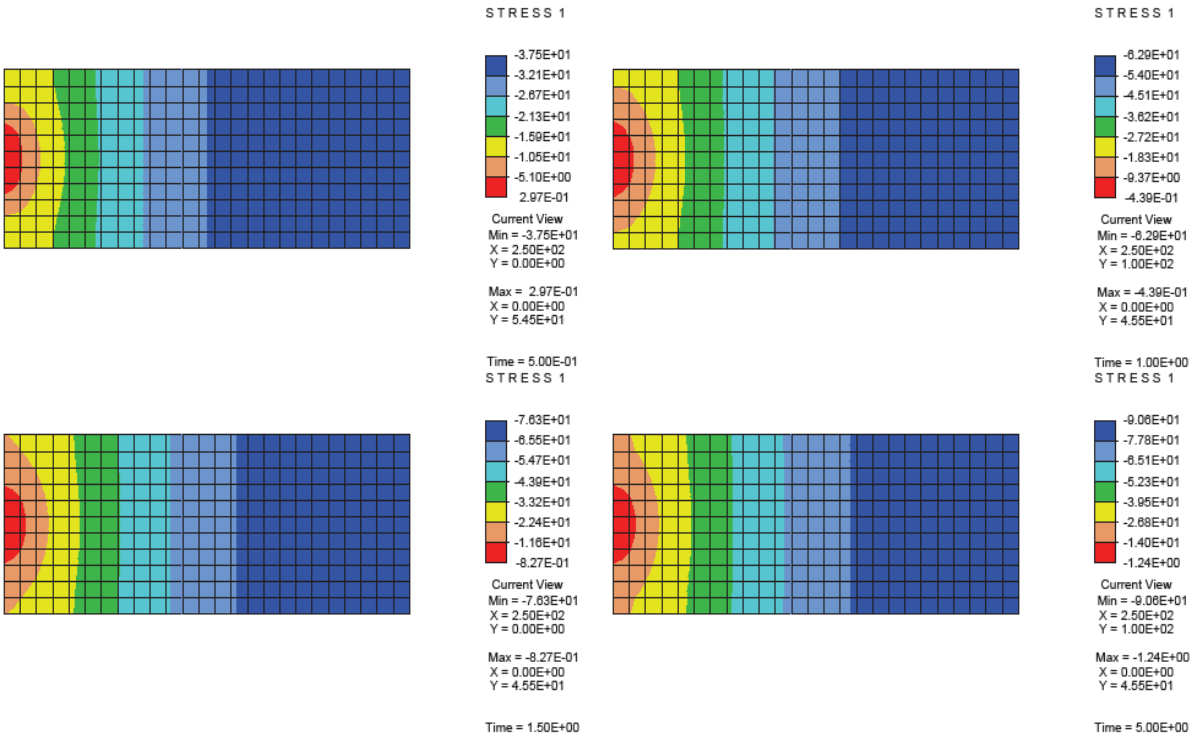

Figure 7-4: CO_2 Chemical Potential in Processes.

the velocities of fluids were mainly affected by concentration. In addition, at the outlet side, the velocities would be impacted by pressure gradient between simulation region and surroundings.

7.16.3 Pressure

The pressure in adsorbent bed was simulated in processes as well. As shown in figure 7-6, the pressure in simulation region was mainly determined by fluid concentration. However, at the outlet side, the pressure would be affected by surroundings conditions.

7.17 Seepage velocity

Since there are no measured values of the seepage velocity on the gas phase, the local concentration of CO_2 in the gas mixture can not be test in experiments. Therefore, the value of CO_2 concentration at different location can be predicted by CO_2 breakthrough time and solid breakthrough capacity, together with seepage velocity on gas phase [113].

As figure 7-7 shown, the CO_2 concentration were predicted at point N1, N2, and N3 respectively. The simulation results were shown in figure 7-8 to figure 7-11 by varying breakthrough capacities and seepage velocities. Meanwhile, the results of the simulation and the experiment were shown with a tolerance of 5%.

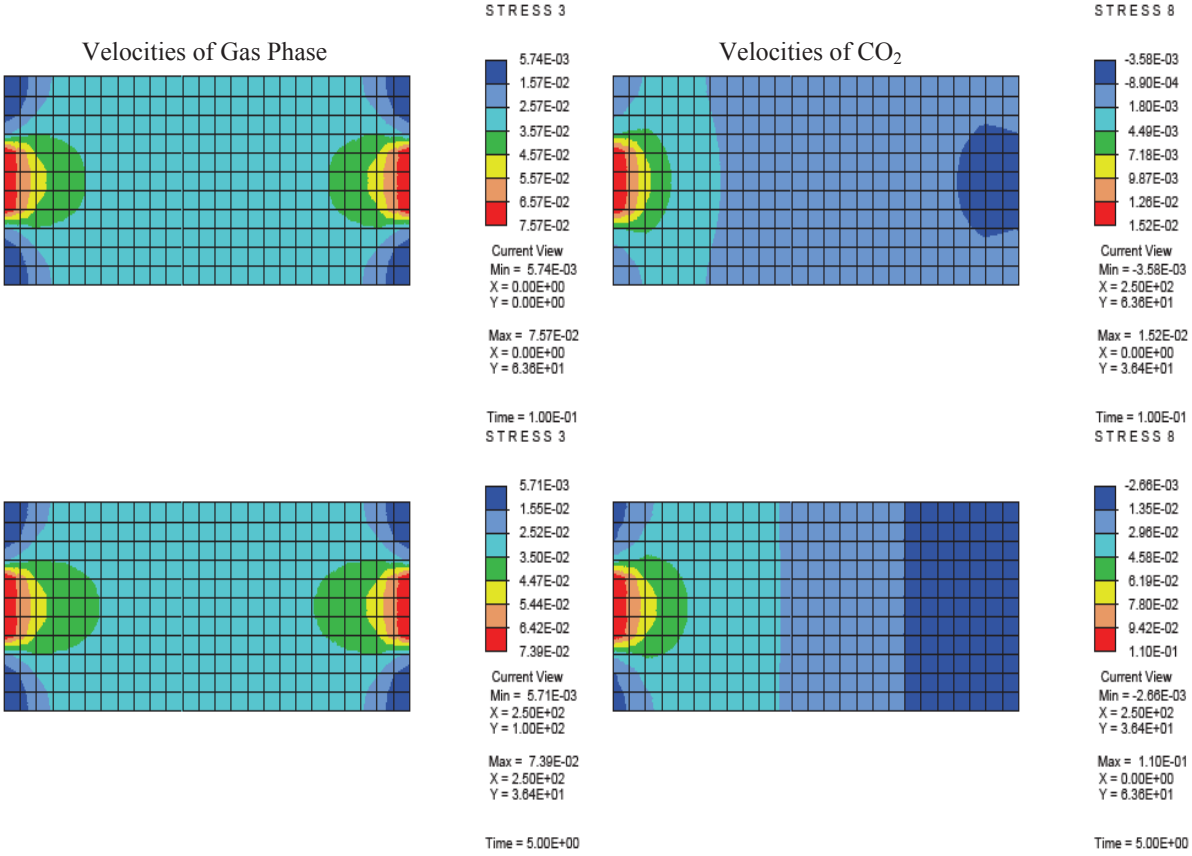

Figure 7-5: The Fluid Velocities in Simulation.

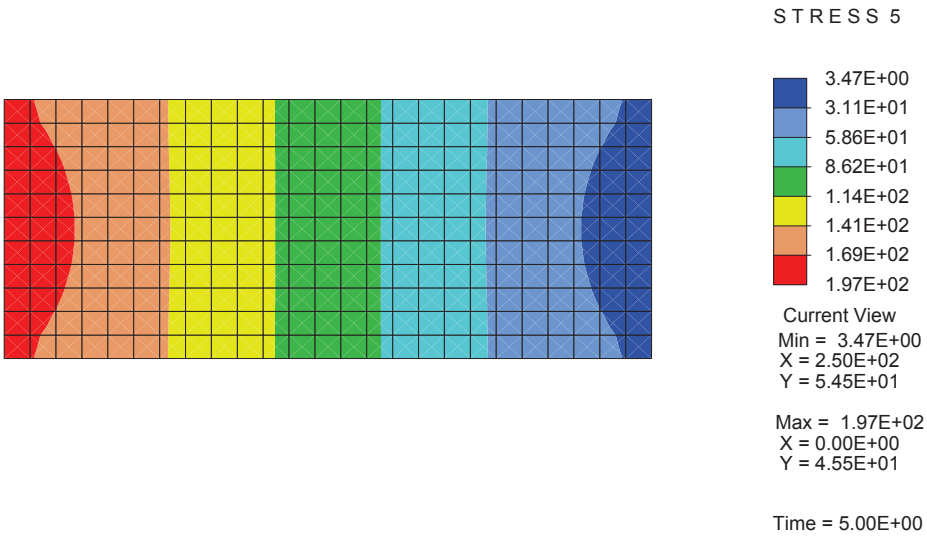

Figure 7-6: Pressure in Simulation Region.

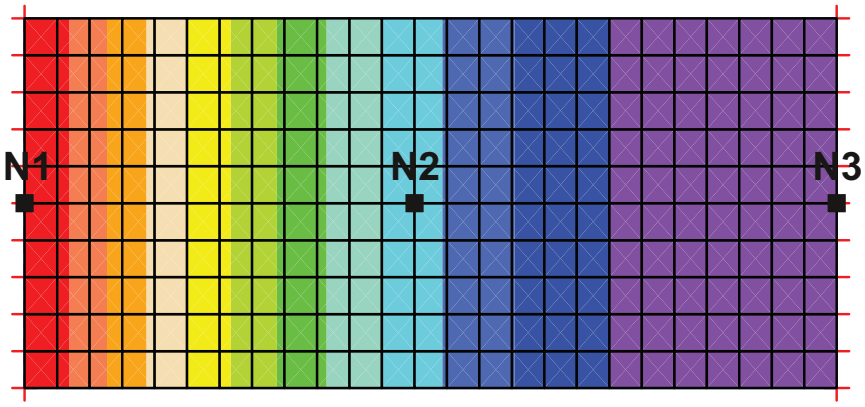

Figure 7-7: Locations in simulation.

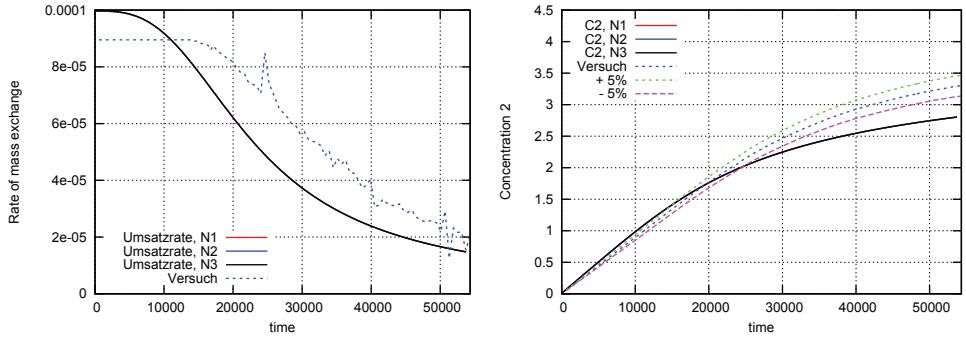

Figure 7-8: c^{S}_{max}=4.0, $\hat{\rho}^{CO_2}_{max}$=1·10^{-4}, $\mathbf{w}_{GS}$=1.1·10^{-3}, $c^{CO_2}_{0}$=0.015.

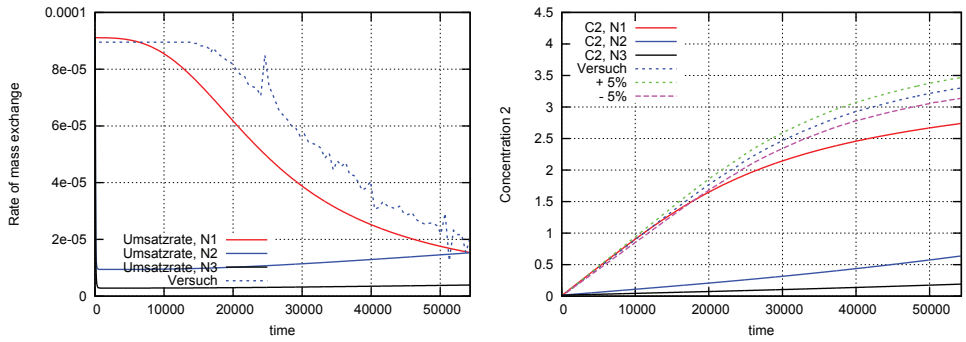

Figure 7-9: c^{S}_{max}=4.0, $\hat{\rho}^{CO_2}_{max}$=9.16·10^{-5}, $\mathbf{w}_{GS}$=1.1·10^{-3}, $c^{CO_2}_{0}$=0.015.

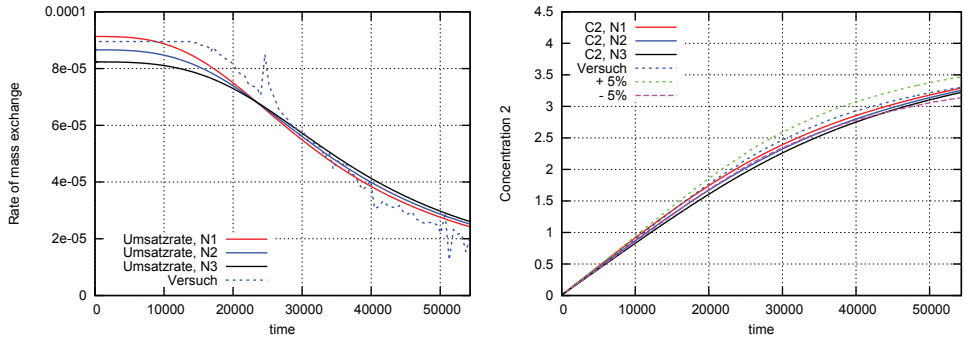

Figure 7-10: c^{S}_{max}=5.3, $\hat{\rho}^{CO_2}_{max}$=9.16·10^{-5}, $\mathbf{w}_{GS}$=0.022, $c^{CO_2}_{0}$=0.015.

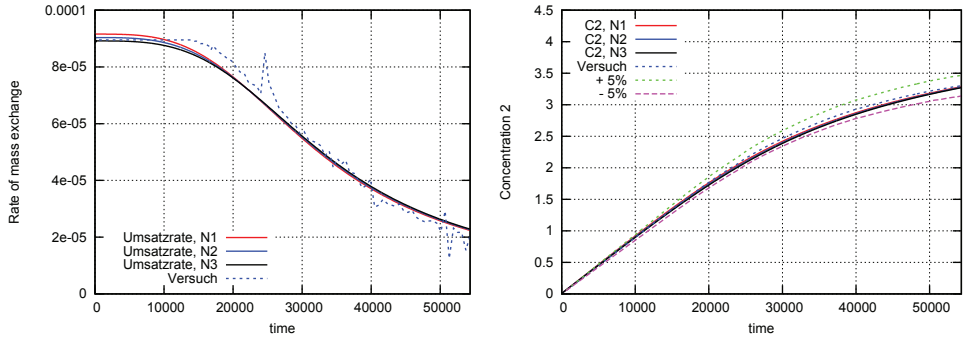

Figure 7-11: c^{S}_{max}=5.3, $\hat{\rho}^{CO_2}_{max}$=9.16·10^{-5}, $\mathbf{w}_{GS}$=0.033, $c^{CO_2}_{0}$=0.015.

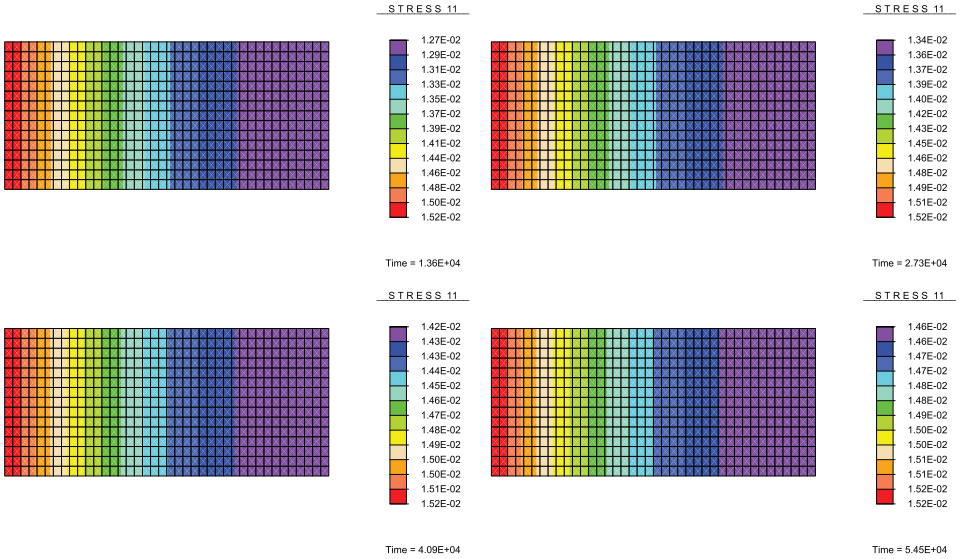

Figure 7-12: Size1: n_x=40, n_y=15.

7.18 Convergence

In order to determine the effect of finite element discretization on simulation results, mesh size was varied in this work. The CO_2 concentratiion at point N3 was considered, and the results were compared with those with various mesh size. The results were shown in figure 7-12 to figure 7-19

7.19 Conclusions

Simulation is an effective method on adsorption theories. According to the properties of landfill gas and bottom ash, the landfill gas adsorption system was formed from gas phase, solid phase, CO_2, CH_4, and N_2. The modeling was analyzed according to mass balance and momentum balance. Moreover, among the phase, the constitutive relations were introduced and developed in models.

At last, as the pretreatments to simulation, the interphase mass transfer models were discussed, and the parameters for simulation were listed. Furthermore, the parameter on seepage velocity of solid-gas phase and convergence were studied in the work of Liedmann [113]. The performance

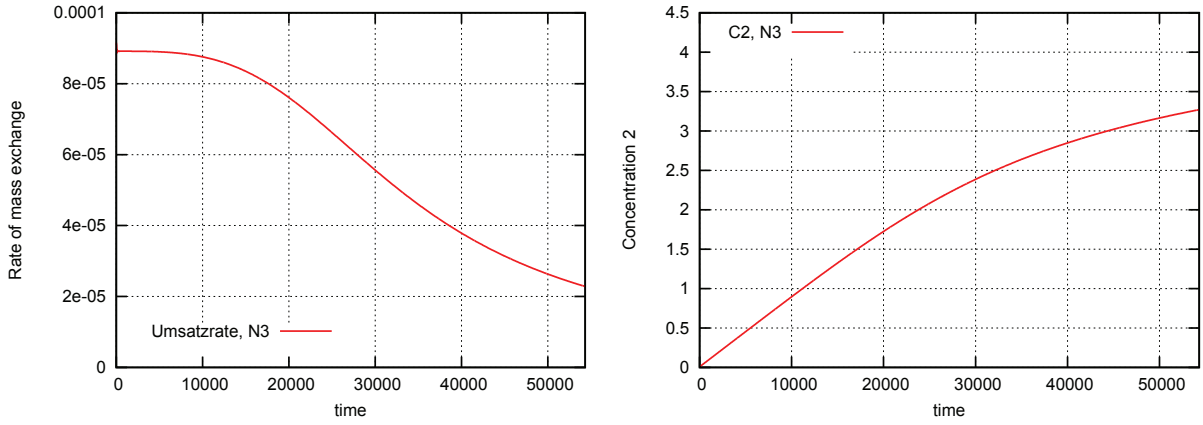

Figure 7-13: Breakthrough time and CO_2 concentration in size1.

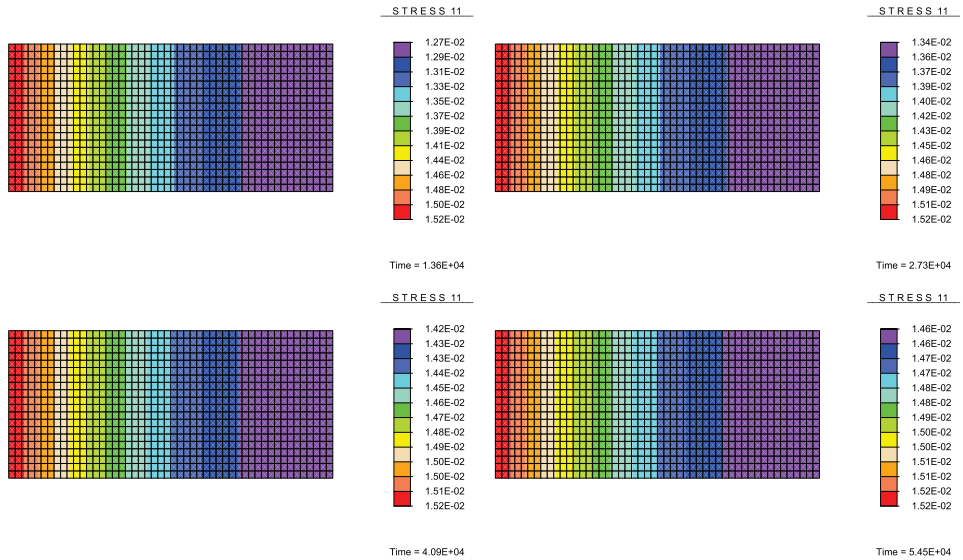

Figure 7-14: Size2: n_x=50, n_y=20.

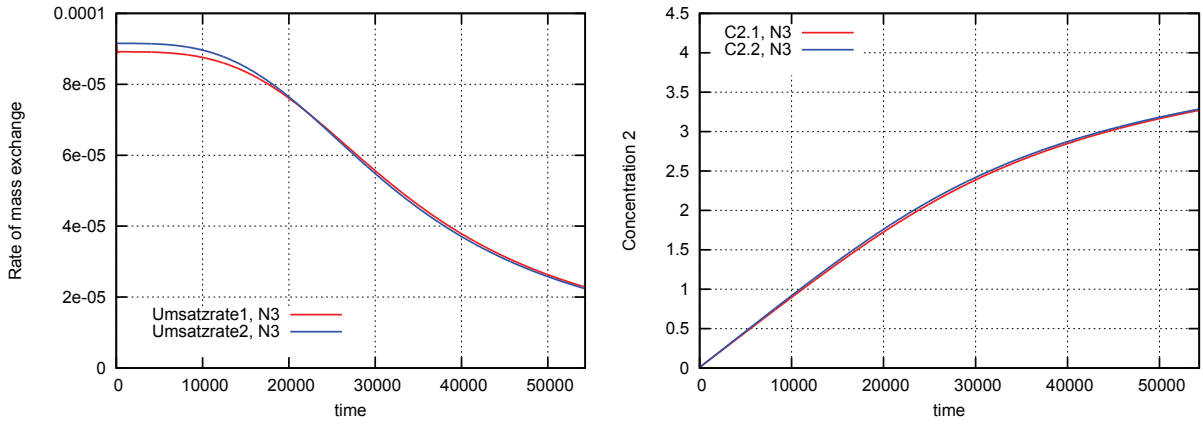

Figure 7-15: Breakthrough time and CO_2 concentration in size1 and size2.

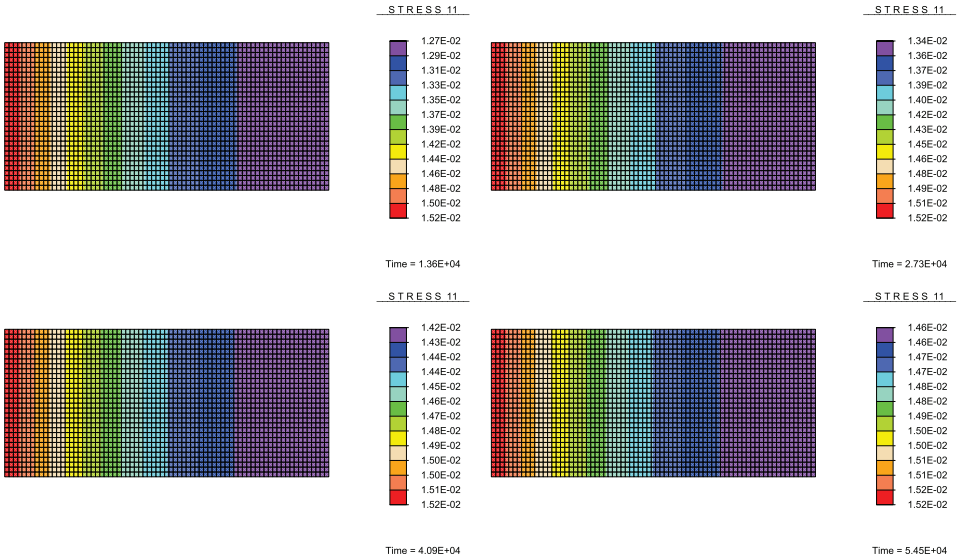

Figure 7-16: Size3: n_x=75, n_y=30.

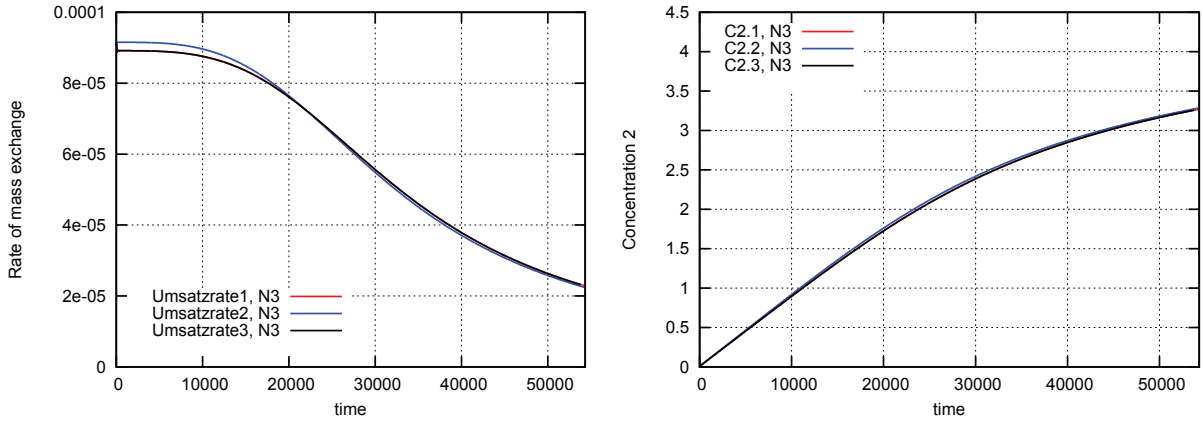

Figure 7-17: Breakthrough time and CO_2 concentration in size1,size2 and size3.

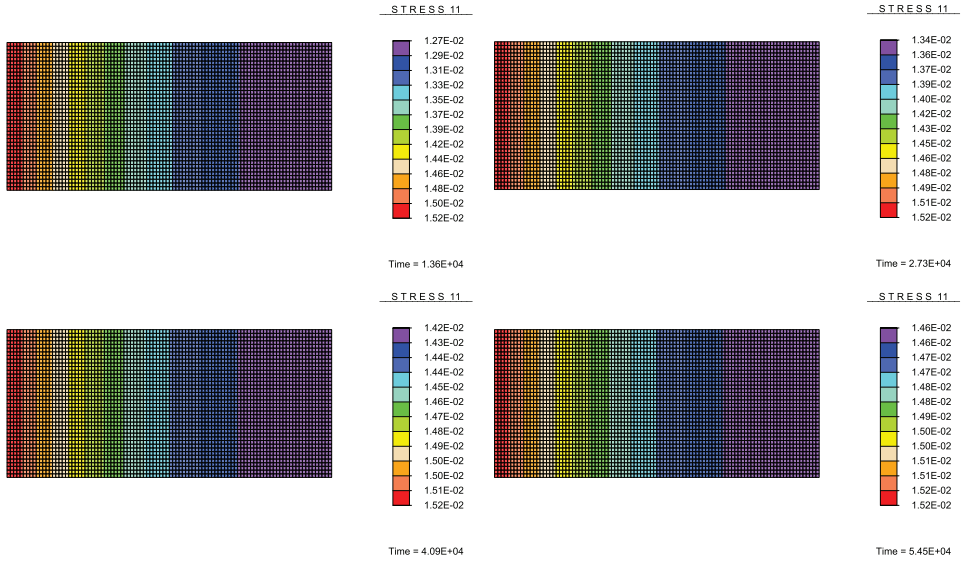

Figure 7-18: Size4: n_x=100, n_y=40.

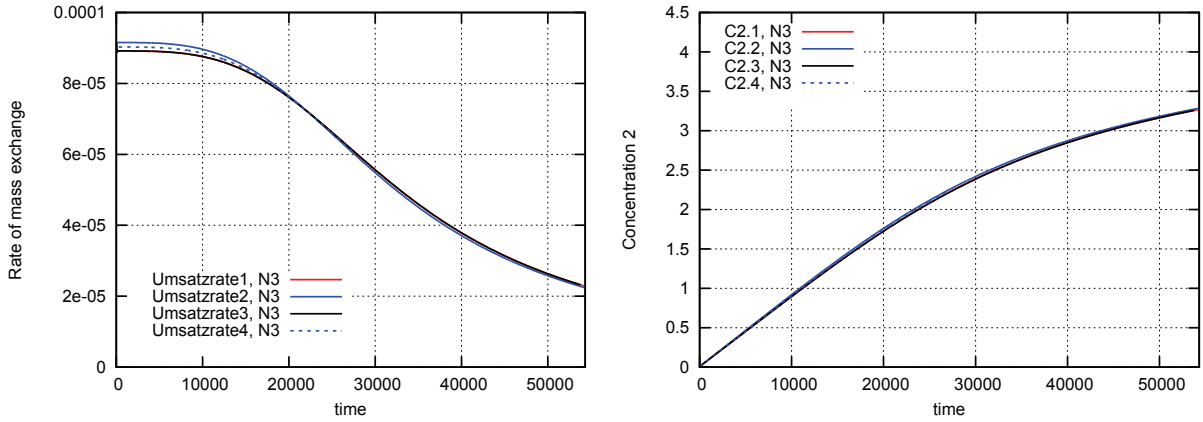

Figure 7-19: Breakthrough time and CO_2 concentration in size1,size2,size3 and size4.

of this adsorption model thus was improved. Therefore, the CO_2 concentration, fluid velocities, and pressure could be predicted by simulation.

8 Conclusions and Outlook

8.1 Conclusions

In this work, the new methods on landfill gas utilization for renewable energy are discussed by simulations and experiments. In addition, the models on landfill gas adsorption are developed.

The landfill gas can be used as fuel for fuel cells via steam-reforming. The simulation on landfill gas steam reforming is discussed in this thesis. In the reforming processes, the production of H_2 will decrease as pressure increasing, and it will increase as temperature increasing. Meanwhile, higher temperature and lower fraction of steam may give rise to methane cracking. In practice, the performance of fuel cell systems is directly related to gas load time. Seen from data of PAFCs system in a sewage plant, biogas and landfill gas may be supplied as fuel to fuel cell systems for long time running.

As experiments illustrated, bottom ash can be used as adsorbent for landfill gas upgrading. The CO_2 breakthrough capacity can be evaluated with breakthrough curves. However, CO_2 capacity is related to input gas flow rate and gas composition. As the same time, owing to the carbonation reaction between bottom ash and CO_2, the alkalinities of used bottom ash eluate decreases significantly.

Simulation is an effective method to predict landfill gas adsorption. The landfill gas adsorption through porous media modelling is developed based on mass balance, momentum balance and constitutive relations among phases. In this simulation work, the diffusion coefficients of landfill gas can be estimated by Fick's law.

8.2 Outlook

In the further research, the Pressure Swing Adsorption (PSA) of landfill gas with bottom ash may be performed experimentally. Currently, landfill gas upgrading process is performed in the range of constant pressure, in which landfill gas is purified by chemisorptions. However, PSA is a physisorption process, in which adsorbent can be used repeatedly. In practice, PSA is normally used to remove moisture from landfill gas, after gas is sucked out of landfill cites. Landfill gas upgraded with bottom ash in PSA may shorten the adsorption process, purified gas may be put into utilization directly.

In the field of gas adsorption modelling, the heat transfer and energy balance may be taken into consideration furthermore. Normally, there exist different temperatures in the different position of an adsorbent bed during gas adsorption processes. These temperature differences may result in heat transfer among gases and solid phases within the adsorbent bed. As consequence, the CO_2 breakthrough capacities of bottom ash may vary with temperature. These phenomena are able to be described by energy balance and to be predicted by models with heat transfer.

List of Reference

References

[1] Federal Ministry for the Environment, Nature Conservation and Nuclear Safety of Germany, *Renewables' Contribution to Energy Supply in Germany Continued to Rise in 2010*, No. 039/11, Berlin, **2011**.
http://www.erneuerbare-energien.de.

[2] Federal Ministry for the Environment, Nature Conservation and Nuclear Safety of Germany, *Renewable energy experiencing double-digit growth worldwide*, No. 094/11, Berlin, **2011**.
http://www.bmu.de.

[3] National Bureau of Statistics of China, *Utilization of Renewable Energy in China's Rural Areas(2009)*,(in Chinese), **2011**.
http://www.stats.gov.cn.

[4] S. Sakai et al., *World Trends in Municipal Solid Waste Management*, Waste Management, 16, pp.341-350, **1996**.

[5] V.K. Gupta et al., *Adsorption of Carmoisine A from Wastwater Using Waste Materials–Bottom Ash and Deoiled Soya*, J. Colloid Interface Sci., **2009**.
doi: 10.1016/j.jcis.2009.03.056.

[6] P.T. Williams, *Waste Treatment and Disposal*, John Wiley & Sons, Ltd, **2005**.
ISBN 0-470-84912-6.

[7] The UK Strategy, *Sustainable Development*, HMSO, London, **1994**.

[8] Department of the Environment and Welsh Office, *Making Waste Work*, HMSO, London, **1995**.

[9] UK Government Strategy Unit, *Waste Not Want Not*, HMSO, London, **2002**.

[10] Association for Sustainable Use and Recovery of Resources in Europe (ASSURE), *Towards Integrated Management of Municipal Solid Waste*, ASSURE, Brussels, Belgium, **1998**.

[11] Basel Convention, *Basel Convention on the Control of Transboundary Movements of Hazardous Wastes and Their Disposal*, **2005**.
http://www.basel.int/pub/pub.html.

[12] European Commission, Environmental Data Centre on Waste, Municipal waste, **2011**.
http://epp.eurostat.ec.europa.eu.

[13] Federal Statistical Office of Germany, *Environment Time series - Waste accumulation 1996-2009*, **2011**.
http://www.destatis.de.

[14] National Bureau of Statistics of China, *Urban Environment(2000-2009)* (in Chinese),**2011**. http://www.stats.gov.cn.

[15] European Environment Agancy, *Household and Municipal Waste: Comparability of Data in EEA Member Countries*, **2000**.

[16] Federal Statistical Office of Germany, *Decoupling of Generation from Economic Output(2002 - 2007)*, **2009**.
http://www.bmu.de/english/waste_management.

[17] The Central People's Government of the People's Republic of China, *Restrictions on Manufacture, Sale and Usage of Plastic* (in Chinese), **2008**.
http://www.gov.cn.

[18] National Bureau of Statistics of China, *The Main Data on Sixth Population Censuses of China* (in Chinese),**2011**.
http://www.stats.gov.cn.

[19] C. Fischer, M. Werge, *EU as a Recycling Society Present recycling levels of Municipal Waste and Construction & Demolition Waste in the EU* European Topic Centre on Resource and Waste Management, **2009**.

[20] Waste Management Statistics, *Composition of Household Waste (2007),Source: Statistisches Bundesamt 2009*, Federal Ministry for the Environment, Nature Conservation and Nuclear Safety of Germany, **2009**.
http://www.bmu.de.

[21] *The Directive on Furthering Treatment of Municipal Solid Waste*, (in Chinese), The State Council of the People's Republic of China, **2011**.
http://www.gov.cn.

[22] *European Parliament and Council Directive 94/62/EC of 20 December 1994 on packaging and packaging waste*, last amended by Directive 2004/12/EC, **2004**.

[23] K. Blumenthal, *Generation and treatment of municipal waste*, Eurostat, European Commission, **2011**.

[24] Ramboll, *Waste to Energy in Denmark*, **2006**.
www.zmag.dk/showmag.php?mid=wsdps.

[25] Federal Statistical Office of Germany, *Environment - Waste Balance 2009*, pp.2, **2011**.

[26] Federal Ministry for Environment, Nature Conservation and Nuclear Safety of Germany, *Waste incineration-A potential danger? Bidding farewell to dioxin spouting*, **2005**.

[27] D.O. Reimann, *Treatment of Waste Water From Refuse Incineration Plants*, Waste. Manag. Res. January., vol.5, no.1, pp.147-157, **1987**.
doi: 10.1177/0734242X8700500118.

[28] The Administrative Center for China's Agenda 21. *The White Paper on China's Population, Environment and Development in 21st Century*, (in Chinese), **1997**.
http://www.acca21.org.cn.

[29] National Bureau of Statistic of China, *Handbook on Statistical Data of BRICs*, (in Chinese), **2011**.
http://www.stats.gov.cn.

[30] National Bureau of Statistic of China, *Investment in urban environmental infrastructure in cities(2009)*, (in Chinese), **2011**.
http://www.stats.gov.cn.

[31] National Bureau of Statistics of China, *Urban Environment in Different Region of China(2009)* (in Chinese), **2011**.
http://www.stats.gov.cn.

[32] National Bureau of Statistics of China, *Environment in cities of China(2000-2009)* (in Chinese), **2011**.
http://www.stats.gov.cn.

[33] B. Solenthaler, R. Bunge, *Waste Incineration in China*, Institute for Applied Environmental Technology, Hochschule Rapperswil.**2003**.

[34] Yumen Ni, Haijun Zhang, Su Fan,etc., *Emissions of PCDD/Fs from municipal solid waste incinerators in China*, Chemosphere 75, pp.1153-P1158, **2009**.

[35] Juliang Wang, *Comparison in Waste Management and Sorting Methods between China and Germany* (in Chinese).
http://www.cn-hw.net/html/32/200905/10503.html.

[36] Qin Wang, *Aspects of Pretreated Hospital Waste Biodegradatiion in Landfills*, Doctoral Thesis in Unversity of Duisburg-Essen, **2004**.

[37] S. Roe, J. Reisman, R. Strait and M. Doorn, *Emerging Technologies for The Management and Utilization of Landfill Gas*, Technical Report EPA-600/R-98-021, **1998**.

[38] National Research Council and National Academy of Engineering, *The Hydrogen Economy: Opportunities, Costs, Barriers, and R&D Needs*, National Academies Press, **2004**.

[39] R.B. Williams, K. Kornbluth, P.A. Erickson, etc., *Estimates of Hydrogen Production Potential and Costs from California Landfill Gas*, 15th European Biomass Conference & Exhibition, 7-11 May, Berlin, Germany, **2007**.

[40] W.J. Cook, L.A. Siwajek, W.R. Brown, *Landfill Gas Conversion to a Contaminant-Free Methane-Carbon Dioxide Reformer Feedstock for Methanol Synthesis*.
http://www.netl.doe.gov/publications/proceedings/97/97ng/ng97_pdf/NGP4.PDF

[41] C. Deed, J. Cronow, A. Rosevear, etc., *Guidance on gas treatment technologies for landfill gas engines*, R&D Technical Report, pp.1-330, Environment Agency, Bristol, UK., **2004**.

[42] SCS Engineers, *Comparative Analysis Of Landfill Gas Utilization Technologies*, File No. 0293066, SCS Engineers, Washington, D.C., **1997**.

[43] T. Tsatsarelis, A. Karagiannidis, N. Moussiopoulos, etc., *Technologies of Landfill Gas Management and Utilization*, Waste-to-Energy Research and Technology Council, Greece. **2008**.
http://ttpl.chemeng.ntua.gr/wte/Pdfs/Karagiannidis_LFG_management.pdf

[44] P. Jaramillo and H. S. Matthews. *Landfill-gas-to Energy Projects: Analysis of Net Private and Social Benefits*, Environmental Science & Technology, Vol. 39, No.19, 7365-7373, **2005**.

[45] United States Environmental Protection Agency. *Auxiliary and Supplemental Power Fact Sheet: Microturbines*. Online publication, EPA Number: 832F05014, **2005**.

[46] United States Environmental Protection Agency, *LFG Energy Project Development Handbook, Chapter 3. Project Technology Options*.
http://www.epa.gov/landfill/res/pdf/pdh_chapter3.pdf

[47] Electricity-Generation Technologies for Landfill Gas, *U.S. Climate Change Technology Program-Technology Options for the Near and Long Term*, 156-158, November, **2003**.

[48] EG&G Technical Services, Inc., *Fuel Cell Handbook (Seventh Edition)*, U.S. Department of Energy, Morgantown, West Virginia, **2004**.

[49] J. C. Trocciola and J.L. Preston, *Demonstration of Fuel Cells to Recover Energy from Landfill Gas- Phase III.Demonstration Tests, and Phase IV.Guidelines and Recommendations*, Research and Development EPA-600/SR-98-002, **1998**.

[50] P. Lunghi, R. Bove, U. Desideri, *Life-Cycle-Assessment of Fuel-Cells-Based Landfill-Gas Energy Conversion Technologies*, Journal of Power Sources 131, 120-126, **2004**.

[51] J. Staniforth,K. Kendall, *Cannock Landfill Gas Powering a Small Tubular Solid Oxide Fuel Cell: A Case Study*, Journal of Power Sources 86, 401-403, **2000**.

[52] S. G. Meibuhr, *Review of United States Fuel-Cell Patents Issued from 1860 to 1947*, Electrochim. Acta, vol.11, pp.1301-1308, **1966**.

[53] P.W. Atkins, *Physical Chemistry*(3rd Edition), W.H. Freeman and Company, New York, NY, **1986**.

[54] A United Technologies Company, *UTC Fuel Cells*, **2005**.

[55] Fuel Cell Markets, *PAFC - Phosphoric Acid Fuel Cells Portal Page*, **2010-2011**.
http://www.fuelcellmarkets.com/fuel_cell_markets

[56] N. Giordano, *Fuel Cells Activity at CNR, TAE Institute*, CNR/TAE, Italy, **1992**.

[57] Westinghouse/DOE, *Gas Cooled Fuel Cell Systems Technology Development*, WAES-TR-92-001, **March 1992**.

[58] K. Harasawa, I. Kanno, I. Masuda, *Fuel Cell R&D and Demonstration Programs at Electric Utilities in Japan*, in Fuel Cell Seminar Abstracts, Tucson, AZ, **November 29-December 2, 1992**.

[59] M. Krueger, S. Beckmann, B. Engelen, etc. *Microbial Methane Formation from Hard Coal and Timber in an Abandoned Coal Mine*, J. Geomicrobiology, Vol.25, Issue 6, pp.315-321, **2008**.

[60] M. B. Wold, L. D. Connell, S. K. Choi, *The Role of Spatial Variability in Coal Seam Parameters on Gas Outburst Behaviour during Coal Mining*, International Journal of Coal Geology, Vol. 75, Issue: 1, pp.1-14, **2008**.

[61] Eds: P. Lens, P. Westermann, M.Haberbauer, etc., *Biofuels for Fuel Cells: Biomass Fermentation towards Usage in Fuel Cells*, IWA Pulishing, ISBN: 1843390922, **2005**.

[62] R. Holub, P. Voňka, *The Chemical Equilibrium of Gaseous Systems*, D.Reidel Publishing Company,Inc., ISBN: 9027705569, **1976**.

[63] Ch. Miao, Ch. Pasel, M. Luckas, J.-D. Herbell, *Thermodynamics on Landfill Gas Reforming*, Chem. Eng. Technol., 32, No. (10), pp.1617-1624, **2009**.

[64] Ch. Miao, T. Mietzel, et al., *Simulation Study for Landfill Gas Steam Reforming*, Proceeding of ISARET 2009, 28-29 April **2009**, UNITEN, Malaysia, ISBN 978-983-43357-6-2.

[65] Ch. Miao, T. Mietzel, M. Luckas, J.-D. Herbell, *Simulation on Landfill Gas-Steam Reforming*, Journal of Energy & Environment, (**in pressing**).

[66] M. Luckas, J. Krissmann, *Thermodynamik der Elektrolytlösungen*, Springer, ISBN: 3-540-41905-5, **2001**.

[67] C. Deed, J. Cronow, A. Rosevear,etc., *Guidance on Gas Treatment Technologies for Landfill Gas Engines*, R&D Technical Report pp.1-330, Environment Agency, Bristol, UK, **2004**.

[68] N. Muradov, F.Smith, *Thermocatalytic Conversion of Landfill Gas and Biogas to Alternative Transportation Fuels*, J. Energy & Fuels, 22, pp.2053-2060, **2008**.

[69] R. Bove, P. Lunghi, *Electric Power Generation from Landfill Gas Using Traditional and Innovative Technologies*, Energy Convers Manage., 47(11-12), pp.1391-1401, **2006**.

[70] W. Urban, et al., *Catalytically Upgraded landfill Gas as a Cost-Effective Alternative for Fuel Cells*, J.Power Sources, **2009**, doi:10.1016/j.jpowsour.2008.12.029.

[71] R.P. Ribeiro, T.P. Sauer, et al., *Adsorption of CO_2,CH_4, and N_2 in Activated Carbon Honeycomb Monolith*, J.Chem.Eng.Data, 53, pp.2311-2317, **2008**.

[72] C. Petit, T.J. Bandosz, *Complexity of Ammonia Interactions on Activated Carbons Modified with V_2O_5*, J. Colloid Interface Sci., 325, pp.301-308, **2008**.

[73] Q.L. Huang, S.M. Sundaram, et al., *Revisiting Transport of Gases in the Micropores of Carbon Molecular Sieves*, Langmuir, 19, pp.393-405, **2003**.

[74] M. Seredych, T.J. Bandosz, *Desulfurization of Digester Gas on Industrial-Sludge-Derived Adsorbents*, Energy Fuels, 21, pp.858-866, **2007**.

[75] S.U. Rege, R.T. Yang, et al., *Air-Prepurification by Pressure Swing Adsorption using Single/Layered Beds*, Chem. Eng. Sci., 56, pp.2745-2759, **2001**.

[76] G. Pigorini, M.D. LeVan, *Equilibrium Theory for Pressure Swing Adsorption. 2. Purification and Enrichment in Layered Beds*, Ind. Eng. Chem. Res., 36, pp.2296-2305, **1997**.

[77] P. Mostbauer, S. Lenz, et al., *MSWI Bottom Ash for Upgrading of Biogas and Landfill Gas*, Environ. Technol., 29, pp.757-764, **2008**.

[78] G. Ducom, D. Radu-Rirnoveanu, et al., *Biogas-Municipal solid Waste Incinerator Bottom Ash Interactions: Sulphur Compounds Removal*, J. Hazard. Mater., **2009**, doi: 10.1016/j. jhazmat. 2008.12.024.

[79] C.S. Kirby, J. Donald Rimstidt, *Mineralogy and Surface Properties of Municipal Solid Waste Ash*, Environ. Sci. Technoi., 27, pp.652-660, **1993**.

[80] C. Speiser, T. Baumann, R. Niessner, *Morphological and Chemical Characterization of Calcium-Hydrate Phases Formed in Alteration Processes of Deposited Municipal Solid Waste Incinerator Bottom Ash*, Environ. Sci. Technoi., 34, pp.5030-5037, **2000**.

[81] Y.C. Zhao, Song Lijie, *Treatment of MSW Incinerator Bottom Ash*, Huanjing Wuran YU Fangzhi, vol.25, 2, pp.95-97, **2003**(In Chinese).

[82] A. Bagchi, D. Sopcich, *Characterization of MSW Incinerator Ash*, J. Envir. Engrg., 115, pp.447-452, **1989**.

[83] R.R. Greenberg, G.E. Gordon, et al., *Composition of Particles Emitted from the Nicosia Municipal Incinerator*, J. Environ. Sci. Technol., 12, pp.1329-1332, **1978**.

[84] D.D. Do, *Adsorption Analysis: Equilibria and Kinetics*, Imperial College Press, **1998**. ISBN 1-86094-130-3, ISBN 1-86094-137-0 (pbk).

[85] J. Rouquerol, D Avnir, et at., *Recommendations for the Characterization of Porous Solids*, Pure & Appl. Chem., Vol. 66, No. 8, pp.1739-1758, **1994**.

[86] ASTM International, *Standard Test Method for Determination of the Accelerated Hydrogen Sulfide Breakthrough Capacity of Granular and Pelletized Activated Carbon*, Designation:D 6646-03, **2003**.

[87] ASTM International, *Standard Guide for Gas-Phase Adsorption Testing of Activated Carbon*, Designation:D 5160-95, **Reapproved 2003**.

[88] J.C. Maxwell, *On the Dynamical Theory of Gases*, Phil. Trans. Roy. Soc., 157, pp.49-88, **1866**.

[89] J. Stefan, *Über das Gleichgewicht und die Bewegung, insbesondere die Diffusion Von Gasmengen*, Sitzungsber. Akad. Wiss. Wien, 63, PP.63-124, **1871**.

[90] R. Taylor, R. Krishna, *Multicomponent Mass Transfer*, John Wiley & Sons, Inc., **1993**.

[91] R.C. Reid, J.M. Prausnitz, B.E. Poling, *The Properties of Gases & Liquids*(4th Edition), McGraw-Hill, **1987**.

[92] E.L. Cussler, *Diffusion-Mass Transfer in Fluid Systems*(3rd Edition), Cambridge University Press, **2009**.

[93] A. Fick, *On Liquid Diffusion*, Phil. Mag., 10, pp.30-39, **1855**.

[94] D.D. Do, *Adsorption Analysis: Equilibria and Kinatics*, Imperial College Press, **1998**.

[95] R.A. Svehla, *Estimated Viscosities and Thermal Conductivites of Gases at High Temperatures*, NASA Technical Report R-132, **1962**.

[96] R. De Boer, *Trends in Continuum Mechanics of Porous Media*, Springer, Netherlands, ISBN 1-4020-3143-2(HB), ISBN 1-4020-3144-0(e-book), **2005**.

[97] L.W. Morland, *A Simple Constitutive Theory for a Fluid-Saturated Porous Solid*, J. Geophys. Res., 77(5), pp.890-900, **1972**.

[98] M.A. Goodman and S.C. Cowin, *A Continuum Theory for Granular Materials*, Arch. Rational. Mech. An., 44, pp.249-266, **1972**.

[99] J.W. Nunziato and S.L. Passman, *A Multiphase Mixture Theory for Fluid Saturated Granular Material*, APS Selvadurai(ed), Mechanics of Structured Media A, Elsevier Science Publishers B. V., Amsterdam, pp.243-254, **1981**.

[100] R. De Boer and S.J. Kowalski, *Thermodynamics of Fluid-Saturated Porous Media with a Phase Change*, Acta. Mech. 109, pp.167-189, **1995**.

[101] X.Y. Li and X.W. Li, *On the Thermoelasticity of Multicomponent Fluid-Saturated Reacting Porous Media*, Int. J. Eng. Sci. 30, pp.891-912, **1992**.

[102] R. De Boer, *Highlights in the historical Development of the Porous Media Theory - toward a Consistent Macroscopic Theory*, Appl. Mech. Rev. 49, pp.201-262, **1996**.

[103] R. De Boer, *Theory of Porous Media - highlights in the historical development and current state*, Springer-Verlag, Berlin, **2000**.

[104] T. Ricken, R.de Boer, *Multiphase Flow in a Capillary Porous Medium*, Comput. Mater. Sci., 28, pp.704-713, **2005**.

[105] T. Ricken, *Lecture notes on Computational Multiphase Modeling of Porous Media* COMMAS Summer School October 12 - October 16, **2009**.

[106] J. Bluhm, *Modelling of saturated thermo-dlastic porous solids with different phase temperatures*, Porous Media: Theory, Experiments and Numerical Applications, Springer, **2002**.

[107] X.C. Fu, W.X. Shen, etc. (Eds.), *Physical Chemistry*(5th Edition,in Chinese), Higher Education Press, **2005**.

[108] Kaj Thomsen, *Chemical potential*, updated on **2011**, http://www.phasediagram.dk/chemical_potentials.htm.

[109] J. Bluhm, *A Consistent Model for Saturated and Empty Porous Media*, Forschungsberichte aus dem Fachbereich Bauwesen, Universität- GH Essen. ISSN 0947-0921, **1997**.

[110] O.C. Zienkiewicz, R.L. Taylor, *The Finite Element Method, Volume 1, The Basis*(fifth edition), Butterworth-Heinemann, ISBN 0 7506 5049 4, **2000**.

[111] G.F. Pinder, W.G. Gray, *Essentials of Multiphase Flow and Transport in Porous Media*, John Wiley & Sons, **2008**.

[112] S. Kato, H. Inazumi, and S. Suzuki, *Mass Transfer in a Ternary Gaseous Phase*, Int. Chem. Eng., 21, pp.443-452, **1981**.

[113] J. Liedmann, *Parameterstudie für ein gekoppeltes Mehrphasenelement bezüglich der Adsorption von Gasen in porösen Medien*; Bachelor-Thesis, Technische Universität Dortmund, **2011**.